ANALYSIS AND CONTROL OF PERIODIC GAITS IN LEGGED ROBOTS

A DISSERTATION SUBMITTED TO
THE GRADUATE SCHOOL OF ENGINEERING AND SCIENCE
OF BILKENT UNIVERSITY
IN PARTIAL FULFILLMENT OF THE REQUIREMENTS FOR
THE DEGREE OF
DOCTOR OF PHILOSOPHY
IN
ELECTRICAL AND ELECTRONICS ENGINEERING

By
Hasan Hamzaçebi
November 2017

ANALYSIS AND CONTROL OF PERIODIC GAITS IN LEGGED ROBOTS

By Hasan Hamzaçebi

November 2017

We certify that we have read this dissertation and that in our opinion it is fully adequate, in scope and in quality, as a dissertation for the degree of Doctor of Philosophy.

Ömer Morgül (Advisor)

Hitay Özbay

Uluç Saranlı

Melih Çakmakçı

M. Kemal Leblebicioğlu

Approved for the Graduate School of Engineering and Science:

Ezhan Karaşan
Director of the Graduate School

ABSTRACT

ANALYSIS AND CONTROL OF PERIODIC GAITS IN LEGGED ROBOTS

Hasan Hamzaçebi
Ph.D. in Electrical and Electronics Engineering
Advisor: Ömer Morgül
November 2017

The analysis, identification and control of legged locomotion have been an interest for various researchers towards building legged robots that move like the animals do in nature. The extensive studies on understanding legged locomotion led to some mathematical models, such as the Spring-Loaded Inverted Pendulum (SLIP) template (and its various derivatives), that can be used to identify, analyze and control legged locomotor systems. Despite their seemingly simple nature, as being a simple point mass attached to a massless spring from dynamics perspective, the SLIP model constitutes a restricted three-body problem formulation, whose non-integrability has been proven long before. Thus, researchers came up with approximate analytical solutions or they used some other different techniques such as partial feedback linearization for the sake of obtaining analytical Poincaré return maps that govern the motion of the desired legged locomotor system.

In the first part of this thesis, we consider a SLIP-based legged locomotion model, which we call as Multi-Actuated Dissipative SLIP (MD-SLIP) that extends the simple SLIP model with two additional actuators. The first one is a linear actuator attached serially to the leg spring to ensure direct control on the compression and decompression of the leg spring. The second actuator is a rotatory one that is attached to hip, which provides ability to inject some torque inputs to the system dynamics, which is mainly inspired by biological legged locomotor systems.

Following the analysis of MD-SLIP model, we utilize a partial feedback linearization strategy by which we can cancel some nonlinear dynamics of the legged locomotion model and obtain exact analytical solutions without needing any approximation. Having exact analytical solutions is crucial to investigate stability

characteristics of the MD-SLIP model during its hopping gait behavior. We illustrate and compare the applicability of our solutions with open-loop and closed-loop hopping performances on various rough terrain simulations.

Finally, we show how the MD-SLIP model can be anchored to bipedal legged locomotion models, where we assign two independent MD-SLIP models to each leg and investigate the system performance under their simultaneous but independent control. The proposed bipedal legged locomotion model is called as Multi-Actuated Dissipative Bipedal SLIP (MDB-SLIP) model. The key idea here is that we can still utilize the partial feedback linearization concept that we applied for the original MD-SLIP model and ensure exact analytical solutions for the MDB-SLIP model as well. We also provide detailed investigations for open-loop and closed-loop walking gait performance of the MDB-SLIP model on different noisy terrain profiles.

Keywords: Legged Locomotion, Stability Analysis, Periodic Gaits, Partial Feedback Linearization, Spring-Loaded Inverted Pendulum (SLIP) Model, Robotics.

ÖZET

BACAKLI ROBOTLAR İÇİN PERİYODİK YÜRÜME DAVRANIŞLARININ ANALİZİ VE KONTROLÜ

Hasan Hamzaçebi
Elektrik ve Elektronik Mühendisliği, Doktora
Tez Danışmanı: Ömer Morgül
Kasım 2017

Bacaklı hareketlerinin analizi, sistem tanılaması ve kontrolü, doğadaki canlılar gibi hareket eden robotların geliştirilebilmesi amacıyla birçok araştırmacı tarafından yoğun ilgi görmüştür. Bacaklı hareketliliği anlamak amacıyla yapılan çalışmalar, bu sistemlerin tanılaması, analizi ve kontrolü için kullanılabilecek Yaylı Ters Sarkaç (YTS) modeli (ve çeşitli türevleri) gibi matematiksel modellerin ortaya çıkmasına olanak sağlamıştır. YTS modeli, dinamik denklemleri bakımından kütlesiz bir yaya eklenen basit bir noktasal kütle olarak ifade edilmektedir. Ancak bu basit görünümlü yapısına rağmen, YTS modeli, integrali alınamadığı daha önce kanıtlanmış olan kısıtlı üç cisim problemi formülasyonuna sahiptir. Bu nedenle, YTS modelinin hareket denklemlerinin elde edilebilmesi amacıyla çeşitli yakınsamalı analitik çözümler türetilmiştir. Ayrıca, bazı araştırmacılar kısmi geri beslemeli doğrusallaştırma yöntemleri gibi bazı teknikler kullanarak da YTS modelinin hareket denklemleri için çeşitli çözümler üretmiştir.

Bu çalışmada ilk olarak, basit YTS modelini iki ek eyleyici ile genişleten Çoklu-eyleyicili Tüketimli YTS (ÇT-YTS) modeli olarak adlandırdığımız bir YTS tabanlı bacaklı hareketlilik modeli değerlendirilmiştir. Bu eyleyicilerden birincisi, bacak yayına seri halde bağlanarak bacak yayının sıkışması ve gevşemesi üzerinde direkt kontrol sağlayacak bir doğrusal eyleyicidir. İkincisi ise, kalçaya sabitlenen ve bacağın dönüş ekseninde tork girdisi sağlayan bir dönel eyleyicidir. Bu tip eyleyiciler temel olarak doğadaki canlı dinamiklerinden esinlenilmiş ve bacaklı hareketlilik modellerine dahil edilmiştir.

Çalışmanın devamında, değerlendirilen bacaklı hareketlilik modelinde (ÇT-YTS) yer alan bazı doğrusal olmayan dinamiklerin etkisini ortadan kaldıracak ve bu sayede herhangi bir yakınsama ihtiyacı olmadan tam analitik çözümler elde edebilmemize olanak sağlayacak bir kısmi geri beslemeli doğrusallaştırma

yönteminin sunulmasıdır. Tam analitik çözümlerin elde edilebilmesi, ÇT-YTS modelinin zıplama davranışı sırasında kararlılık analizinin yapılabilmesi için oldukça önemlidir. Sunulan çözüm yönteminin uygulanabilirliği açık döngü ve kapalı döngü zıplama davranışı performanslarına bakılarak çeşitli engebeli arazi simülasyon çalışmaları üzerinde karşılaştırmalı olarak gösterilmiştir.

Son olarak, ÇT-YTS modelinin çift bacaklı yürüyüş hareketleri için de uygulanabileceğini göstermekteyiz. Bu kapsamda, iki bacağa da ayrı ve bağımsız ancak eşzamanlı olarak kontrol edilebilen ÇT-YTS modelleri atanmıştır. Ortaya çıkan bu yeni çift bacaklı yürüyüş modeli ise Çoklu-eyleyicili Tüketimli Çift bacaklı YTS (ÇTÇ-YTS) modeli olarak adlandırılmıştır. Buradaki kilit fikir, ÇT-YTS modeli için önerilen kısmi geri beslemeli doğrusallaştırma yönteminin aslında çift bacaklı ÇTÇ-YTS modeli için de aynı şekilde kullanılarak tam analitik çözümlerin elde edilebilmesidir. Çalışmalarımızı desteklemek amacıyla, ÇTÇ-YTS modelinin de açık döngü ve kapalı döngü yürüyüş davranışının birbirinden farklı engebeli yer profilleri üzerinde ayrıntılı performans değerlendirmeleri sunulmuştur.

Anahtar sözcükler: Bacaklı Hareketlilik, Kararlılık Analizi, Periyodik Yürüyüş Şekilleri, Kısmi Geri Beslemeli Doğrusallaştırma, Yaylı Ters Sarkaç (YTS) Modeli, Robotik.

Acknowledgement

I would like to express my special thanks to my supervisor Ömer Morgül for his patience, guidance and invaluable comments during my doctoral studies. He was always there to kindly listen and give advice. In this sense, he is one of the very few people who deserves all the respect. I really appreciate all the hard work he has done for helping me to improve my work.

I would like to thank to Hitay Özbay and Uluç Saranlı for being members of my thesis progress committee. I would also express my gratitudes to Hitay Özbay, Uluç Saranlı, Melih Çakmakçı and M. Kemal Leblebicioğlu for reading this thesis and for being the members of my thesis defense jury.

I would like to thank İsmail Uyanık and Anıl Türel Uyanık for their support during this thesis and being incredibly good family friends. I would also like to thank İsmail Uyanık and Ali Nail İnal for sharing their office with me during my Ph.D. study.

I would like to give my special thanks to my friends İsmail Uyanık, Ali Nail İnal, Deniz Kerimoğlu, Görkem Seçer, Burak Kürkçü and Mustafa Mert Ankaralı for their support during the development of this thesis. I also thank to the other members of our research group Bahadır Çatalbaş, Hasan Eftun Orhon, Caner Odabaş, Mustafa Gül, Elvan Kuzucu Hıdır, Dilan Oztürk, Mansur Arısoy and Ahmet Safa Öztürk. Additionally, I would like to thank to my friends from Bilkent University Veli Tayfun Kılıç, Serkan Sarıtaş, Furkan Çimen, Ali Alp Akyol, Ahmet Dündar Sezer, Serdar Ögüt, Necip Gürler and Merve Begüm Terzi.

I would like to thank Bilkent University Electrical and Electronics Engineering Department and especially to faculty members for giving me this opportunity by teaching me well. I also want to thank Mürüvet Parlakay, Aslı Tosuner, Ergün Hırlakoğlu, Onur Bostancı, Ufuk Tufan and Yusuf Çalışkan for their administrative and technical support.

I would like to thank The Scientific and Technological Research Council of Turkey (TÜBİTAK) for the financial support during my Ph.D. study.

Also, I would like to thank to Aselsan A.Ş. for the support and encouragements during my Ph.D. study.

I thank my managers at Aselsan A.Ş. Semra Doğandağ, Hüseyin Özgün, Ali Kaderli, Birol Erentürk and Mustafa Erbudak for the support and encouragements during my Ph.D. study.

I would like to thank my mentors from Aselsan A.Ş and friends Emre Turgay, İsmail Özsaraç (and to their family) who taught me so much. I would like to thank to my coworkers Faruk Yurtsever, Mustafa Karakurt, Burak Kürkçü, Çağlar Uzun, Caner Orhan, Kemal Önder Bilgiç, Görkem Çağlar Sayan, Alican Eslek, Görkem Dayı, Yunus Emre Doğan, Mehmet Sami Tok, Gökhan Özdoğan, Murat Müminoğlu, Mustafa Eral, Ufuk Doğan, Murat Uyanıkoğlu, Berkay Fidan, Uğur Çavuş, Sefa Parlakyıldız and Kahraman Yiğit.

Finally, I would like to offer my sincere love to my family, for their support and encouragement in my whole life. I thank my wife Bahar Hamzaçebi and my son Furkan Hamzaçebi for their patience and help during this thesis. I also thank to my family Halim Hamzaçebi, Mevlüde Hamzaçebi, Kamile Hamzaçebi, Melek Hamzaçebi, Elif Soydeğer, Yunus Emre Soydeğer, Bilal Hamzaçebi, Medine Hamzaçebi, Burak Hamzaçebi, Hasan Ertürk, Gülser Ertürk, Ebubekir Ertürk, Sümeyra Ertürk, Edanur Ertürk, Ayşenur Ertürk and Aleyna Ertürk.

Contents

List of Figures

List of Tables

to my beloved family

Chapter 1

Introduction

One common objective of almost all robotics researchers is to build some useful machines that can serve for their interest. Actually, the exponential growth and spread of knowledge made this possible for some kind of applications such as industrial robots that replace human workers in factories for decades. However, area of legged locomotion, which aims to understand animal movements in nature and tries to build robot platforms inspired by these observations, is not as mature as the field of wheeled or tracked robotics. However, there is ample evidence, which both theoretically and practically indicates that the legged morphologies perform better than the wheeled/tracked ones, especially on rough terrains [1, 2, 3]. Therefore, the main research direction in the field of legged locomotion is to first analyze and understand legged locomotion [4, 5], then build legged robots with high maneuverability and control their locomotion by inspiring from nature [3, 6, 7, 8, 9, 10]. Detailed reviews about legged robots can be found in [11, 12]

1.1 Models for Running with Legged Robots

There are various approaches that are used to identify, analyze and control legged locomotion models. One of the most common method is to derive physics-based

mathematical models for the legged locomotor systems by using the principles of Lagrangian dynamics. Such methods are quite successful for describing center of mass trajectories of legged locomotion models [13, 14, 15] even in physical robotic systems [16, 17, 18]. On the other hand, data-driven techniques can also be utilized to estimate transfer functions [19, 20, 21, 22, 23] as well as state space models [24, 25] for legged locomotor systems using input-output data. Different than these approaches, central pattern generators based models are also considered in literature to investigate legged locomotion models [26, 27, 28].

Among the alternatives, it would be fair to say that a vast majority of the current literature exclusively focus on developing physics-based mathematical models and performing parametric fit to the data. Note that such robot structures may have many legs and depending on their configurations, the resulting dynamical equations usually become very complex, which makes both the analysis and control of such systems extremely difficult. One way of dealing with the complexities resulting from dynamics of many-legged systems is to obtain reduced order models that are easy to quantify some essential features, such as the center of mass dynamics, of legged locomotor systems, see e.g. [29]. The key reason behind this approach is that such templates and their anchors are easier to analyze and control. Since their behaviour captures some essential features of the original system, the results obtained from these templates are expected to be applicable to the analysis and control of the original structure. The Spring-Loaded Inverted Pendulum (SLIP) model is one of such templates which attracted considerable attention and received wide spread acceptance in the community of biology [30, 31, 32] and robotics [1, 33, 34, 35, 36]. It has been observed both theoretically and experimentally that SLIP template, and their anchors, can successfully predict the center of mass (COM) trajectories of different animals, regardless of the number of legs, see e.g. [2, 29, 37, 38]. Likewise, it has also been observed that SLIP templates yield accurate ground reaction force profiles resulting in the actual motion of such legged animals, see [29, 37, 39]. Hence, the SLIP model is also used as control targets for legged locomotor systems [18, 40, 41]. Motivated mainly from these observations, in this work we will focus on some properties of various SLIP templates as a model to study one-legged locomotion. For more

information on legged locomotion, the resulting dynamics and related subjects, the reader may resort to e.g. [2, 11], and the references therein. Also note that there are some successful extensions of such models for 3D legged locomotion models [42, 43, 44, 45, 46].

Despite its simplicity, COM trajectories of SLIP model constitute a three-body problem during the phase in which the leg is in contact with the ground (stance phase) [47], and non-integrability of such systems have been shown before [48]. Having this problem in its formulation, SLIP model does not have exact analytic solutions to their stance phase dynamics. One ad-hoc solution to overcome this issue is to proceed with numerical integrations, so that non-integrable nature of the system dynamics will not cause any problem. However, having solutions to the equations of motion, especially for the stance phase, might bring a huge computational advantage for some applications, see e.g. [49, 50]. In such cases, the utilization of semi-analytic approximation would be much more computationally effective than the numerical integration of stance dynamics, especially in feedback control of such systems which require high performance.

Once we turn our directions to computationally efficient analytical solutions, two main directions come forward to obtain analytic solutions to the equations of motion of the SLIP-like models. Our first choice is to utilize approximations to the non-integrable stance dynamics of the SLIP model. For this purpose, there are iterative methods in literature that approximates the stance dynamics of a 2-DOF SLIP model by using the main principles from mean value theorem [47]. Although the method is analytic by nature, its accuracy depends on the number of iterations performed during each run. Different from this method, simpler approximate analytic solutions have also been developed by assuming constant angular momentum, small angular sweep and low spring compression during the stance phase [51]. The main problem with this method comes from constant angular momentum assumption that yields high prediction performance for symmetric trajectories (see Figure 2.3 for visualization of such a trajectory) that correspond to trajectories where leg length is even symmetric while leg angle is odd symmetric around the time halfway during the stance phase [1]. However, its accuracy deteriorates when the trajectory is non-symmetric [51]. Arslan et al.

[52] proposed an extension to [51] in order to relieve the constant angular momentum assumption, so that the approximation holds also for the non-symmetric trajectories. The effectiveness and performance of such analytical approximate solutions have also been validated on a physical one-legged hopping robot platform [53]. There are also some other approximate analytical solutions for various type of SLIP-based legged locomotion models in the literature [15, 37, 54, 55].

Apart from using analytic approximations, partial feedback linearization also yields closed-form expressions for originally non-integrable system dynamics by eliminating some nonlinear components in the equations of motion with the help of control input. The key idea in partial feedback linearization is to find a transformation, which yields an equivalent controllable linear system through the use of some input signals that can cancel some nonlinearities in the original system. The theoretical foundations for the existence of such a transformation has been proven before [56] using Lie derivatives and brackets. Also, there are successful examples of using partial feedback linearization for various type of robotics systems [57, 58, 59, 60, 61]. More importantly, Piovan et al. [62] use a linear actuator input, connected in series with the leg spring, in order to cancel the nonlinearities in the SLIP dynamics to obtain exact closed-form expressions as an example of using partial feedback linearization for legged locomotor system dynamics. The important point here is to notice that partial feedback linearization also allows enforcing specific, analytic trajectories to the stance phase dynamics, while eliminating the nonlinearities in the system dynamics [63]. Our previous studies also show how this idea can be extended for obtaining exact analytical solutions to the stance dynamics of different legged locomotion models [64, 65].

1.2 Extending SLIP Model with Multiple Actuators

SLIP template consists of a point mass attached to a massless leg. In order to increase its practicality, many researchers anchored to SLIP template to obtain

more complex models for running with legged robots [35, 53, 66, 67], whose COM trajectories can be accurately defined with SLIP template, see Section 1.1. This section details our extensions to SLIP template based on biological observations and engineering requirements.

Our first goal is to present a focused understanding of stability properties of hopping that are common to a wide range of legged robots. Therefore, we first extend the SLIP template with a passive, compliant damping in the leg, which is inevitable for physical robot platforms. Note that extending the SLIP template with a damping element has been utilized in literature [68] and its effectiveness for modeling losses in a physical robot has been shown experimentally [53].

On the other hand, existence of damping in the leg requires energy injection to the system in order to compensate for losses. Therefore, we first consider a single linear actuator, which is serial to leg spring, as in [62, 69]. Physical significance of using a linear actuator in the leg has been validated in [70] by modeling muscle activation in the leg, which injects energy to legged animals during the stance phase, with a force-free leg length actuation. Note that addition of a linear actuator serial to the leg spring brings a mass to the robot leg. Various studies investigating the effect of leg mass suggest that it affects system dynamics both due to its inertia and due to the losses during the impact collisions [71]. However, effect of inertia has been found to have a minor effect on system trajectories as compared to impact collisions [71]. For the case of impact collisions, note that the linear actuator is placed between the body mass and the leg spring. Thus, linear actuator can be modeled as a part of body mass instead of leg mass. On the other hand, it has been shown that effect of leg mass during the impact collisions can be modeled with a simple inelastic collision map after the liftoff event [53]. Therefore, we neglect the mass of the linear actuator and continue our analysis with massless leg assumption in our simulation studies. For physical implementations, the inelastic collision map, which will not affect our stance dynamics solutions, can be used to consider the mass of the robot leg.

However, using a single linear actuator as in [62] limits us to enforce closed-form trajectories to either radial or angular trajectories (several equations allow

enforcing constrained trajectories to radial and angular motion simultaneously [62]). Hence, we utilize a torque actuation at the hip in order to obtain analytical solutions to both radial and angular trajectory at the same time. Various studies indicate that torque-actuated SLIP model yields more accurate predictions for the ground reaction forces (GRF) as compared to basic SLIP models and their GRF responses fit better to animal locomotion data [37]. Hence, torque actuation is utilized both in theoretical analysis as well as on experimental legged robot platforms [37, 68, 72, 73]. We assume fixed body orientation for torque actuation that allows the reaction force at the hip to be applied on body mass, which is assumed to be a point mass in our analysis. Note that although our assumption for fixed body orientation seems to be impractical, planarizers for legged robots make this assumption valid for template models [74]. On the other hand, a humanlike body orientation without a planarizer will need a properly chosen body angle for our desired hip torque actuation profile. However, this approach is left out of the scope of the current study.

1.3 Extending Bipedal SLIP Model with Multiple Actuators

Although the SLIP model and its variants are capable of representing the COM trajectories for different legged locomotor systems, a detailed analysis on more complex legged locomotion models require anchoring the model to some different legged locomotor systems [66, 75]. Our goal in this part is to first extend the MD-SLIP model for a bipedal legged locomotion model and then apply the proposed feedback linearization also on this model.

One of the initial ideas of bipedal legged locomotion models started by Geyer's use of simple spring-mass models to represent walking gaits in a bipedal legged locomotion model [76]. The new model basically consists of two springy legs and called as bipedal SLIP (B-SLIP) model in the literature. A key advantage of using bipedal SLIP model is the ability to obtain walking and running gaits, which are

the mostly used gaits in humans [77, 78]. The walking gait that are produced by B-SLIP model includes a non-instantaneous double support (DS) phase, in contrast to the passive dynamic walkers [79, 80, 81]. In addition, the B-SLIP model is reported to produce ground reaction forces that better match the human data, which is important towards building humanoid robot platforms. Motivated by these advantages, some researches aimed to achieve dynamic walking with the B-SLIP model [82, 83, 84] as well as with more complex models [45, 85, 86, 87, 88] through the embedding of B-SLIP models.

Motivated by these ideas, we extend upon our MD-SLIP model to a bipedal legged locomotion model considering the principles from B-SLIP model [76]. Our goal is not to simply extend the MD-SLIP model to a bipedal case but also to show that partial feedback linearization also allows obtaining exact analytical solutions for the bipedal legged locomotion models, which would be otherwise too challenging even with the approximations.

1.4 Contributions

This thesis aims to contribute on the analysis and control of periodic gaits in legged locomotion. To this end,

- We first demonstrate extensive simulation studies on investigating stability characteristics of a variety of SLIP-based legged locomotion models.
- We consider a multi-actuated SLIP model, called MD-SLIP, to enhance the stability region of the SLIP-based models that are currently available in the literature. The model we investigate includes a linear actuator to compress leg spring as well as a rotary actuator to inject torque inputs to the system.
- We utilize the partial feedback linearization theory to obtain the exact analytical solutions for the MD-SLIP model. The way we utilize the partial feedback linearization for the MD-SLIP model allows enforcing specified trajectories for the equations of MD-SLIP model.

- Another contribution of this thesis is the extension of our multi-actuated SLIP model for double support phase of bipedal legged locomotion models, which is called as MDB-SLIP model. We present how the multi-actuated structure for each leg can be utilized to increase stability of bipedal legged locomotion models. Besides, we can also utilize the partial feedback linearization to enforce some desired locomotion trajectories.

- Last but not least, we show the stability and robustness performance of the proposed models (as well as the partial feedback linearization strategy) on various noisy terrain locomotion simulations via a dead-beat control strategy.

1.5 Organization of the Thesis

This thesis is organized as follows. In Chapter 2, background about various SLIP models, such as the dissipative SLIP model including some analytical approximate solutions, active SLIP model and torque-actuated dissipative SLIP model are reviewed. Besides, we show systematic simulation studies to investigate the stability properties of these SLIP-based models. In Chapter 3, we propose the multi-actuated SLIP (MD-SLIP) model as well as our partial feedback linearization strategy to obtain closed-form solutions to equations of motion of the MD-SLIP model. We also present our investigations on stability characteristics of the MD-SLIP model and its performance on rough terrain under a dead-beat control strategy. Chapter 4 introduces our extensions of the MD-SLIP model for a bipedal legged locomotion model called MDB-SLIP model. We show how our multi-actuated model and partial feedback linearization strategy can be utilized to obtain closed-form solutions for the bipedal legged locomotion models. Then, in Chapter 5, we present our investigations on the performance of the MDB-SLIP model on sloped and noisy grounds via extensive simulation studies. Finally, in Chapter 6, we give the concluding remarks and possible future works of the current study.

Chapter 2

On the Stability of SLIP Models

This section is devoted to investigating stability characteristics of various SLIP-based models including approximate analytical solutions to their normally non-integrable dynamics. In the first part of this chapter, we introduce the background material on system models and equations of motions for different SLIP models. Then, the second part presents our efforts on investigating stability characteristics of these SLIP-based models.

2.1 SLIP Models

2.1.1 Dissipative SLIP Model

The dissipative spring-loaded inverted pendulum model is an extended version of the well-known SLIP model, where a parallel damping element is added to capture dissipation behavior of the leg during the stance phase. The model consists of a body, which is assumed to be a point mass, attached to a massless leg to preserve the simplicity of the model. The leg spring has parallel compliance and damping elements as illustrated in Figure 2.1.

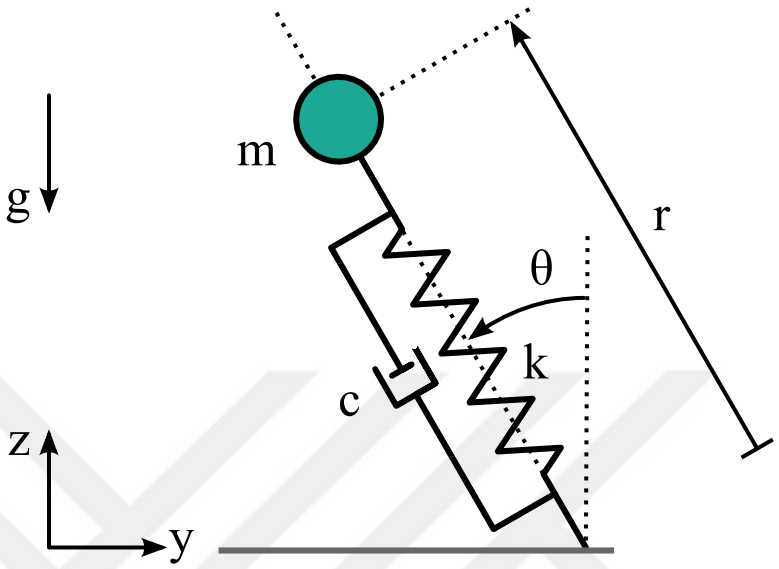

Figure 2.1: The dissipative SLIP model, coordinate system and model parameters

The model has hybrid system dynamics by nature and there are two switching subsystems that are triggered one after another during locomotion, as illustrated in Figure 2.2. First phase is called flight when the toe of the robot is on the fly and the second phase is called stance when the toe of the robot is in contact with the ground. The periodic locomotion of the robot is realized via consecutive activation of these two phases. Actually, these phases can also be divided into sub-phases of locomotion to investigate the overall behavior in detail. The flight phase have two sub-phases as *ascent* and *descent* based on the increase or decrease in the vertical position of the robot. Similarly, stance phase can be observed in two sub-phases as *compression* and *decompression*, which are discriminated as the compression and decompression behavior of the leg spring as the name refers to.

The transitions from and to the sub-phases of locomotion are described by events which are given by some predefined boundary conditions for system dynamics during associated phase of locomotion. Starting from descent phase, the robot first faces with *touchdown* event which triggers the transition from descent phase to the stance phase, where the foot gains ground contact. In the first sub-phase of stance, body mass starts to compress the leg spring until the bottom point where the *bottom* event occurs. The *bottom* event triggers the transition

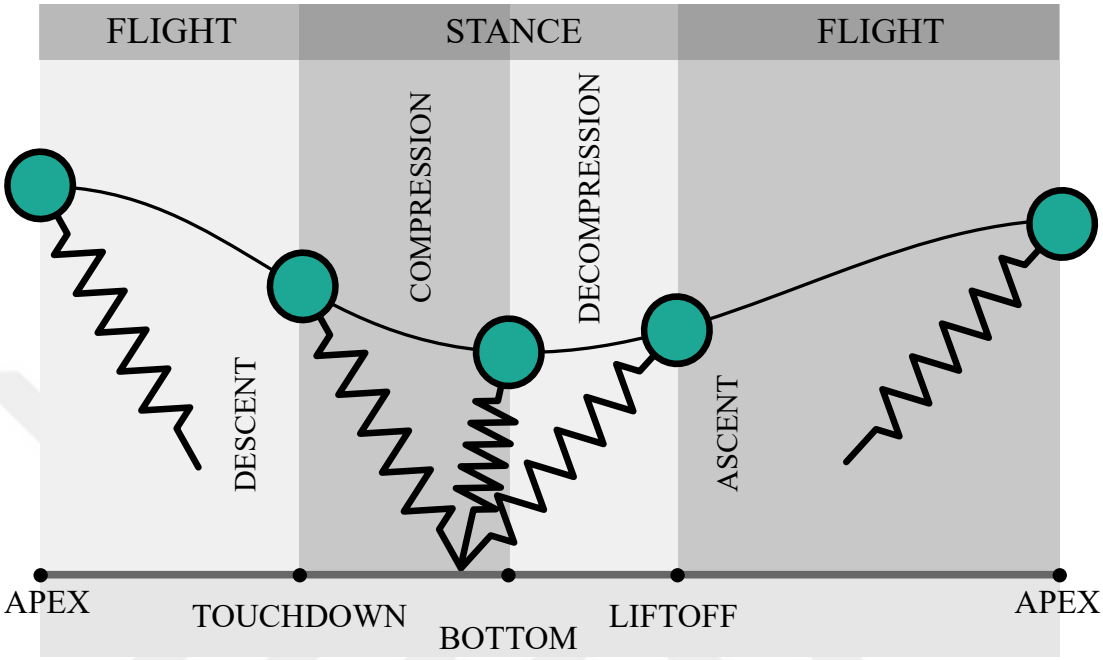

Figure 2.2: The phases of a single-stride locomotion of the SLIP model

from compression to decompression phase, where the body velocity changes its direction during stance and leg spring starts pushing the body upwards by using the potential energy stored in the leg spring. After some point the *liftoff* event occurs, when the toe of the robot loses the contact with the ground and robot starts to fly upwards due to the push of the leg spring. Finally, the robot reaches a maximum height where the ascent phase ends. This event is called *apex* event, which triggers the transition from ascent to descent, which will be frequently used in the thesis.

In addition to various terms defined above which are utilized in the thesis, at this point, we will clarify some terminology regarding the locomotion trajectory. Note that Figure 2.2 represents a sample trajectory for the SLIP model. This trajectory, starting and ending at two subsequent apexes, is called a *stride*. By an abuse of notation, we will also call this motion (stride) as a gait in this thesis. Obviously the concept of gait, albeit containing the motion depicted in Figure 2.2, corresponds to various coordination modes of animal (or robot) legs in literature [5, 14, 27]. However, one-legged template structure of the SLIP model does not allow a multi-legged gait description for one stride. On the other hand, [31]

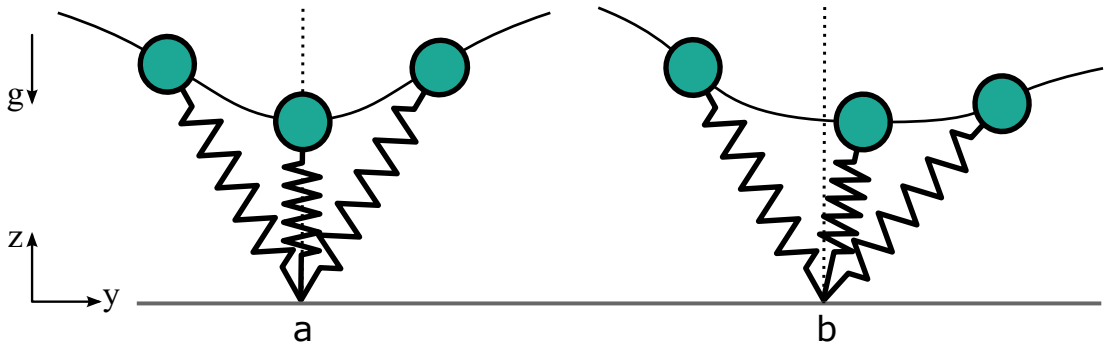

Figure 2.3: A sample illustration of a) symmetric gait and b) asymmetric gait.

describes the locomotion performed by kangaroos as hopping gait that is also one of the locomotion types performed by using the SLIP model. Therefore, we focus on hopping gait in our analysis and we will refer to this type of locomotion as hopping gait (or simply gait) and the path it follows during the locomotion will be called trajectory throughout the thesis. The locomotion of SLIP is then subsequent recursion of strides depicted in Figure 2.2. A periodic motion, or simply a periodic gait is such a motion where initial and final apex states are equal. The locomotion containing such periodic gaits is then called as a periodic locomotion. A periodic gait could be symmetric or asymmetric, as depicted in Figure 2.3. In symmetric gaits, at the bottom event, the SLIP is vertically upwards and the resultant trajectory has the following properties; leg length is even symmetric while leg angle is odd symmetric around the bottom state [1]. Otherwise the trajectory is called asymmetric.

Our aim in this work is to analyze the existence and stability of periodic gaits of SLIP dynamics under some control laws. The main motivation behind such an aim is that such gaits could be preferred as steady-state targets in the feedback control of SLIP locomotion. Likewise, deviations from such a periodic gait could be utilized as a locomotion performance measure. In fact, if one can relate various properties of such stable periodic gaits with the control law properties, various other measures could be considered to improve the locomotion performance. For instance, a periodic locomotion could be generated by using symmetric or asymmetric gaits. While symmetric gaits are easier to analyze since they yield approximate analytical solutions, see [51], asymmetric gaits may

Table 2.1: Dimensionless counterparts of the physical quantities

Quantity	Description
$t := \bar{t}/\sqrt{r_0/g}$	time
$y := \bar{y}/r_0$	length
$\dot{y} := \dot{\bar{y}}/\sqrt{gr_0}$	velocity
$\ddot{y} := \ddot{\bar{y}}/g$	acceleration
$\theta := \bar{\theta}$	angle
$\dot{\theta} := \dot{\bar{\theta}}\sqrt{r_0/g}$	angular velocity
$\ddot{\theta} := \ddot{\bar{\theta}}r_0/g$	angular acceleration
$E := \bar{E}/(mgr_0)$	energy
$k := \bar{k}r_0/(mg)$	leg stiffness
$c := \bar{c}\sqrt{r_0/g}/m$	damping constant
$\tau := \bar{\tau}/(mgr_0)$	torque

be used to improve the stability of periodic gaits. They may be utilized to adjust foot placement, to regulate the energy or to control the horizontal position with better locomotion performance. Further information about the symmetric and asymmetric trajectories of the SLIP template can be found in [1] and the references therein.

In order to make sure that our analysis are parameter independent and obtain general forms, all the works in this thesis will be presented with dimensionless formulation. To obtain dimensionless quantities, time and length will be scaled with $\sqrt{r_0/g}$ and leg rest length r_0, respectively. Conversion from physical quantities to non-dimensional counterparts can be obtained by using the equations in Table 2.1, where variables with bars are the physical quantities of the corresponding non-dimensional parameters. Additionally, notations used for SLIP model throughout the thesis are given in Table 2.2. Note that our formulations are in the non-dimensional coordinates to generalize our solutions. However, in order to book-keep the notations of background materials, the reviews about such background works will be given in their original coordinate frames.

System dynamics of the dissipative SLIP model during the flight phase is fairly simple, since the point mass follows a ballistic trajectory during its fly, which is given as

$$\ddot{y} = 0, \ddot{z} = -1 \tag{2.1}$$

Table 2.2: Notation for SLIP model used throughout the thesis

SLIP Parameters	
y, z	Body horizontal and vertical positions
$\dot{y}, \dot{z}$	Body horizontal and vertical velocities
$\ddot{y}, \ddot{z}$	Body horizontal and vertical accelerations
r, θ	Leg length and angle
$\dot{r}, \dot{\theta}$	Leg compression and swing rates
m, g	Body mass and gravitational acceleration
c, k	Leg damping constant and stiffness
r_0	Leg rest length
p_θ	Angular momentum
t_s	Stance duration
t_{td}, t_{lo}	Touchdown and liftoff times
r_{td}, θ_{td}	Touchdown leg length and angle
r_{lo}, θ_{lo}	Liftoff leg length and angle
$\dot{r}_{td}, \dot{\theta}_{td}$	Touchdown leg compression and swing rates
$z_a, \dot{y}_a$	Apex height and horizontal velocity

in Cartesian coordinates.

However, system dynamics during stance is not as simple as in the flight phase. In order to obtain the equations of motion during the stance phase, Lagrangian method is used in this thesis. In the non-dimensional formulation, Lagrangian of the system dynamics can be obtained as

$$L = \frac{1}{2}(\dot{r}^2 + r^2\dot{\theta}^2) - \frac{k}{2}(1-r)^2 - r\cos\theta. \tag{2.2}$$

In addition, we have a Rayleigh dissipation function due to the damping term as

$$D = \frac{1}{2}c\dot{r}^2. \tag{2.3}$$

By using the classical Lagrange's equations

$$\frac{d}{dt}\left(\frac{\partial L}{\partial \dot{q}_j}\right) - \frac{\partial L}{\partial q_j} + \frac{\partial D}{\partial \dot{q}_j} = 0, \tag{2.4}$$

with $q_1 = r$ and $q_2 = \theta$, we obtain the following equations of motion for the stance phase

$$\ddot{r} = r\dot{\theta}^2 + k\,(1-r) - \cos\theta - c\dot{r}, \tag{2.5}$$

$$\ddot{\theta} = \frac{1}{r}\left(\sin\theta - 2\dot{r}\dot{\theta}\right). \tag{2.6}$$

It has been shown that the equations of the form given by (2.5) and (2.6) are non-integrable [48]. Hence, exact analytical solution of the stance dynamics given by (2.5) and (2.6) are not available. Although numeric integration is a first choice to obtain stance trajectories, it is not an efficient solution for online computation when solutions with different parameter sets are needed to optimize the controller parameters [50]. Some researchers proposed analytical approximate solutions to the stance dynamics [13, 51], some with iterative solutions [47] and some of these approximations are validated on physical robot platforms [53]. On the other hand, some studies in literature focus on using partial feedback linearization, which aims at deriving exact analytical solutions with the utilization of additional actuators [62].

2.1.2 Simple Approximate Stance Map by Geyer et al.

In this section, we briefly review the approximation method proposed in [51]. If a sufficiently small angular span Δq_θ is assumed for the stance phase, the effect of gravity can be linearized, yielding simplified equations of motion

$$m\ddot{r} = mr\dot{\theta}^2 + k(r_0 - r) - mgr, \tag{2.7}$$

$$\frac{d}{dt}(mr^2\dot{\theta}) = 0, \tag{2.8}$$

which are now integrable since the angular momentum, $p_\theta := mr^2\dot{\theta}$ and the total energy

$$E = \frac{m}{2}\dot{\theta}^2 + \frac{{p_\theta}^2}{2mr^2} + \frac{k}{2}(r_0 - r)^2 + mgr, \tag{2.9}$$

become constants of the motion. Defining the parameters

$$\rho := \frac{r - r_0}{r_0} \leq 0, \tag{2.10}$$

$$\epsilon := \frac{2E}{m{r_0}^2}, \tag{2.11}$$

$$\omega := \frac{p_\theta}{m{r_0}^2}, \tag{2.12}$$

$$\omega_0 := \sqrt{\frac{k}{m}} \tag{2.13}$$

and substituting them into (2.9), yields

$$\epsilon = \dot{\rho}^2 + \omega^2/(1+\rho)^2 + {\omega_0}^2\rho^2 + 2g(1+\rho)/r_0. \tag{2.14}$$

If the relative spring compression $|\rho| \ll 1$ is assumed, then the term $1/(1+\rho)^2$ can be approximated by a Taylor series expansion around zero to yield

$$1/(1+\rho)^2\big|_{\rho=0} = 1 - 2\rho + 3\rho^2 - O(\rho^3). \tag{2.15}$$

Under these assumptions and further simplifications [51], an approximate analytical solution to $r(t)$ can be found as

$$r(t) = r_0(1 + a + b\sin(\hat{\omega}_0 t)), \tag{2.16}$$

where some variables are defined as

$$\hat{\omega}_0 := \sqrt{{\omega_0}^2 + 3\omega^2}, \tag{2.17}$$

$$a := (\omega^2 - g/r_0)/\hat{\omega}_0^2, \tag{2.18}$$

$$b := \sqrt{a^2 + (\epsilon - \omega^2 - 2g/r_0)/\hat{\omega}_0^2}. \tag{2.19}$$

The equation (2.16) can also be used to determine the times for critical events relative to an unknown time origin as

$$t_{td} = (\pi - \arcsin(-a/b))/\hat{\omega}_0, \tag{2.20}$$

$$t_{lo} = (2\pi + \arcsin(-a/b))/\hat{\omega}_0, \tag{2.21}$$

assuming that $r_{lo} = r_{td} = r_0$.

Given the approximate analytical solution for the radial motion and the conservation of the angular momentum, angular velocity can be obtained as

$$\dot{\theta} = \omega/(1+\rho)^2 = \omega(1 - 2\rho). \tag{2.22}$$

Recalling that $\rho := (r - r_0)/r_0 = a + b\sin(\hat{\omega}_0 t)$, an approximate analytic solution to the angular motion can be found as

$$\theta(t) = \theta_{td} + \omega(1-2a)(t - t_{td}) + \frac{2b\omega}{\hat{\omega}_0}\left(\cos(\hat{\omega}_0 t) - \cos(\hat{\omega}_0 t_{td})\right), \tag{2.23}$$

where $t_{td} \le t \le t_{lo}$, and t_{td} and t_{lo} are as in (2.20) and (2.21).

As a summary the following four equations are obtained as approximate analytical solutions of stance dynamics given by (2.5) and (2.6):

$$r(t) = r_0(1 + a + b\sin(\hat{\omega}_0 t)), \tag{2.24}$$

$$\dot{r}(t) = r_0\hat{\omega}_0 b\cos(\hat{\omega}_0 t), \tag{2.25}$$

$$\theta(t) = \theta_{td} + \omega(1-2a)(t - t_{td}) + \frac{2b\omega}{\hat{\omega}_0}\left(\cos(\hat{\omega}_0 t) - \cos(\hat{\omega}_0 t_{td})\right), \tag{2.26}$$

$$\dot{\theta}(t) = \omega(3 - \frac{2r}{r_0}). \tag{2.27}$$

2.1.3 Gravity Correction to Geyer et al. by Arslan et al.

The angular momentum during stance phase is conserved for symmetric trajectories [52]. However, conservation of angular momentum becomes inaccurate for non-symmetric trajectories. The angular momentum around the toe, $P(t)$, during stance can be calculated as

$$P(t) = P_{t_0} + \int_{t_0}^{t} \tau(\zeta)d\zeta, \tag{2.28}$$

$$\tau(t) := mgr(t)\sin(\theta(t)), \tag{2.29}$$

where $\tau(t)$ is the torque due to gravity around the toe and P_{t_0} is the angular momentum at touchdown instant. These expressions are too complex for integration so (2.28) can be simplified by an n-point approximation as

$$P(t) \approx P_{t_0} + (t - t_0)\left(\frac{1}{n}\sum_{k=0}^{n-1} mgr_d[k]\sin(\theta_d[k])\right), \tag{2.30}$$

where $r_d[k]$ and $\theta_d[k]$ are (functions of $r(t)$ and $\theta(t)$, respectively) defined as

$$r_d[k] := r(t_0 + \frac{k}{n}(t - t_0)), \tag{2.31}$$

$$\theta_d[k] := \theta(t_0 + \frac{k}{n}(t - t_0)), \tag{2.32}$$

respectively.

An average leg length between times t_i and t_f where $t_{td} \leq t_i < t_f \leq t_{lo}$ can be

calculated as

$$r_{av}(t_i, t_f) \approx \frac{1}{t_f - t_i} \int_{t_i}^{t_f} r_0(1 + a + b\sin(\hat{\omega}_0 t))dt, \tag{2.33}$$

$$= r_0(1 + a) - \frac{b}{\hat{\omega}_0(t_f - t_i)} \left(\cos(\hat{\omega}_0 t_f) - \cos(\hat{\omega}_0 t_i)\right), \tag{2.34}$$

and using it in (2.30), the total effect of gravity becomes

$$P_c := \frac{(t_f - t_i)mgr_{av}(t_i, t_f)}{2} \left(\sin(\theta(t_i)) + \sin(\theta(t_f))\right). \tag{2.35}$$

P_c is proposed to be added to the original angular momentum term, p_θ

$$\hat{p}_\theta = p_\theta + P_c, \tag{2.36}$$

which replaces p_θ in all derivations. Using touchdown and liftoff times as initial and final stated yields the corrective method for the apex return map [52].

2.1.4 Active SLIP Model

In this section, we give a brief review of the active SLIP model proposed in [62]. Note that [62] utilizes partial feedback linearization to obtain exact analytical solutions to originally non-integrable system dynamics. More precisely, a linear actuator is attached to the leg spring serially and the length of the actuator can be adjusted. By adjusting actuator length, some nonlinear elements are cancelled and the resulting system dynamics may have analytical solutions.

The addition of linear actuator changes the leg length as

$$r(t) = r_{act}(t) + r_k(t) \tag{2.37}$$

where $r_{act}(t)$ represents the linear actuator length and $r_k(t)$ is leg spring length. In the same formulation, the symbols $r_{act,0}$ and $r_{k,0}$ are used to describe the rest lengths of the linear actuator and the leg spring, respectively. Therefore, the leg rest length can be represented as $r_0 = r_{k,0} + r_{act,0}$.

Actuator displacement is defined as $\Delta r_{act} = r_{act} - r_{act,0}$ in [62]. For Δr_{act}, the following control law is proposed in [62]

$$\Delta r_{act} = \frac{m}{k}\left(\ddot{r} + g\cos\theta - r\dot{\theta}^2\right) + r - r_0, \tag{2.38}$$

for the actuator displacement to make the point mass to follow the desired trajectory.

In order to obtain analytically tractable equations of motion for the stance phase, [62] forces the point mass to follow some specified symmetric gaits. For instance, the following equation for the angular velocity is used to enforce the symmetric gait in [62]

$$\dot{\theta}(t) = A\cos\theta(t) + c_1, \tag{2.39}$$

where A and c_1 are determined from the boundary conditions between descent and compression subphases at the touchdown instant. The solutions of A, c_1, $r(t)$ and more details can be found in [62].

2.1.5 Torque-Actuated Dissipative SLIP Model

In this section, we review the torque-actuated dissipative SLIP (TD-SLIP) model, proposed by Ankarali and Saranli [37]. One of the main contributions of this model is that a rotary actuator is attached to the hip to compensate the damping loss of the dissipative SLIP model. The aim of this work is to approximate stance dynamics of the proposed model and to perform limit-cycle identification and characterization.

It has been shown in [37] that, TD-SLIP model is marginally stable without applying an explicit control but asymptotically stable locomotion can be achieved for fixed touchdown angles by applying torque inputs via the hip actuator.

For the hip actuator, the following torque function is proposed in [37]

$$\tau(t) = \begin{cases} \tau_0(1 - t/t_f) & \text{if } 0 \le t \le t_f \\ 0 & \text{if } t > t_f \end{cases} \tag{2.40}$$

where $\tau_0 := \alpha/\dot{\theta}_{td}$. The α parameter is called as constant touchdown parameter. This function is simple and uses some constants that is determined before touchdown event. Also, the decreasing nature of this function avoids the application of negative work during stance. In order to ensure that torque applied at the liftoff instant is zero, t_f is chosen as the liftoff time. By this way, the hip torque does not cause early liftoffs and the stance duration approximation does not become difficult. More details about this model and derivations can be found in [37].

2.2 Stability Analysis

In this section, we seek to analyze the stability characteristics of the periodic gaits. Such periodic gaits are crucial for their use as steady-state control targets in legged locomotion. Hence, stability of such periodic gaits are important for their use in motion planning. In order to achieve this, we first define apex to apex return map, which is a mathematical description of locomotion from one apex state to the next one. Once we have this apex to apex return map, we can solve it to find fixed points, which maps an apex state to the same apex state in a single stride. Hence, fixed points generate the periodic gaits for legged locomotion. To investigate their stability, we first derive the Jacobian matrix for the periodic apex to apex return map by taking its numerical derivative with respect to cyclic state parameters, apex height and apex speed. Having this at hand, one can determine the stability by checking the eigenvalues of the Jacobian matrix.

2.2.1 Apex to Apex Return Map

The apex to apex return map analysis for the SLIP model starts by dividing the locomotion into repetitive sub-phases and associated transition events. In order to define an initial point, we choose a Poincaré section at the apex state and define the apex to apex return map until the next apex state. Assume that the chosen apex state have the apex height z_{a0} and apex velocity $\dot{y}_{a0}$. The first phase of locomotion is called descent phase, where the body exhibits a ballistic

trajectory (2.1) until the toe contact with the ground. Mathematically, this boundary condition can be formulated as $z = \cos\theta_{td}$. The interim period between the apex state and the touchdown instant can also be mathematically formulated via the following map

$$(\dot{z}_{td}, \dot{y}_{td}) = H_a^{td}(z_{a0}, \dot{y}_{a0}), \tag{2.41}$$

where terms with subscript td corresponds to their values at touchdown and H_a^{td} is the apex to touchdown map. Note that the vertical and horizontal velocities at touchdown; $\dot{z}_{td}$ and $\dot{y}_{td}$ are defined in Cartesian coordinates. One important point to notice that H_a^{td} is a function of θ_{td} and hence it can be used as a control parameter to regulate the output of the apex to touchdown return map. Similar control examples are often appeared in the literature, see e.g. [1, 49, 50].

The touchdown event initiates the stance phase, where the body follow the dynamics represented in (3.1) and (3.2). These can be solved as (3.9) and (3.17). To preserve our mathematical formulation, we write the stance phase as

$$(r_{lo}, \dot{r}_{lo}, \theta_{lo}, \dot{\theta}_{lo}) = H_{td}^{lo}(\dot{r}_{td}, \dot{\theta}_{td}), \tag{2.42}$$

where the variables with subscript lo corresponds to their values at liftoff instant, which can be defined as the time when the toe loses contact with the ground. Besides, H_{td}^{lo} is a mathematical descriptor function for touchdown to liftoff map. Similar to apex to touchdown event, H_{td}^{lo} depends on the control parameter θ_{td}.

The ascent phase, coming after the liftoff event, has the ballistic flight trajectory dynamics with the descent phase except their initial conditions. Hence, the mathematical formulation for ascent subphase can be given as

$$(z_{a1}, \dot{y}_{a1}) = H_{lo}^{a}(\dot{z}_{td}, \dot{y}_{td}, r_{lo}, \theta_{lo}), \tag{2.43}$$

where H_{lo}^{a} corresponds to the liftoff to apex map.

Having all subphase maps at hand, apex to apex return map can be obtained by combining these phases from one apex state to the next one as

$$H_a^a = H_{lo}^a \circ V_{lo} \circ H_{td}^{lo} \circ V_{td} \circ H_a^{td}, \tag{2.44}$$

where H_a^a is apex to apex return map. In addition to subphases, we include simple coordinate transformation matrices V_{td} and V_{lo} to switch between Cartesian and polar coordinates while deriving our solutions. Hence, combining all these subphases, apex to apex return map can be defined via a single mathematical function as

$$(z_{a1}, \dot{y}_{a1}) = H_a^a(z_{a0}, \dot{y}_{a0}), \tag{2.45}$$

where z_{a1} and $\dot{y}_{a1}$ correspond to height and velocity at the resulting apex state. Again, the full apex to apex return map function is defined in terms of the parameter θ_{td}. Hence, one can design controllers by adjusting θ_{td} to regulate the outputs of H_a^a. The importance of H_a^a for our analysis is indicated in the following fact whose proof is self-evident and omitted.

Remark 1. *The apex to apex return map, H_a^a, is important in studying the possible running gait patterns of the SLIP dynamics as well as stability of such gaits. A gait is periodic if and only if it is a fixed point of H_a^a. Similarly, a gait is a stable periodic gait if and only if it is a stable fixed point of H_a^a.* ■

2.2.2 Stability of the SLIP Model

To begin our investigations on analyzing the stability of the dissipative SLIP model, we first try to define the set of all fixed-points for this model in our parameter space. Here, fixed-point refers to an apex state that maps to same apex state in a single stride and we compute such fixed points through numerical analysis. Note that this set of fixed points forms a manifold and we will refer to this set as fixed point manifold throughout the thesis. Having obtained the fixed point manifold, we can now check the stability for each point in this set. However, due to the dissipation term in the dissipative SLIP model, obtaining a periodic motion, hence a fixed point, is not possible. Therefore, in this part, we choose the dissipative term to be zero, which corresponds to lossless SLIP model. Then, we obtain the fixed-point manifold of the SLIP model. The resulting fixed-points are illustrated in Figure 2.4, where the necessary control input, touchdown leg angle, to generate a fixed-point for the given initial conditions can be observed. Using this manifold, one can design stabilizing controllers for the SLIP model

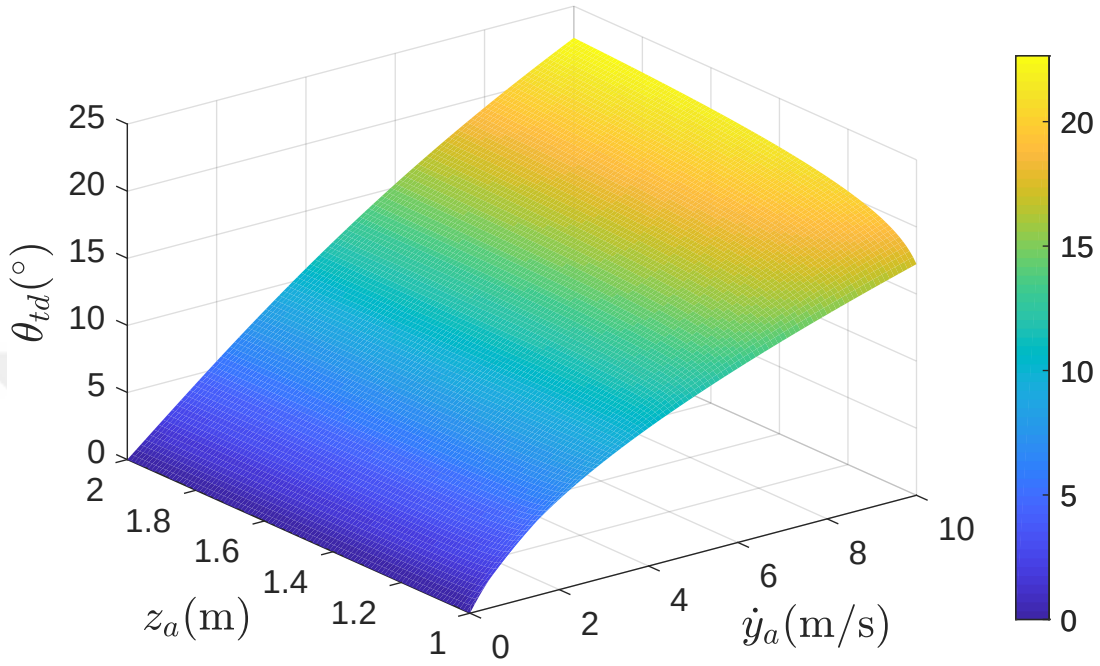

Figure 2.4: Touchdown angles that result periodic gaits for the SLIP model.

to obtain a periodic locomotion. The parameters used for the SLIP model in this section for the fixed-point and stability analysis is given in Table 2.3. Note that these parameters except the leg stiffness are chosen in accordance with [51]. The leg stiffness is greater the typical biological stiffness range [89]. However, the parameters used in the simulations of the following chapters comply with [51, 89].

Unfortunately, obtaining a fixed-point manifold would not be sufficient without considering the stability of the resulting fixed-points. Since there will be disturbances and parametric uncertainties during SLIP locomotion, we need to

Table 2.3: SLIP model parameters used in fixed-point and stability analysis

SLIP Model Parameters	
Body mass, m	$80kg$
Gravitational acceleration, g	$9.81m/s^2$
Leg rest length, r_0	$1m$
Leg compression rate, k	$80kN/m$
Apex vertical position, z_a	$[1-2]m$
Apex horizontal speed, $\dot{y}_a$	$[0-10]m/s$

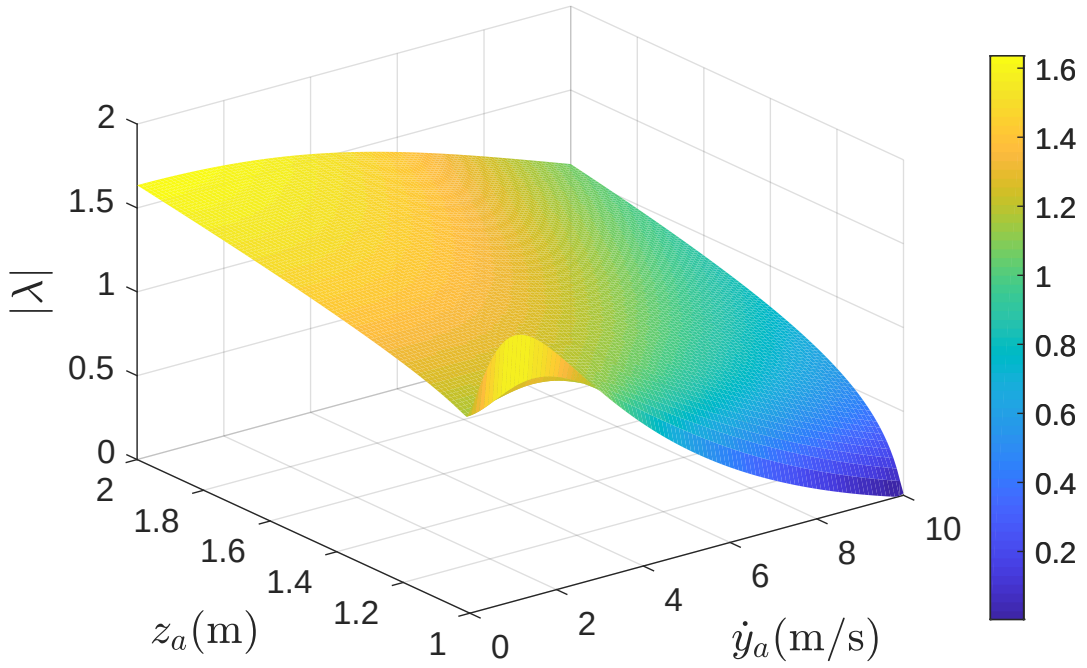

Figure 2.5: Absolute value of the related eigenvalue of the Jacobian matrix of the periodic gaits for SLIP model.

characterize the stability regions of the fixed-points. Therefore, we performed a stability analysis of the fixed-points in the fixed-point manifold represented in Figure 2.4.

In order to perform a stability analysis, we first computed the eigenvalues of the numerical Jacobian matrix of the system. Note that, since the system is time invariant and the motion is periodic, one of the eigenvalues of the Jacobian matrix is always 1, see [90]. Therefore, to determine the stability, one has to consider the remaining eigenvalues of the Jacobian matrix. Hence, the periodic gait is asymptotically stable if these remaining eigenvalues are inside the unit circle of the complex plane. Figure 2.5 illustrates the absolute value of the other eigenvalues of the system.

Stable and unstable regions are also shown in Figure 2.6. Green colored (horizontally-dashed) and blue colored (vertically-dashed) regions represent stable and unstable regions, respectively.

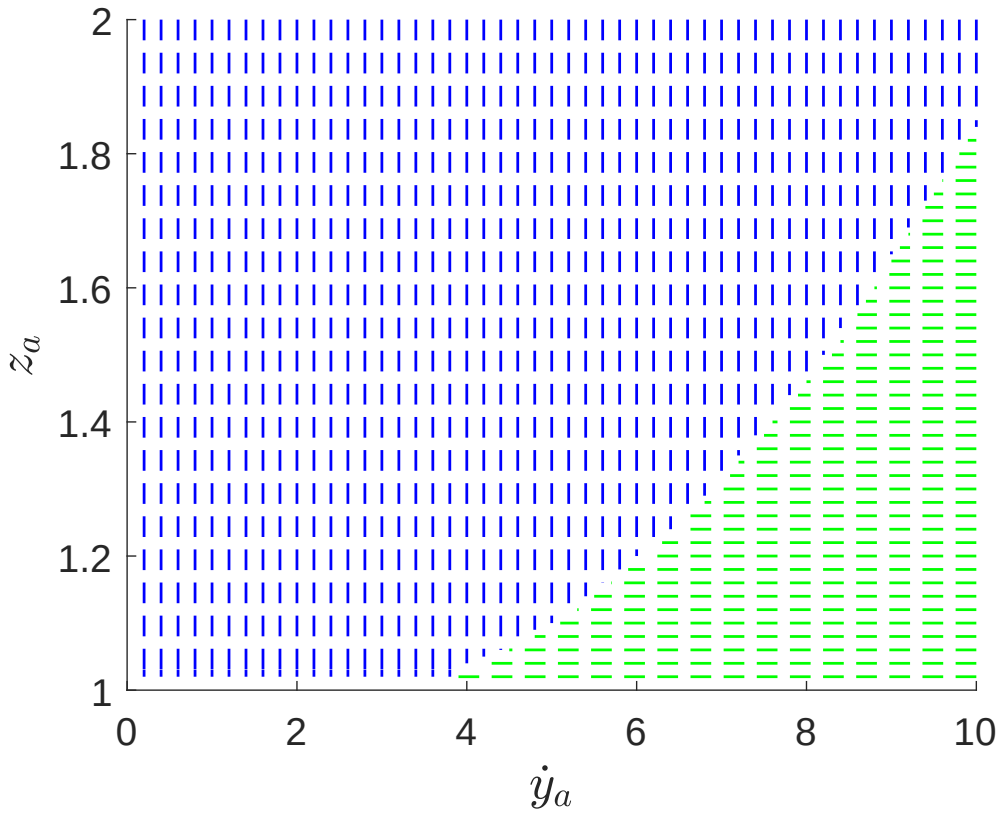

Figure 2.6: Stability region of the SLIP model. Blue (vertically-dashed) region illustrates the unstable gaits whereas green (horizontally-dashed) region illustrates the stable region for the SLIP model.

2.2.3 Stability of Approximate Analytic solution of Geyer et al.

After obtaining a fixed-point manifold for the dissipative SLIP model and performing a stability analysis for the resulting fixed-points, we started to work on approximate analytical solutions for the SLIP model in order to make a comparison. Different than previous section, this time we will use the approximate analytic solutions of [51] to obtain a fixed-point manifold for the SLIP model instead of numerically integrating the nonlinear system dynamics. Our goal is to observe the differences that may result in fixed-point and stability analysis between the actual system dynamics and analytical approximations.

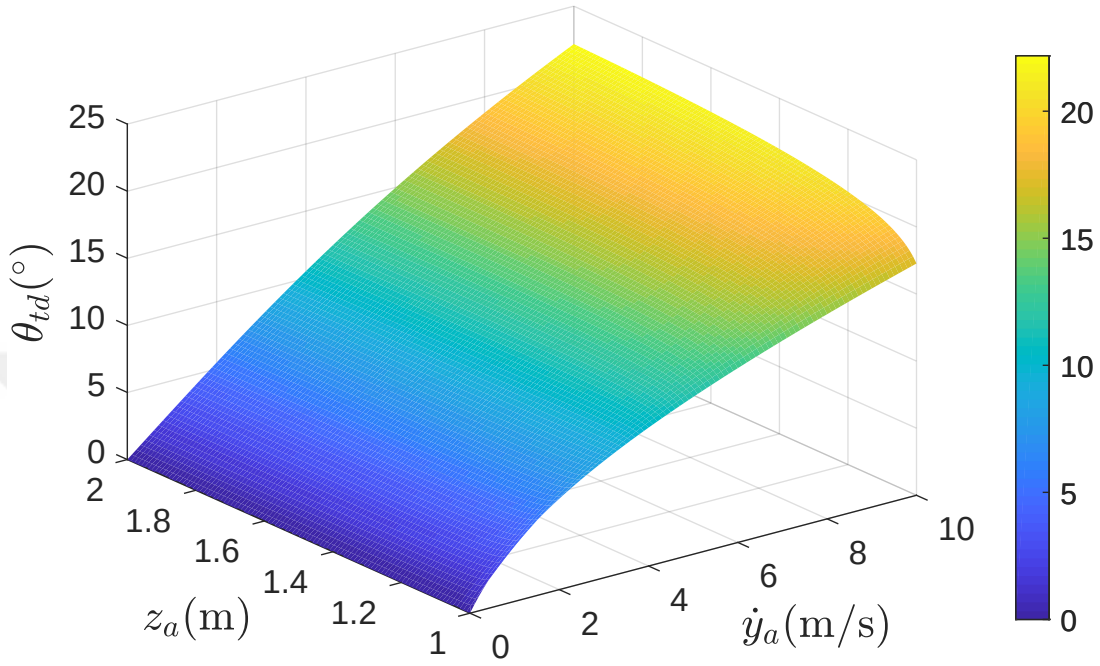

Figure 2.7: Touchdown angles that result periodic gaits for the approximate analytic solution of SLIP model.

In order to make a fair comparison, we used the same parameters as in the previous section and performed a fixed-point analysis for the SLIP model by using analytical approximate solutions given in (2.24)–(2.27). Our goal is again to find the control inputs, touchdown angle for the SLIP case, which result in periodic gaits for the SLIP model. Figure 2.7 illustrates the fixed-point manifold for the analytic approximate solutions.

Our goal is to evaluate the performance of the approximate analytical solutions to the SLIP dynamics in the sense of fixed-points. Therefore, we decided to compare the resulting control input, touchdown angle, to obtain a fixed-point for the same initial conditions. We derived the percentage error of the touchdown angles obtained through approximate solutions with respect to ground truth touchdown angles that are obtained via actual dynamics. Mathematically, this error function can be defined as

$$PE_{\hat{\theta}_{td}} = 100\frac{|\hat{\theta}_{td} - \theta_{td}|}{\theta_{td}} \tag{2.46}$$

where θ_{td} is the ground truth solution obtained via numerically solving the system

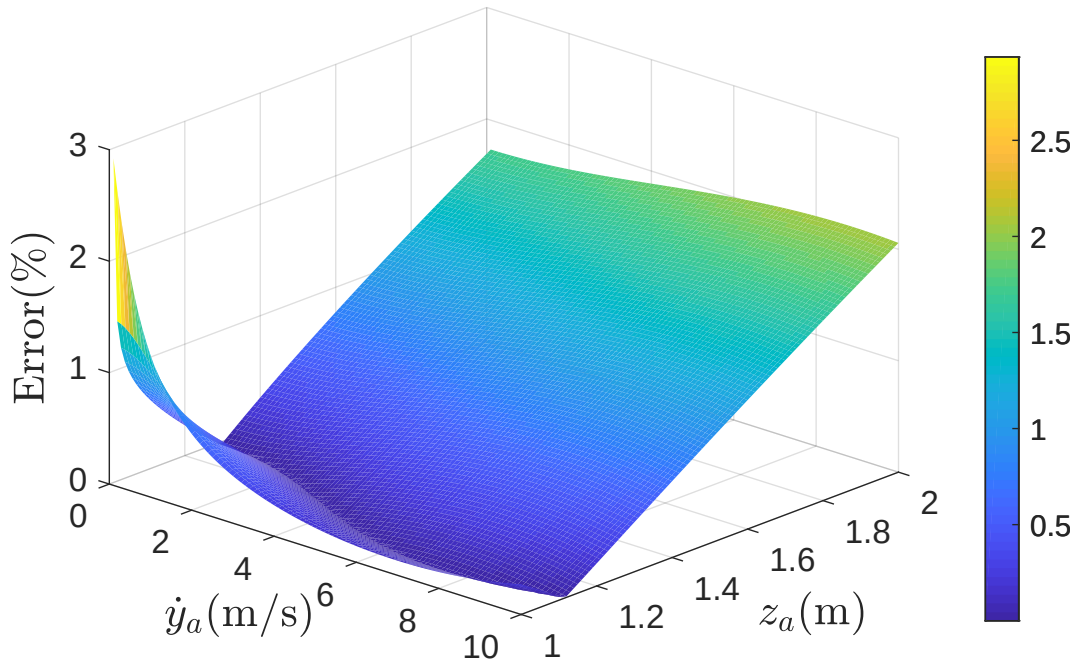

Figure 2.8: Percentage error of the touchdown angles that result periodic gaits obtained by using approximate analytic solution of SLIP model.

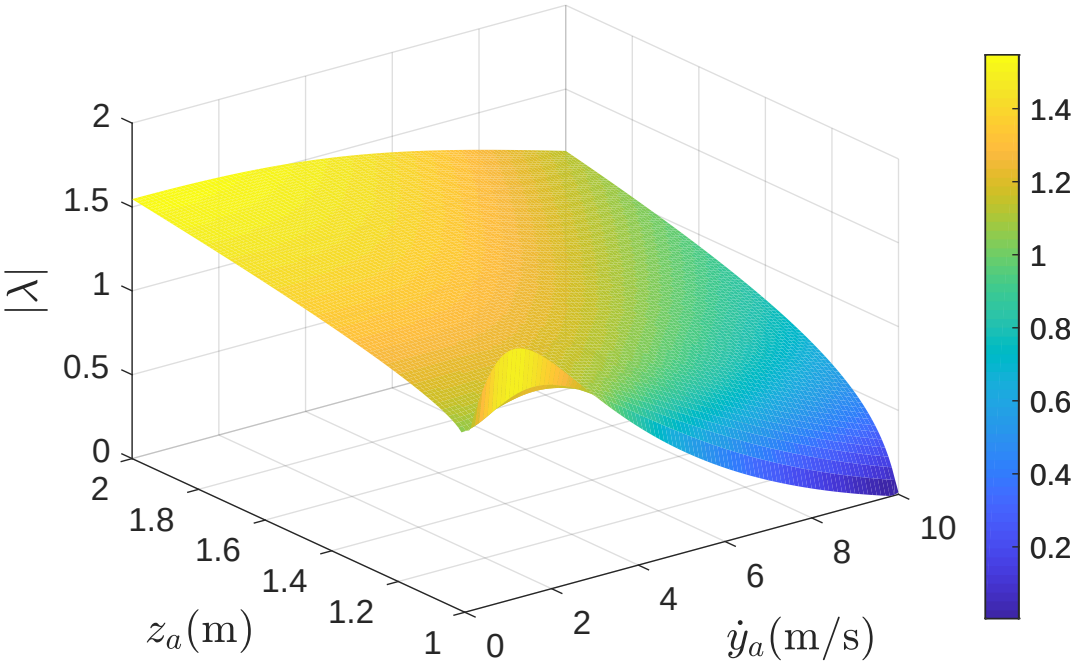

Figure 2.9: Absolute value of the related eigenvalue of the Jacobian matrix of the periodic gaits for the approximate analytic solution of SLIP model.

dynamics and $\hat{\theta}_{td}$ is predicted touchdown angles using the approximate analytical solution of [51]. Figure 2.8 shows the percentage control input error with respect to initial conditions. Note that touchdown angle prediction errors stay well below %3 yielding successful description of the control parameters.

Finally, we performed a stability analysis for the SLIP model by using analytic approximate solutions. We again computed the eigenvalues of the numeric Jacobian. Similarly, one of these eigenvalues is again on the unit circle. Figure 2.9 illustrates the other eigenvalues of the system.

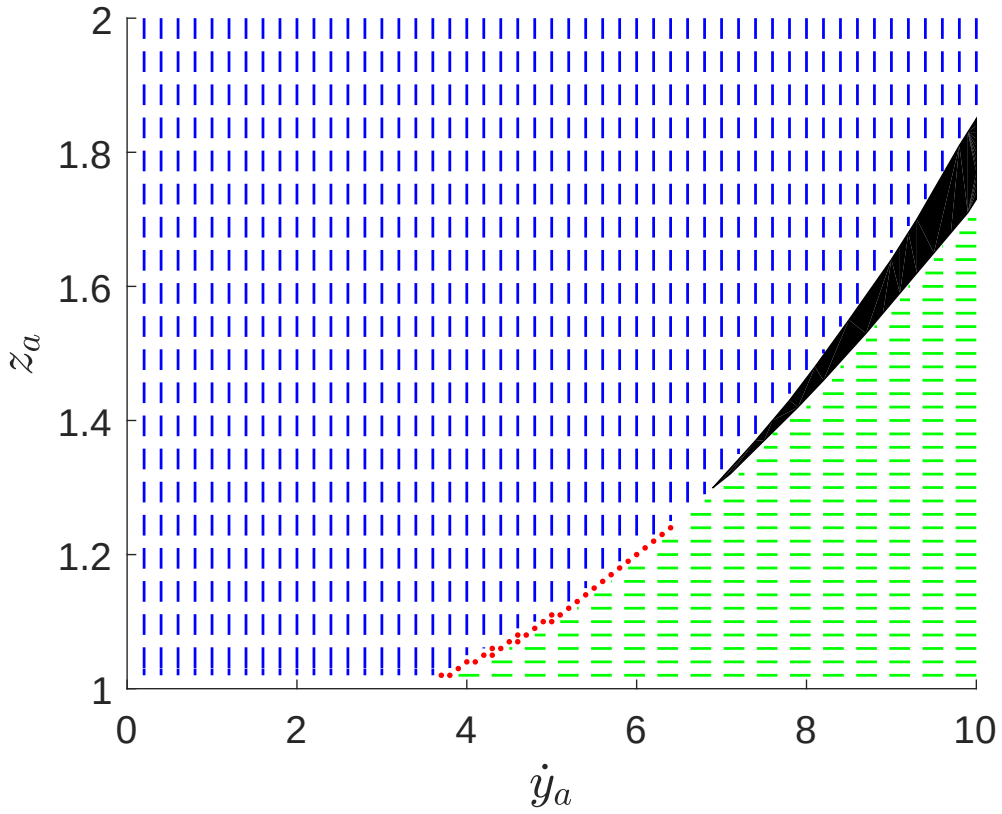

Figure 2.10: Stability region of the approximate analytical solution of SLIP model. Blue (vertically-dashed) region and green (horizontally-dashed) region correctly classified as unstable and stable fixed-points, respectively. However, black (shaded) and red (dotted) regions are falsely classified as unstable and stable, respectively.

Stable and unstable regions are also shown in Figure 2.10. Blue and red regions represent stable and unstable regions, respectively. These are the regions where the approximate solution complies with the ground truth solution, which can be obtained by numerical solution of the system dynamics. However, there are some small regions in the boundary of the stable and unstable regions, where approximate analytical solution yields incorrect results with the actual dynamics. The approximate solution is successful as classifying blue (vertically-dashed) region and green (horizontally-dashed) region as unstable and stable, respectively. However, black (shaded) and red (dotted) regions are falsely classified as unstable and stable, respectively. Falsely classified regions should be handled with care when designing controllers with the approximate analytical solution.

2.2.4 Stability of Gravity Correction of Arslan et al.

In this part, we seek to analyze the stability characteristics of the gravity correction method proposed in [52]. Note that for the lossless SLIP model, the fixed-points that we are using for analyzing stability of a gait results in always symmetric trajectories. This point is also observed and analytically justified in [91]. This is valid for both the numerical solutions as well as approximate analytical solutions.

The main contribution of [52] is to adjust angular momentum for non-symmetric gaits to increase the region of validity of [51]. Thus, for symmetric gaits, we expect no difference between [51] and [52] at all. This also means that their fixed point stability analysis should be very similar.

Let the superscripts G and A represent the approximation model of Geyer et al. [51] and Arslan et al. [52], respectively. One of the eigenvalues of the Jacobian matrix of the fixed point gaits equal to 1 for both models, since the motion is time invariant and periodic, see [90]. Let λ^G and λ^A represent other eigenvalues for the approximation model of Geyer et al. [51] and Arslan et al. [52], respectively. Then, the percentage change $\Delta|\lambda|$ of the eigenvalues of the Jacobian matrix of

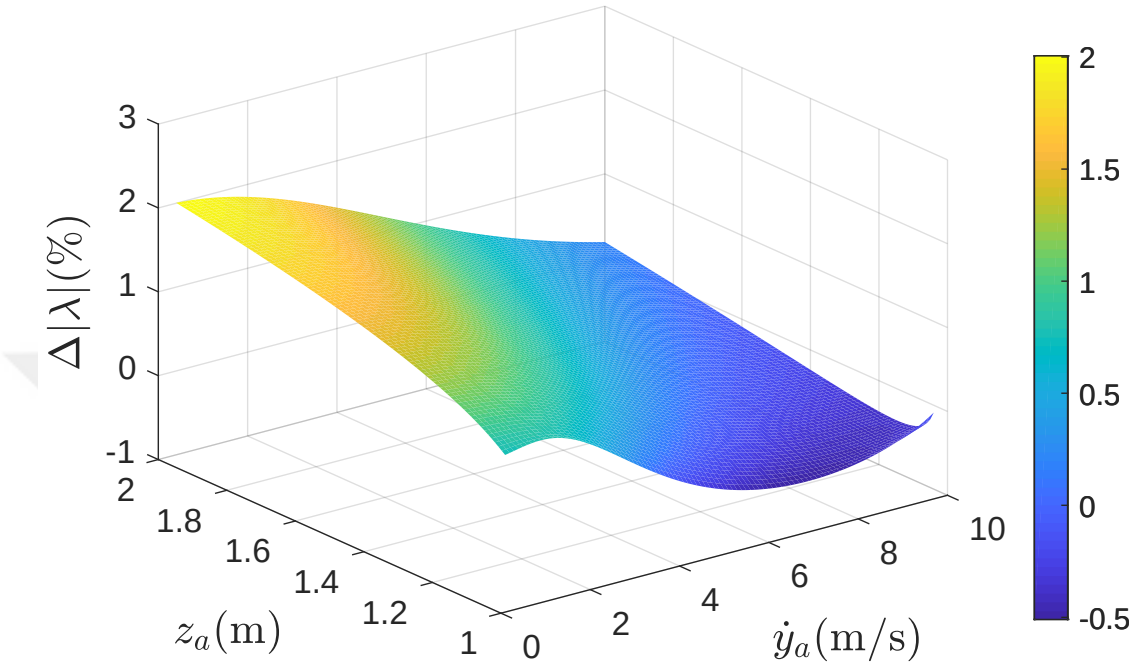

Figure 2.11: Percentage difference between the eigenvalues of Geyer et al. and Arslan et al.

the fixed point gait is defined as

$$\Delta|\lambda| = 100\frac{|\lambda^A| - |\lambda^G|}{|\lambda^G|}. \tag{2.47}$$

and is illustrated in Figure 2.11. The simulation results prove that there is a negligible difference between the eigenvalues of the two models. A key comment that needs to be noted here is that [51] reports stable when [52] is stable and vice versa (at least for the resolution of initial conditions we used in our simulations). The only difference we observed is that, $|\lambda^A| > |\lambda^G|$ for the unstable region (see blue (vertically-dashed) and black (shaded) regions in Figure 2.10) and $|\lambda^A| < |\lambda^G|$ for the stable region (see green (horizontally-dashed) and red (dotted) regions in Figure 2.10). The simulation results show that [52] actually does not have a considerable effect on the stability characteristics of the fixed points, since for the lossless model fixed-points are always symmetric.

Chapter 3

Multi-Actuated Dissipative SLIP (MD-SLIP) Model

There is a large variety of SLIP-based mathematical models to represent legged locomotion. However, as shown in Chapter 2, there is a non-negligible unstable region on the stability diagrams of the SLIP models. Motivated by this problem, we seek to obtain a novel legged locomotion model that considers both a linear actuator to compress the leg spring and a radial actuator to inject torque inputs. One of the main advantage of such an actuator-enhanced model is that we obtain a relatively large stability region, which increases the mobility and robustness of the legged locomotion model. Besides, this multi-actuated model allows enforcing desired trajectories by the use of partial feedback linearization. The following sections in this chapter introduces the Multi-Actuated Dissipative SLIP (MD-SLIP) model and our extensive simulation studies on assessing stability and robustness characterising of the proposed model under different scenarios.

3.1 Multi-Actuated Dissipative SLIP Model

3.1.1 Model and Dynamics

The proposed model differs from the original SLIP template by the addition of two actuators as stated earlier. These actuators help us to use partial feedback linearization methods to obtain analytic solutions to the stance dynamics. The first actuator is a linear motor that is attached serially to the leg spring. The second actuator on the other hand is a rotary actuator that is attached to the point mass at the hip to apply the rotational torque τ. This model is called as multi-actuated dissipative SLIP template and can be seen in Figure 3.1, where the coordinate system, model parameters and the additional actuators are also illustrated. Note that although the SLIP template (and hence our proposed model) can be used to represent center of mass trajectories of different animals with varying number of legs (see Section 1.1), the SLIP model itself (and hence our proposed model) corresponds to a one-legged hopping robot when simulated in computerized environments.

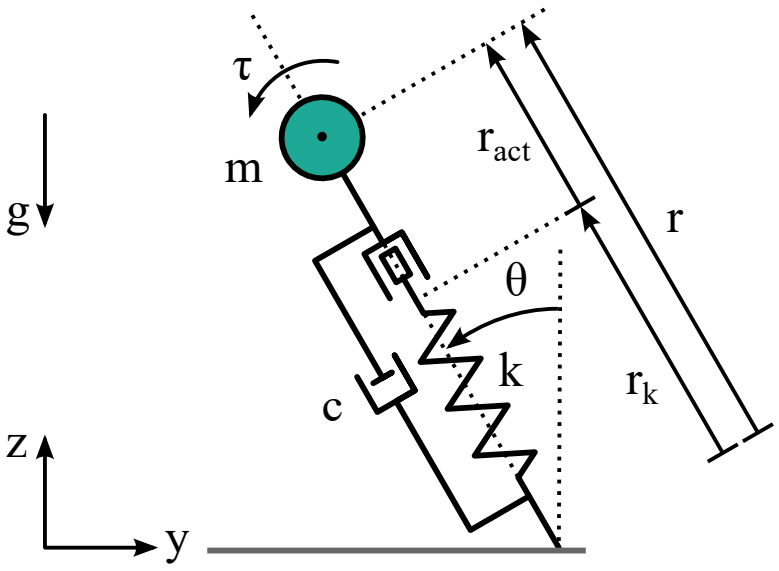

Figure 3.1: Multi-actuated dissipative SLIP model, coordinate system and model parameters. The difference of this model with the dissipative SLIP model (illustrated in Figure 2.1) is the addition of the linear and the rotary actuators.

Note that our additional actuators do not violate or change the assumptions on the original SLIP model such as point mass, massless leg, etc. Therefore, point mass still follows a ballistic trajectory during the flight phase, so the equations of motion will be the same as in (2.1). However, addition of two new actuators changes the stance dynamics, since now we are capable of injecting and removing energy from the system. Therefore, the modified stance dynamics for the multi-actuated dissipative SLIP (MD-SLIP) model can be given as

$$\ddot{r} = r\dot{\theta}^2 + k\left(1 - r + \Delta r_{act}\right) - \cos\theta - c\dot{r}, \tag{3.1}$$

$$\ddot{\theta} = \frac{1}{r}\left(\sin\theta - 2\dot{r}\dot{\theta}\right) + \frac{\tau}{r^2}, \tag{3.2}$$

where Δr_{act} and τ represent the linear actuator displacement and the rotary actuator torque, respectively. The linear actuator displacement is defined as $\Delta r_{act} := r_{act} - r_{act,0}$, where $r_{act,0}$ is the rest length of the linear actuator.

We note that, all time-dependent functions in Section 3.1 use touchdown time as reference for the sake of simplicity.

3.1.2 Solving Stance Dynamics

As mentioned before, the stance dynamics of the SLIP model does not have exact analytical solution due to its highly nonlinear and non-integrable nature. This problem may become more complex if Δr_{act} and τ in (3.1)-(3.2) are not chosen appropriately. In this part, we explain how we can obtain exact analytical solutions to the stance dynamics of the MD-SLIP model by canceling some nonlinear terms in the system dynamics. We show that the equations (3.1) and (3.2) can be solved when partial feedback linearization is used to cancel out some nonlinear terms. Besides, partial feedback linearization can also be used to enforce specific solutions to the equations (3.1) and (3.2) such as specifying some desired trajectories to the point mass during its stance locomotion.

To cancel some of the nonlinear terms in the equation (3.1), linear actuator

displacement is chosen as

$$\Delta r_{act} = \frac{1}{k}(\cos\theta - r\dot{\theta}^2 + c\dot{r}) - A_0 + C_0 t, \tag{3.3}$$

where A_0 can be used to adjust the initial value and C_0 can be used as an additional control parameter.

At touchdown instant, a force is applied to the point mass in order to compensate the losses due to leg damping. To achieve this, Δr_{act} is chosen as $c\dot{r}_{td}/k$ at touchdown instant. Using this idea and evaluating (3.3) at touchdown instant, we obtain:

$$A_0 = \frac{\cos\theta_{td} - r_{td}\dot{\theta}_{td}^2}{k}. \tag{3.4}$$

Substituting (3.3) in (3.1) results in

$$\ddot{r} + kr = k(1 - A_0 + C_0 t). \tag{3.5}$$

The solution of (3.5) can be obtained as

$$r(t) = A_1 \sin(\omega t) + A_2 \cos(\omega t) + 1 - A_0 + C_0 t \tag{3.6}$$

where $w = \sqrt{k}$.

At this point, if we compare the exact analytical solution given by (3.6) with the approximate analytical solution of original SLIP dynamics given by (2.16), we observe that they have quite similar structure when $C_0 = 0$. Hence, although the control law given by (3.3) seems quite nonintuitive, the resulting behaviour is actually quite close to the natural behaviour of original SLIP dynamics. We also note that, although (2.16) represents an approximate solution of (2.5), (3.6) is an exact solution of (3.1).

Applying the boundary condition at touchdown instance, i.e. the leg length should be equal to the leg rest length, A_2 can be found as $A_2 = A_0$.

In order to find the A_1, the radial velocity

$$\dot{r}(t) = A_1\omega\cos(\omega t) - A_0\omega\sin(\omega t) + C_0, \tag{3.7}$$

should be equal to its touchdown value at touchdown instant, which results in

$$A_1 = \frac{\dot{r}_{td} - C_0}{\omega}. \tag{3.8}$$

As a result, the leg length during stance phase can be found as

$$r(t) = 1 - A_0 + A_0 \cos(\omega t) + A_1 \sin(\omega t) + C_0 t, \tag{3.9}$$

where A_0 and A_1 are given by (3.4) and (3.8), respectively.

For the angular velocity equation (3.2), we propose an approach similar to the one utilized in [62]. By adding an additional control parameter C_1, similar to (2.39), we propose the following desired angular velocity equation

$$\dot{\theta} = B_0 \cos(\theta + C_1) + B_1. \tag{3.10}$$

The required torque to enforce (3.10) can be found from (3.2) as

$$\tau = 2r\dot{r}\dot{\theta} - r\sin\theta - B_0 r^2 \sin(\theta + C_1)\dot{\theta}. \tag{3.11}$$

In order to avoid sudden jumps in torque, we chose to apply $\tau = 0$ at touchdown instance. Using this decision in (3.11), we obtain

$$B_0 = \frac{2\dot{r}_{td}\dot{\theta}_{td} - \sin\theta_{td}}{\sin(\theta_{td} + C_1)\dot{\theta}_{td}}. \tag{3.12}$$

Furthermore, by evaluating (3.10) at touchdown instance we obtain

$$B_1 = \dot{\theta}_{td} - B_0 \cos(\theta_{td} + C_1). \tag{3.13}$$

Solving the angular velocity equation (3.10) for the angular position results in

$$\theta(t) = \frac{\pi}{2} - C_1 + 2\text{atan}\left(\frac{B_0 - B_2 \tanh\left(\frac{B_2 t}{2} + B_3\right)}{B_1}\right), \tag{3.14}$$

where B_2 and B_3 are defined as

$$B_2 := \sqrt{B_0^2 - B_1^2}, \tag{3.15}$$

$$B_3 := \operatorname{atanh}\left(\frac{B_0 - B_1 \tan\left(\frac{\theta_{td}+C_1-\frac{\pi}{2}}{2}\right)}{B_2}\right). \tag{3.16}$$

After some lengthy but straightforward calculations, we obtain the following equation for the angular position

$$\theta(t) = \theta_{td} + 2\operatorname{acot}\left(\frac{B_2\dot{\theta}_{td}\coth\left(\frac{B_2 t}{2}\right) + 2\dot{r}_{td}\dot{\theta}_{td} - \sin\theta_{td}}{\dot{\theta}_{td}^2}\right). \tag{3.17}$$

To summarize, if we choose the linear actuator control law as in (3.3), the solution of the radial dynamics given by (3.1) can be obtained as (3.9), where A_0 and A_1 are constants that are obtained as (3.4) and (3.8), respectively, and C_0 is a free control parameter. Likewise, if we use the torque control law as in (3.11), the solution of the angular dynamics given by (3.2) can be obtained as (3.17), where B_0, B_1 and B_2 are constants as given by (3.12), (3.13) and (3.15), respectively, and C_1 is a free control parameter.

Note that stance trajectories generated by (3.9) and (3.17) are not arbitrary functions enforced by partial feedback linearization. Actually, these trajectories are well-fitted locomotion trajectories similar to the ones generated by the SLIP model. A sample stance trajectory can be seen in Figure 3.20.

Remark 2. *We note that both the solutions given by (3.9) and (3.17) depend on the touchdown positions and velocities. Since the flight phase dynamics are integrable, these values can be obtained at the end of the flight phase, then (3.9) and (3.17) could be used as the solutions of stance phase dynamics. Moreover, these formulas contain the free control parameters C_0 and C_1 explicitly, hence by choosing these parameters appropriately, one may achieve various control objectives.* ■

3.1.3 Apex to Apex Return Map

In order to understand and analyze the MD-SLIP model in detail, its locomotion needs to be divided into sub-phases that consecutively repeat themselves. Note that, similar derivations for the original SLIP model have been given in Section 2.2.1. For the sake of completeness, we make similar derivations for the MD-SLIP model in the sequel. In this thesis, we choose the starting phase as the apex instance and use the apex to apex return map to represent the locomotion. The states at the current apex point are chosen as the apex height z_{a0} and apex velocity $\dot{y}_{a0}$. When the locomotion starts from the apex state, it follows the ballistic trajectory (2.1) until the toe touches to the ground. It means, the touchdown event occurs when the equation $z = \cos\theta_{td}$ is satisfied. Hence the state variables of the descent subphase and their relations can be written as

$$(\dot{z}_{td}, \dot{y}_{td}) = F_a^{td}(z_{a0}, \dot{y}_{a0}), \tag{3.18}$$

where the subscript td indicates the touchdown, F_a^{td} is the apex to touchdown map, the velocities $\dot{z}_{td}$ and $\dot{y}_{td}$ are vertical and horizontal velocities in Cartesian coordinates at touchdown instance, respectively. Note that the map F_a^{td} depends on θ_{td} which is considered as a control parameter. The latter approach is utilized in various control schemes proposed for SLIP dynamics, see e.g. [1, 49, 50].

After the toe touches the ground, the point mass starts to follow the stance dynamics (3.1) and (3.2) which are solved as (3.9) and (3.17). The function for the stance phase can be written as

$$(r_{lo}, \dot{r}_{lo}, \theta_{lo}, \dot{\theta}_{lo}) = F_{td}^{lo}(\dot{r}_{td}, \dot{\theta}_{td}), \tag{3.19}$$

where the subscript lo indicates the liftoff and F_{td}^{lo} is the touchdown to liftoff map. Note that the map F_{td}^{lo} depends on the control parameters θ_{td}, C_0 and C_1, see (3.9) and (3.17).

The liftoff event occurs, when the toe loses ground contact. After this instance the point mass follows the ballistic trajectory (2.1) again until its vertical velocity becomes zero at the apex. The ascent subphase can be represented as

$$(z_{a1}, \dot{y}_{a1}) = F_{lo}^{a}(\dot{z}_{td}, \dot{y}_{td}, r_{lo}, \theta_{lo}), \tag{3.20}$$

where F_{lo}^{a} is the liftoff to apex map.

After describing the trajectory from current apex state to the next one, apex to apex function can be written as

$$F_{a}^{a} = F_{lo}^{a} \circ R_{lo} \circ F_{td}^{lo} \circ R_{td} \circ F_{a}^{td}, \tag{3.21}$$

where F_{a}^{a} represents apex to apex return map. Note that R_{td} and R_{lo} stands for the coordinate transformations between Cartesian and polar coordinates. These transformations are required since we use polar coordinates for our stance phase (radial) solutions while the actual map (with descent and ascent phases) are represented in Cartesian coordinates.

Finally, the next apex state can be achieved by using current apex state as

$$(z_{a1}, \dot{y}_{a1}) = F_{a}^{a}(z_{a0}, \dot{y}_{a0}), \tag{3.22}$$

where z_{a1} and $\dot{y}_{a1}$ are the height and the velocity at the next apex point. Note that the map F_{a}^{a} depends on the control parameters θ_{td}, C_0 and C_1. Our aim is now to choose these control parameters appropriately to obtain stable gait patterns.

Remark 3. *The apex to apex return map, F_{a}^{a}, is important in studying the possible running gait patterns of the SLIP dynamics as well as stability of such gaits. For example, any periodic gait is a fixed point of F_{a}^{a}, and any stable gait is a stable fixed point of F_{a}^{a}.* ■

3.1.4 Finding Stance Duration

To find the stance duration, the liftoff condition needs to be determined. In the dissipative SLIP model, leg spring is constrained such that the maximum length of the leg spring is its rest length. On the other hand, dissipation in the SLIP model can yield some early liftoffs. In addition to these two criteria, we avoid negative work by turning off the torque control to eliminate early liftoff. Hence, the liftoff condition can be given as

$$r = 1 + \Delta r_{act} - \frac{c}{k}\dot{r}, \tag{3.23}$$

where Δr_{act} is given by (3.3). Due to the highly nonlinear expressions of the latter, finding an analytical expression for the solution of (3.23) is very difficult. However, the numeric calculation is still a way to find the stance duration.

Under the symmetric stance trajectory assumption, we can find exact solution for the stance duration. To have symmetric stance trajectory, leg length and leg angle need to be even and odd symmetric around the time halfway through the stance phase, respectively [1]. To satisfy these requirements, three conditions need to be met. First, leg length needs to be even symmetric around bottom event, which is possible by choosing $C_0 = 0$. Second, leg angle needs to be odd symmetric, which requires $C_1 = 0$. Third, at bottom time leg angle should be zero. As a result a symmetric gait is formed by choosing control parameters C_0 and C_1 as zero and adjusting θ_{td} to tune the bottom time

$$t_b = \frac{1}{w}\left(\pi - \operatorname{acos}\left(\frac{A_0}{\sqrt{A_0^2 + A_1^2}}\right)\right) \tag{3.24}$$

and the time required to make θ equals to zero

$$t_{\theta=0} = \frac{2}{B_2}\operatorname{acoth}\left(\frac{\sin\theta_{td} - \dot{\theta}_{td}^2\cot(\frac{\theta_{td}}{2}) - 2\dot{r}_{td}\dot{\theta}_{td}}{B_2\dot{\theta}_{td}}\right) \tag{3.25}$$

equal. Then, the stance duration can be calculated as

$$t_s = 2t_b = 2t_{\theta=0}. \tag{3.26}$$

3.2 Periodic Gaits and Their Stability in MD-SLIP Model

As stated in Remark 3, the periodic gaits of the proposed MD-SLIP model are the fixed points of the apex to apex map F_a^a given by (3.21). This fixed point, $(z_a^*, \dot{y}_a^*)$, satisfies the following equation

$$(z_a^*, \dot{y}_a^*) = F_a^a(z_a^*, \dot{y}_a^*). \tag{3.27}$$

The stability of such fixed points can be determined by the eigenvalues of the Jacobian matrix of F_a^a evaluated at the fixed point. The Jacobian matrix is defined for the apex to apex return map as

$$J := \begin{bmatrix} \dfrac{\partial z_{a1}}{\partial z_{a0}} & \dfrac{\partial z_{a1}}{\partial \dot{y}_{a0}} \\ \dfrac{\partial \dot{y}_{a1}}{\partial z_{a0}} & \dfrac{\partial \dot{y}_{a1}}{\partial \dot{y}_{a0}} \end{bmatrix}. \tag{3.28}$$

However, we do not have exact solution of the stance duration for all cases, where numeric calculation might be necessary. In such cases, the Jacobian matrix is approximated in numerical simulations as

$$J_n := \begin{bmatrix} \dfrac{z_{a1z} - z_{a1}}{\Delta z_{a0}} & \dfrac{z_{a1y} - z_{a1}}{\Delta \dot{y}_{a0}} \\ \dfrac{\dot{y}_{a1z} - \dot{y}_{a1}}{\Delta z_{a0}} & \dfrac{\dot{y}_{a1y} - \dot{y}_{a1}}{\Delta \dot{y}_{a0}} \end{bmatrix}, \tag{3.29}$$

where the values for Δz_{a0} and $\Delta \dot{y}_{a0}$ have been chosen as sufficiently small values to approximate the numerical derivatives. After some extensive simulations, we experimentally choose this number as 10^{-5}, since further decrease apparently does not have a meaningful change on the eigenvalues of the Jacobian. The other variables are defined as

$$(z_{a1}, \dot{y}_{a1}) := F_a^a(z_{a0}, \dot{y}_{a0}), \tag{3.30}$$

$$(z_{a1z}, \dot{y}_{a1z}) := F_a^a(z_{a0} + \Delta z_{a0}, \dot{y}_{a0}), \tag{3.31}$$

$$(z_{a1y}, \dot{y}_{a1y}) := F_a^a(z_{a0}, \dot{y}_{a0} + \Delta \dot{y}_{a0}). \tag{3.32}$$

During simulations the non-dimensional parameters and initial conditions are chosen as $z_a \in [1 - 2]$, $\dot{y}_a \in [0 - 3.2]$ and $k \in [15 - 100]$.

3.2.1 Zero Control Parameters C_0 and C_1

The goal of this section is to investigate the stability of the periodic motion for the proposed MD-SLIP model when the gaits are symmetric.

Note that symmetric gaits are obtained by choosing the control parameters C_0 and C_1 as zero leaving us the leg touchdown angle, θ_{td}, as the only control parameter to regulate the gait. In order to begin stability analysis, fixed points of the corresponding Poincaré map should be extracted. To accomplish this, we first find the touchdown angle, θ_{td} that yields same solutions for (3.24) and (3.25) to obtain the fixed point manifold. At this point, we use numeric calculations to solve $t_b = t_{\theta=0}$ in order to find the fixed point manifold since obtaining an analytic solution is very difficult for these equations, see (3.24) and (3.25). The significance of this fixed point manifold is that any point chosen inside the fixed point manifold as an initial condition to our MD-SLIP model yields symmetric periodic locomotion. The fixed point manifold of the MD-SLIP model in terms of a function apex height, apex velocity and touchdown angle is illustrated in Figure 3.2. We also present comparative illustration of the touchdown angles of the MD-SLIP model with the SLIP model.

Another important observation about Figure 3.2 is that the touchdown angle θ_{td} that results in periodic motion is more or less proportional to the apex horizontal velocity $\dot{y}_a$. Note that this property is also observed in the original SLIP template and [1] designed touchdown angle controllers to regulate apex horizontal velocity based on this principle. Figure 3.2 shows that our proposed model also exhibits this property, which would allow simple touchdown angle controllers as in [1] to regulate apex horizontal velocity. We note that average steady-state velocity is utilized as a measure to determine the locomotion performance in [5]. By combining this idea with the observation given above, we could state that if we choose apex horizontal velocity as a measure to evaluate the locomotion performance, we could utilize the touchdown angle as a parameter for optimizations. However, since our main aim in this work is to determine the existence

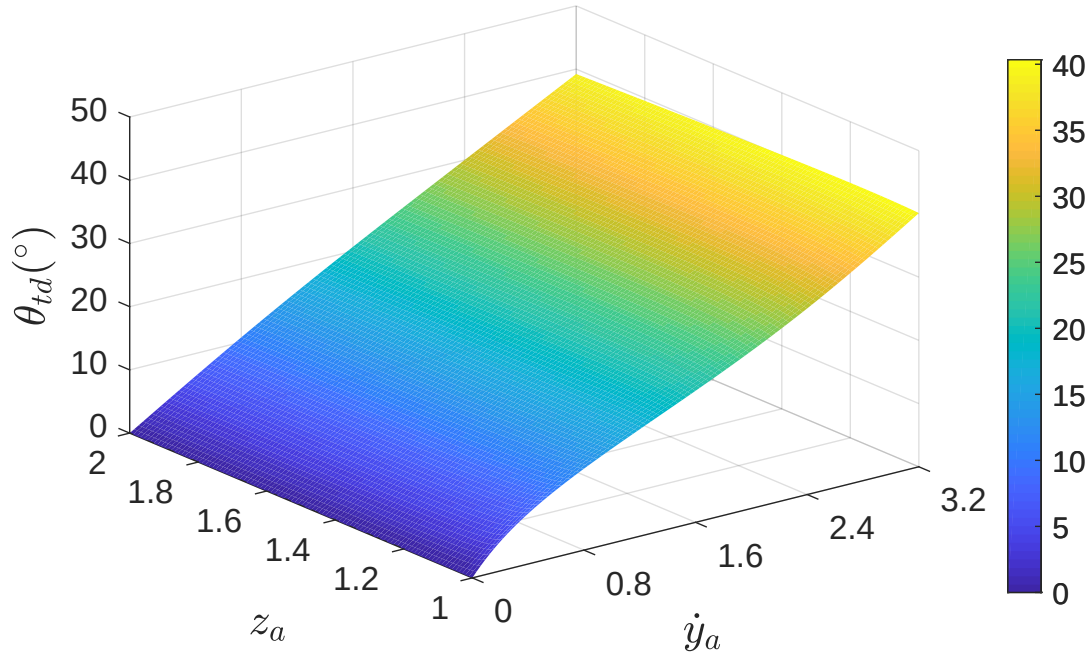

Figure 3.2: Touchdown angles that result symmetric periodic gaits for the MD-SLIP model with control parameters C_0 and C_1 are zero. The dimensionless spring constant k is chosen as 36.

and stability of periodic gaits, we do not elaborate further on this subject which requires and deserves further investigation.

In Figure 3.3, we present a comparative illustration of touchdown leg angle between the MD-SLIP model and the passive SLIP model. Our goal here is to observe the possible similarities and differences between the touchdown leg angles for the two models. As seen in Figure 3.3, for the middle range of initial conditions, the two model utilizes similar touchdown leg angles to obtain fixed points. However, due to the use of active control signals and partial feedback linearization in MD-SLIP model, touchdown leg angles differ on a range of initial conditions, especially when apex horizontal velocity $\dot{y}_a$ is large.

Having zero control parameters assumption, we have analytic solutions to the system dynamics and stance duration and hence we can perform an analytic stability analysis. However, the stance duration is solved only for the symmetric gaits and this analysis requires the general solution for the stance duration. Since

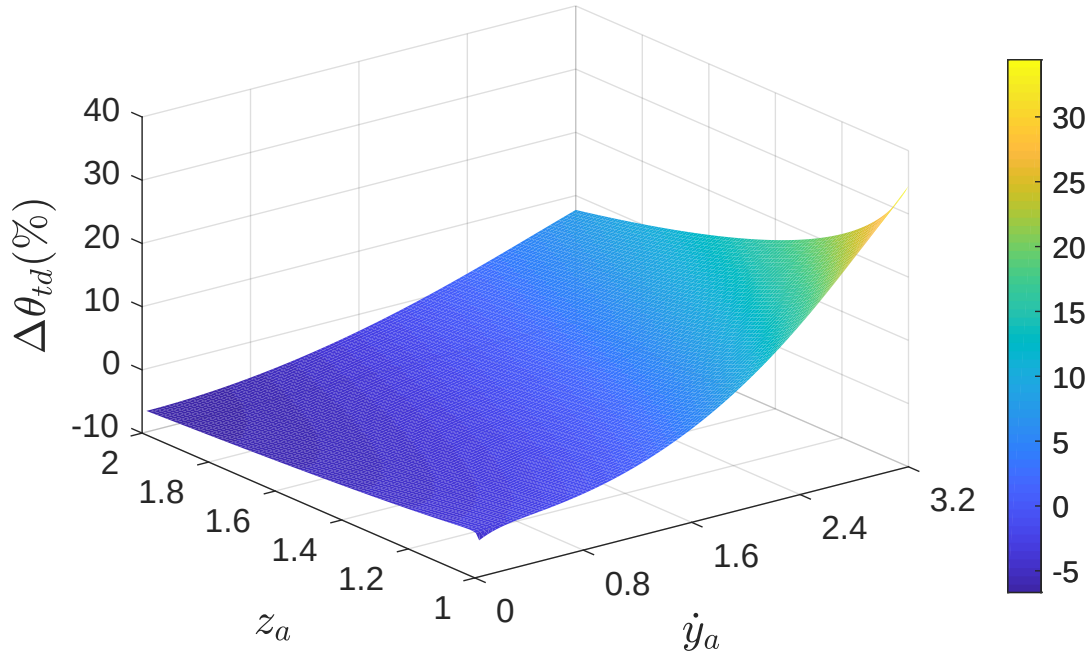

Figure 3.3: The percentage change of the touchdown angles that result periodic gaits for the MD-SLIP model (control parameters C_0 and C_1 are zero) with respect to passive SLIP.

the analysis is performed around the symmetric stance trajectories, we assume that the stance duration equation solved for symmetric gaits can be used in this analysis. Additionally, finding an exact analytic solution for the leg touchdown angle that results in periodic locomotion is very challenging. Therefore, we utilize numeric solution to find leg touchdown angles and plug in these numeric solution into our equations to form the Jacobian matrix. Symbolic Toolbox of the MATLAB is used in all the steps to calculate the eigenvalues for the Jacobian matrix (3.28), because of the complexity of the equations. Since we perform the analysis around the symmetric gaits, magnitude of one of the eigenvalues always results as 1. Therefore, we use the magnitude of the other eigenvalue illustrated in Figure 3.4, to determine the stability of the gaits.

Note that using analytical Jacobian for computing eigenvalues is only valid for symmetric gaits. However, most of the natural gaits generated by animals, and hence our simulation models, correspond to asymmetric trajectories, which requires derivation of numeric Jacobian matrix as in (3.29). In order to validate

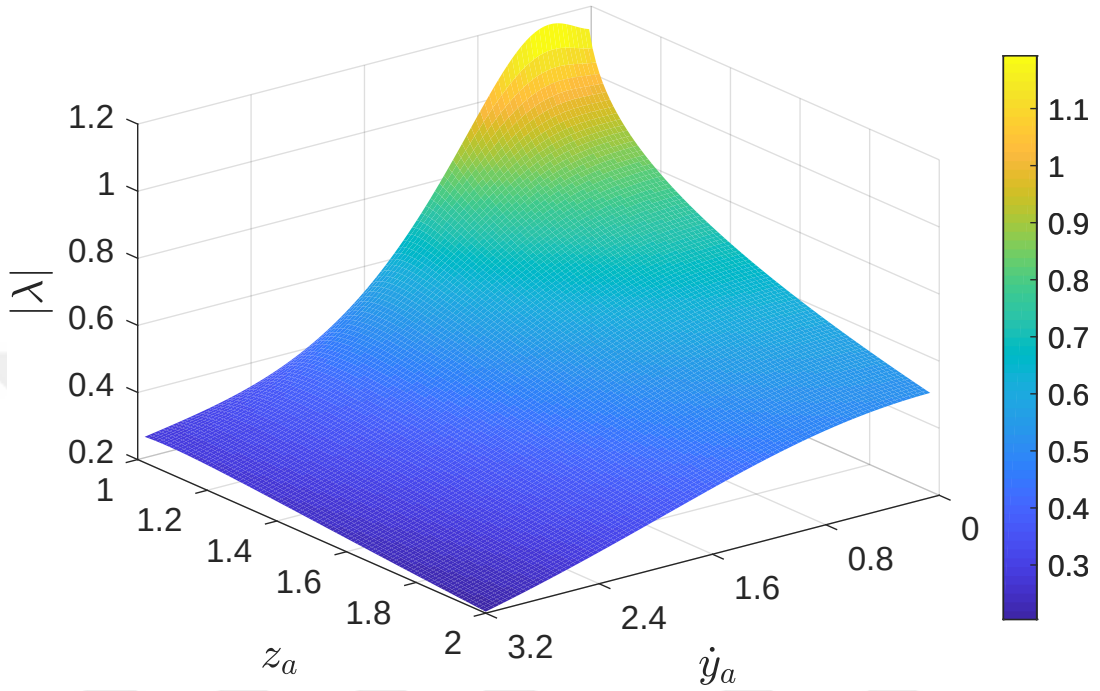

Figure 3.4: Magnitudes of the related eigenvalues of the Jacobian matrix of the periodic gaits for the MD-SLIP model with control parameters C_0 and C_1 are zero.

this approach, we first derived both analytical and numerical Jacobian matrices for the symmetric gait assumption and compared the resulting eigenvalues. Having noticed that the distance between first eigenvalue pair was less than 0.1% (the other eigenvalue pair was equal to 1 in both approaches), we decided to proceed with (3.29) to compute eigenvalues for the non-symmetric gaits.

To compare the stability of the periodic gaits for the MD-SLIP model and the SLIP model, fixed points of the corresponding apex to apex map should be obtained. To find the fixed points of the periodic gaits for the SLIP model, conservation of energy is required. Therefore, we choose the damping constant as zero to find the fixed points of the SLIP model and perform a stability analysis to compare with the MD-SLIP model. In Figure 3.5, stability regions of SLIP model and MD-SLIP model is shown. The SLIP model is only stable in green (horizontally-dashed) region whereas the MD-SLIP model is unstable only in the red (dotted) region, in which the initial states have low speed and height. It is

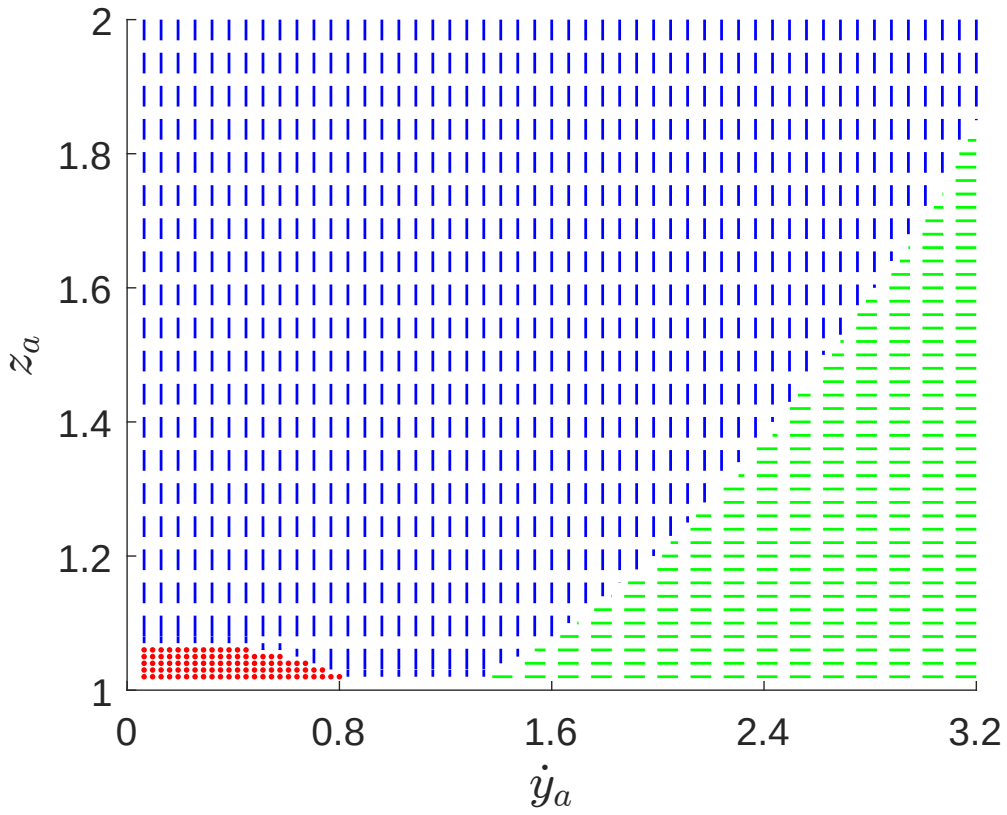

Figure 3.5: A comparison between stability regions of the SLIP and MD-SLIP models. Blue (vertically-dashed) region illustrates the stable gaits of the MD-SLIP model and green (horizontally-dashed) region illustrates the stable region for both SLIP and MD-SLIP models. Finally, the red (dotted) region illustrates the region where both models are unstable. Note that the dimensionless spring constant is chosen as 36 in this analysis.

obvious that MD-SLIP model increases the stable region for the interested region of initial conditions.

Remark 4. *Note that our stability analysis is based on the linearization of nonlinear dynamics around a periodic motion (i.e. limit cycle). As a result of linearization, all of our results are only local, hence stable periodic gait here means an asymptotically (and locally) stable periodic motion, see [92]. There are various ways to measure the stability performance of the periodic gaits considered in this work. An obvious choice would be to characterize or estimate the domain of attraction (DoA) of such a gait, (i.e. the set of all initial apex states from which*

the starting trajectories asymptotically converge to the apex state of the periodic gait). However, finding and/or estimating such a DoA is quite difficult and requires mainly large amount of simulations, see e.g. [92, 93], which is beyond the scope of present work. Another measure is the robustness of such stable gaits against small perturbations, and rough terrain simulations are frequently utilized in literature as a measure of such robustness, [29, 39, 93]. Indeed, our stable gaits are found when SLIP motion is on a flat ground. When the terrain changes, its effect could be considered as a perturbation of apex state and if the resulting motion still converges to the periodic gait in question in rough terrains, this would indicate a sufficiently robust stable gait. Although an exact analytical relation between this type of robustness measure and the size of DoA is not available, we may expect that the better robustness results in rough terrain simulations is an indicator of larger sizes for DoA. This approach will be utilized in Section 3.3, see also [93] for similar stability measures. Another measure for stability performance might be the magnitude of the maximum eigenvalue, see e.g. [93]. Minimization of this quantity as a stability measure will be considered in Section 3.2.2. We note that other measures of stability, as well as estimation of DoA, are subjects which require and deserve further investigations. ■

Since active SLIP model proposed in [62] enforces a symmetric gait for all initial conditions, the Jacobian matrix becomes identity matrix. Hence, the eigenvalues of the Jacobian matrix becomes 1. Therefore, our approach which is based on linearization is inconclusive to determine the stability properties of periodic gaits obtained in [62]. As a result, we cannot compare the stability of the periodic gaits for the MD-SLIP model and the model given in [62] by using our method.

On the other hand, we could compare the properties of stable gaits obtained in our model with the ones obtained in TD-SLIP model. The fixed points of the TD-SLIP are calculated and the stability analysis for TD-SLIP is also performed. In order to make a fair comparison, non-dimensional spring constant k is chosen as 36 and non-dimensional damping coefficient c is chosen as 0.96 to satisfy the value 0.08 for the damping ratio ζ_0 as in [37]. The stability regions of the periodic gaits of TD-SLIP model and MD-SLIP model are illustrated in Figure 3.6. When we

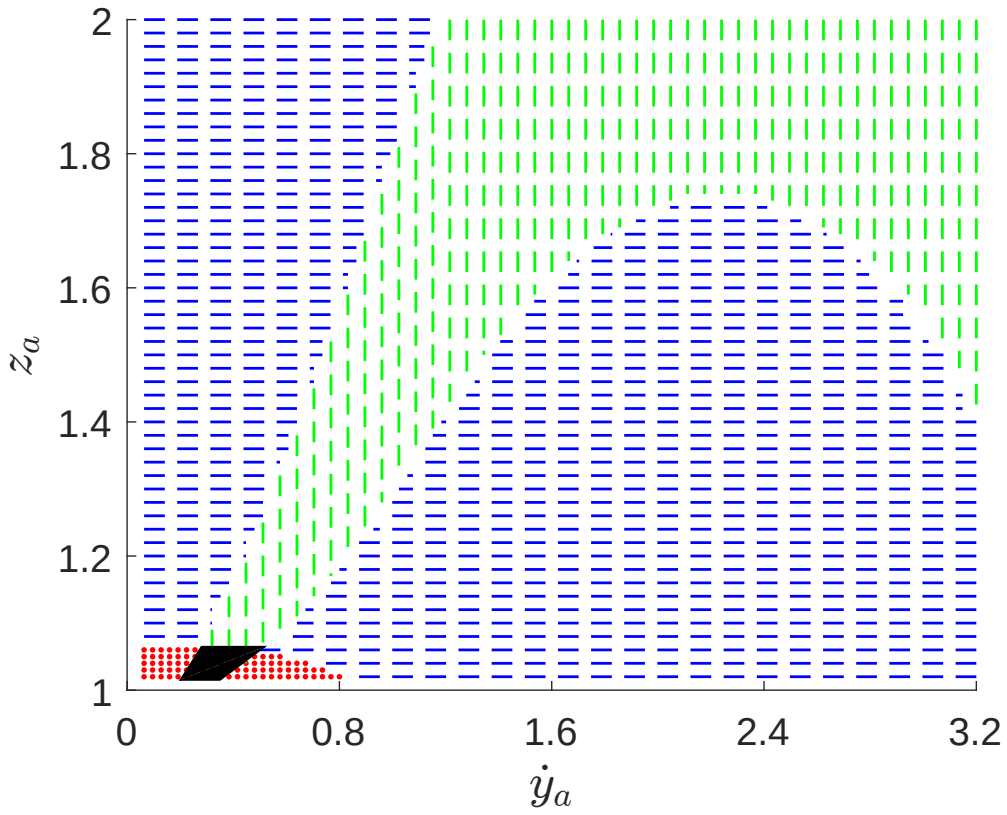

Figure 3.6: Stability regions for the TD-SLIP and MD-SLIP models. Green (vertically-dashed) and red (dotted) regions illustrate the stability and instability for both models, respectively. Blue (horizontally-dashed) region corresponds to stability region for MD-SLIP model, while TD-SLIP is unstable. On the contrary, black (shaded) region represents stability region for the TD-SLIP model while the MD-SLIP model is unstable. The dimensionless spring and damping constants k and c are chosen as 36 and 0.96, respectively.

compare the stability regions of the gaits generated by the proposed model with the TD-SLIP model, we notice that the MD-SLIP model increases the region in which stable motion is observed. There is only a very small portion in our initial condition range, where the TD-SLIP model generates stable gaits but the proposed model gaits are unstable; note that this region is very small and corresponds to initial conditions with heights very close to leg length and very small horizontal velocities. On the other hand, the proposed model exhibits stable gaits in a wide range of initial conditions, where TD-SLIP model is unable to preserve the stability of gaits.

3.2.2 Optimizing Control Parameters C_0 and C_1

In this section, we investigate the stability of periodic gaits when $C_0 \neq 0$ and/or $C_1 \neq 0$ case. As we mentioned before, the case $C_0 = C_1 = 0$ results is symmetric gaits, and when $C_0 \neq 0$ and/or $C_1 \neq 0$, the resulting gait becomes asymmetric. We also observed that in this case, the resulting periodic motion has better stability characteristics as compared to symmetric periodic gait case. Hence, by choosing C_0 and C_1 appropriately we may improve some stability measures. As noted in Remark 4, maximum eigenvalue magnitude will be used as a stability measure in this section. More precisely, let λ_1 and λ_2 be the eigenvalues of the Jacobian matrix. Then the optimization problem considered in this section is given as

$$\min_{\theta_{td}, C_0, C_1} \max\{|\lambda_1|, |\lambda_2|\}. \tag{3.33}$$

For a given $w^* = (z_a^*, \dot{y}_a^*)$ pair, if we choose $C_0 = C_1 = 0$, then there is a single touchdown angle θ_{td} value which makes w^* a fixed point. However, if we choose $C_0 \neq 0$ and/or $C_1 \neq 0$, then there is a range of touchdown angle θ_{td} values which make w^* a fixed point for a given $w^* = (z_a^*, \dot{y}_a^*)$ pair. The magnitudes of the eigenvalues of the corresponding Jacobian matrix for the changing touchdown angle θ_{td} are illustrated in Figure 3.7. Minimizing the touchdown angle while keeping the eigenvalues in the unit circle results in $C_0 = C_1 = 0$. Maximum values for the touchdown angle while keeping the eigenvalues in the unit circle is illustrated in Figure 3.8. Notice that, the range for stable touchdown angle can go up to 10 degrees as illustrated in Figure 3.9 and the percentage of the range of the touchdown angles relative to minimum touchdown angles that result stable periodic gaits for the MD-SLIP model is illustrated in Figure 3.10. Notice that proportionality between the touchdown angle θ_{td} that results in periodic motion and the apex horizontal velocity $\dot{y}_a$ is still valid for asymmetric gaits. Therefore, simple touchdown angle controllers as in [1] can also be used for asymmetric gaits in the proposed model. As noted in Section 3.2.1, following the idea given in [5], if we choose apex horizontal velocity as a measure for locomotion performance, we could utilize touchdown angle as a control parameter for optimization.

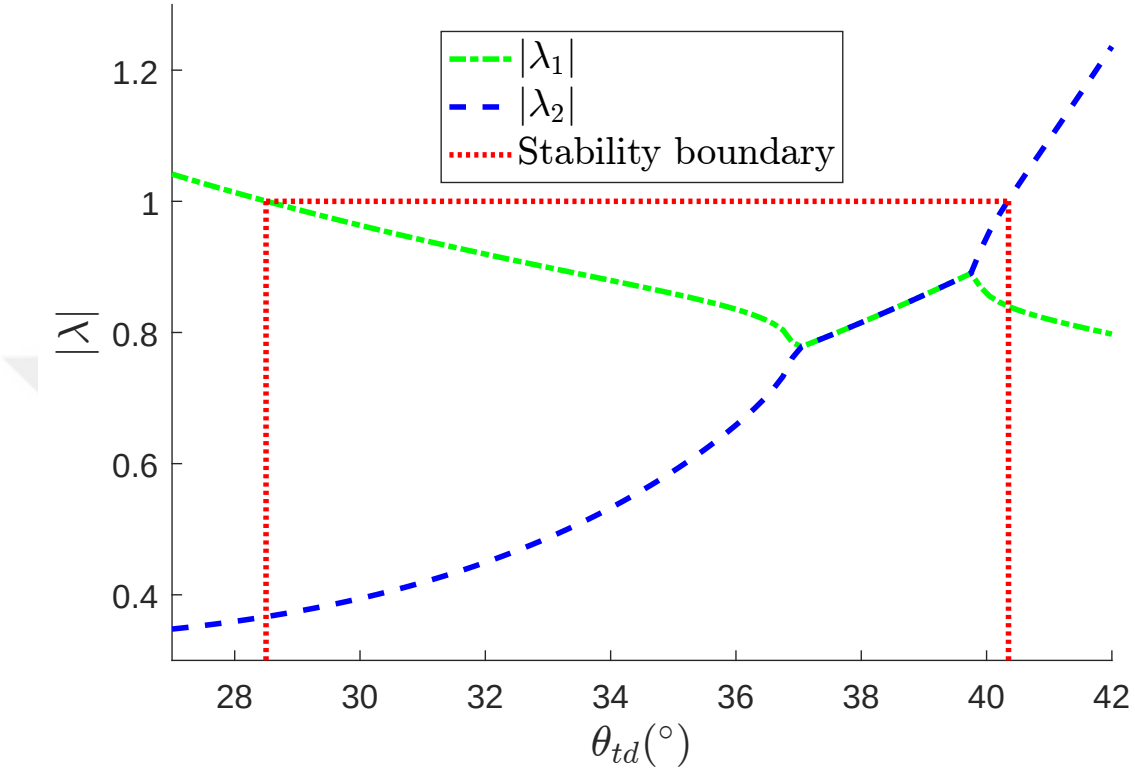

Figure 3.7: Magnitudes of the eigenvalues with respect to touchdown angle. The green and blue lines correspond to two eigenvalues of the system with respect to varying touchdown angles. The red (dotted) lines represent the stability boundary. In this system, the touchdown angle is chosen appropriately by adjusting C_0 and C_1 to make the gaits fixed point. The dimensionless apex height and velocity are 1.02 and 2.3, respectively.

To provide some insight about the asymmetry of the gait, the angle bisector of the touchdown angle θ_{td} and liftoff angle θ_{lo} is chosen as a measure. Notice that increased angle bisector results in increased asymmetry. For stable gaits, it is observed that maximum values for the angle bisector is observed around maximum touchdown angles. Angle bisector for maximum touchdown angle case and its ratio to the touchdown angle is shown in Figure 3.11 and Figure 3.12, respectively. As seen in Figure 3.11, the MD-SLIP model allows asymmetrical bisectors up to 14 degrees based on the initial horizontal velocity. This shows that we can obtain periodic motion even with asymmetrical trajectories. The ability to choose such leg angles increases the possible foot placement locations during motion planning while preserving a stable periodic locomotion. Similarly, in Figure 3.12, we show

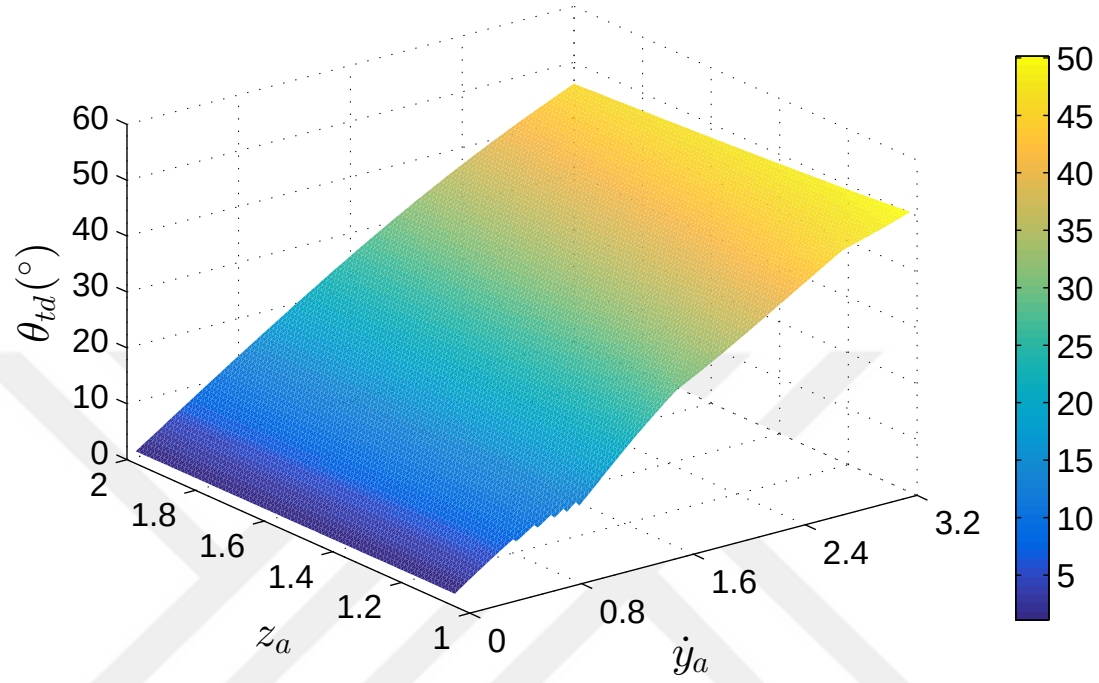

Figure 3.8: Touchdown angles that result periodic gaits for the MD-SLIP model with control parameters C_0 and C_1 are optimized to maximize the touchdown angle while keeping magnitudes of the eigenvalues of the Jacobian matrix of the apex to apex map in the unit circle. The dimensionless spring constant k is chosen as 36.

the percentage ratio of the angle bisector to the touchdown angle. In a great portion of initial conditions, we observe a proportional relationship between the touchdown leg angle and the angle bisector. Such relationships might be useful for deciding the touchdown leg angles, since we can now have an idea about the resulting angle bisector.

Now, we aim to find the control parameters which yield eigenvalues that are closest to the origin that can be obtained by solving the optimization problem defined in (3.33). Figure 3.13 illustrates the touchdown leg angles that yield the most stable case for the eigenvalues. Note that the relation of the touchdown leg angle with respect to initial conditions can be simply approximated with a plane, which would result in simple controllers that will output the necessary touchdown leg angles to minimize the maximum of eigenvalues for a given initial condition. Also, we report the maximum of eigenvalues that are obtained after

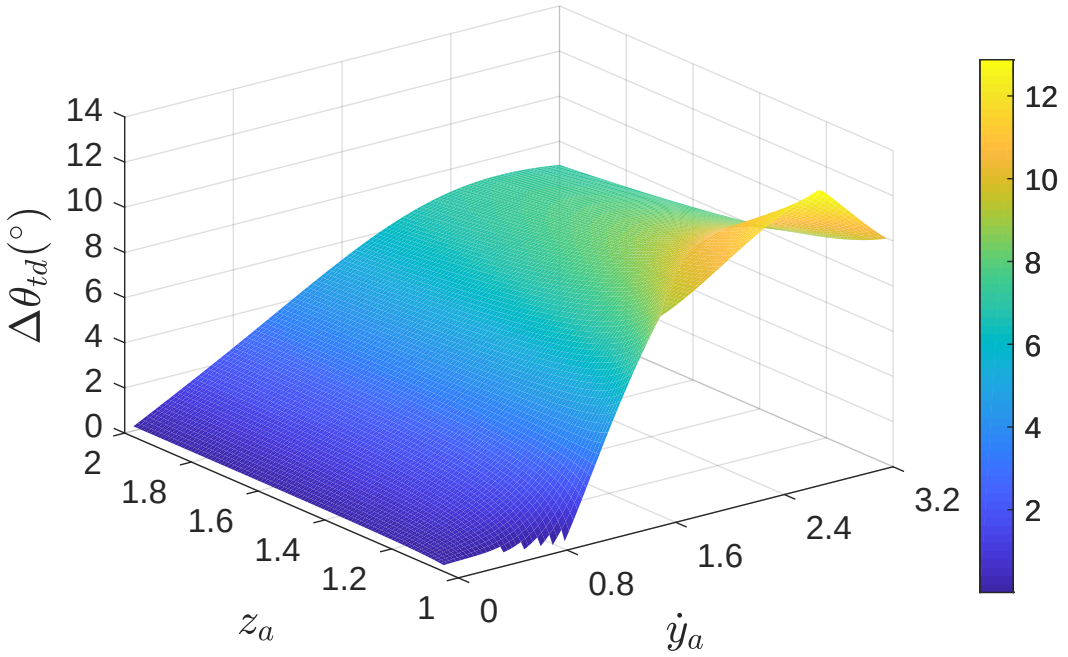

Figure 3.9: Range of the touchdown angles that result stable periodic gaits for the MD-SLIP model. The dimensionless spring constant k is chosen as 36.

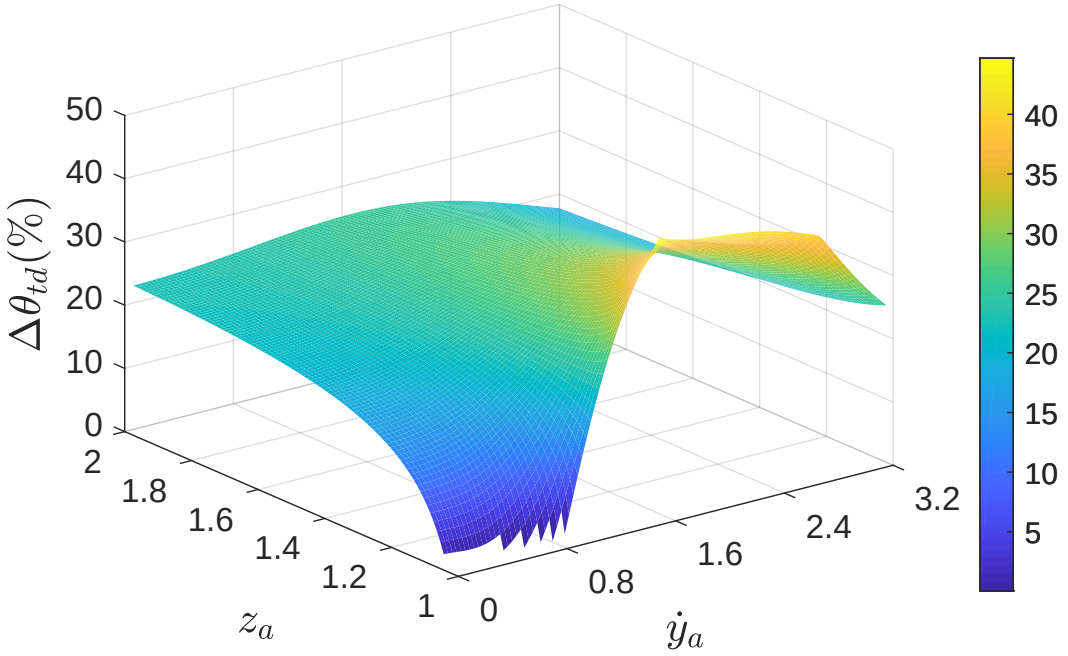

Figure 3.10: The percentage of the range of the touchdown angles relative to minimum touchdown angles that result stable periodic gaits for the MD-SLIP model.

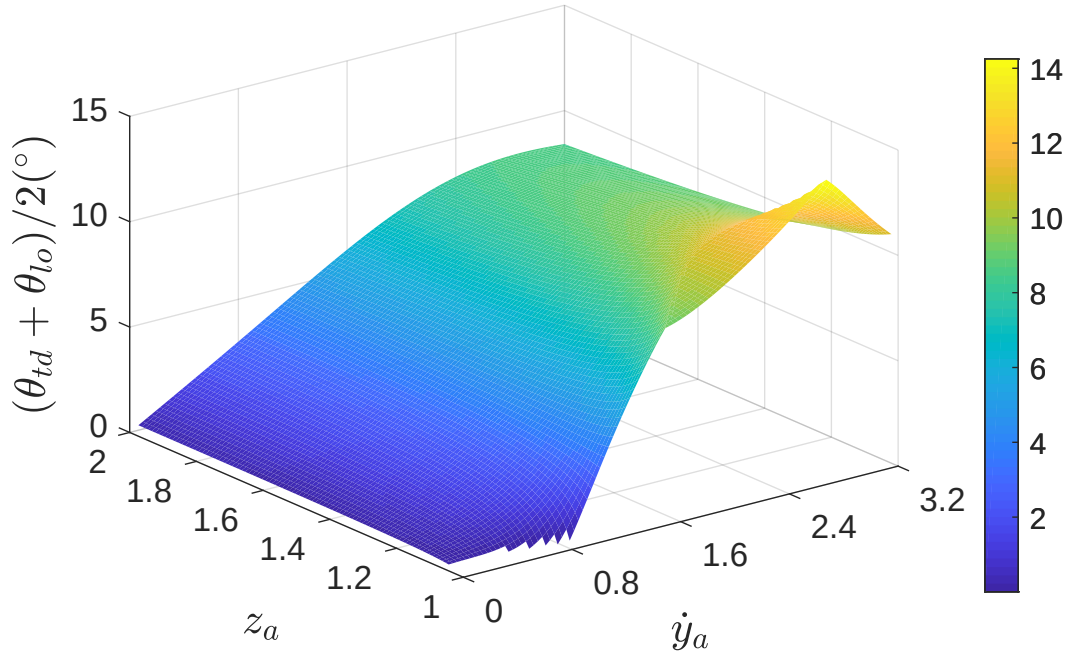

Figure 3.11: Angle bisector of touchdown and liftoff angles of the MD-SLIP model. The control parameters, C_0 and C_1, are adjusted to obtain a stable system (eigenvalues are inside the unit circle) with maximum touchdown angle to compute the angle bisector.

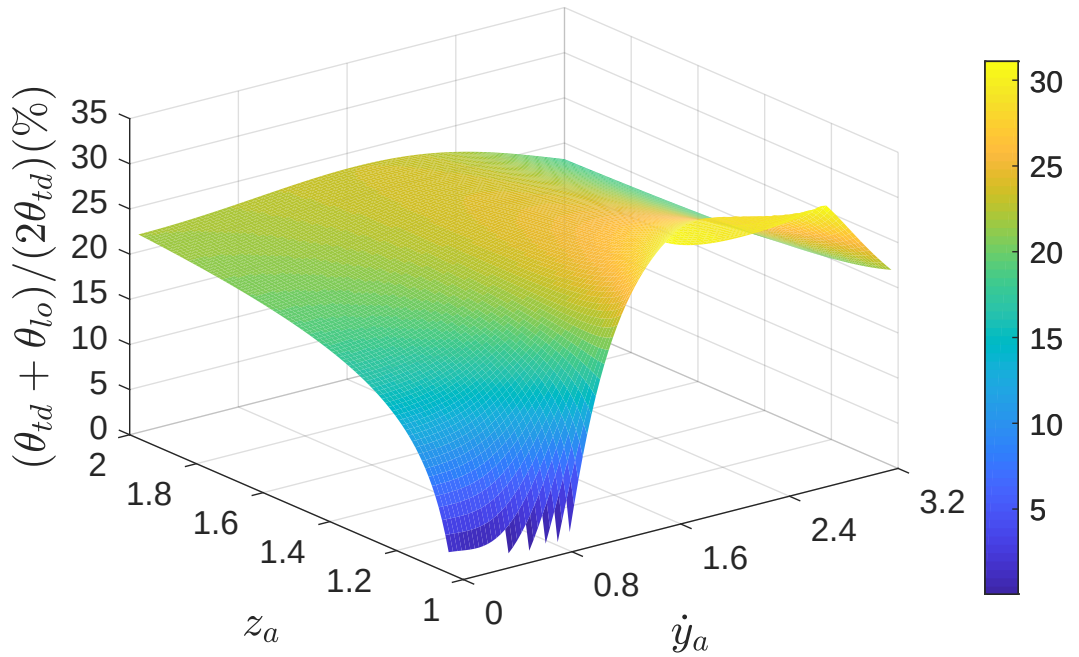

Figure 3.12: The ratio of the angle bisector to the touchdown angle as percentage for maximum touchdown angle case.

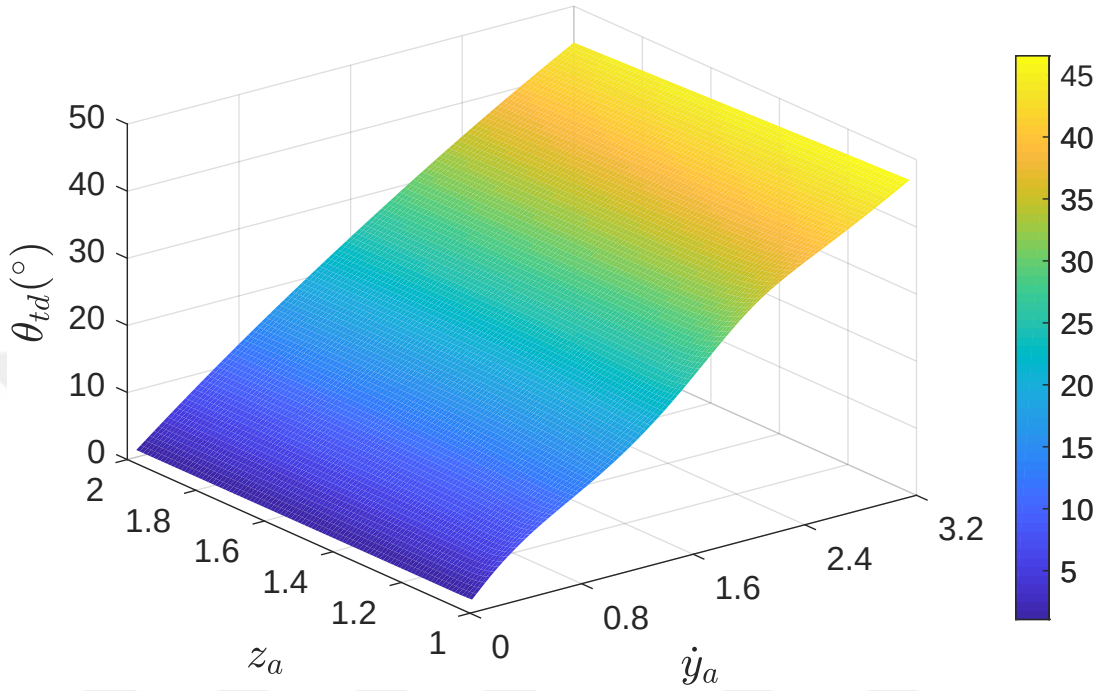

Figure 3.13: The touchdown angles of the stable periodic gaits for the MD-SLIP model.

minimization of the eigenvalues in Figure 3.14. Note that the resulting control constants C_0 and C_1 for the stable gaits have also similar simple dependence on initial conditions as illustrated in Figure 3.15 and Figure 3.16, respectively. These plots together shows that actually, there is a hidden simpler relation between the control parameters, touchdown leg angle and the initial conditions when the goal is to obtain the most stable fixed points. This point requires a detailed investigation, and hence left as a future work, to obtain simpler alternative formulations in controller design for the seemingly complex legged locomotion models.

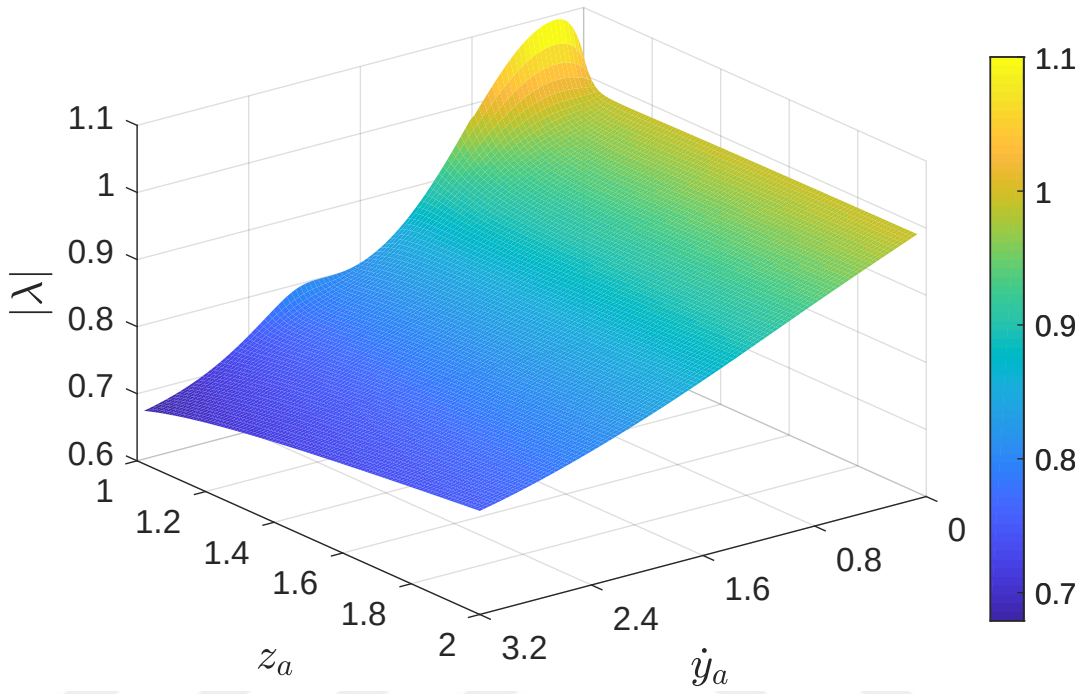

Figure 3.14: Maximum of the magnitudes of the eigenvalues of the Jacobian matrix of the stable periodic gaits for the MD-SLIP model.

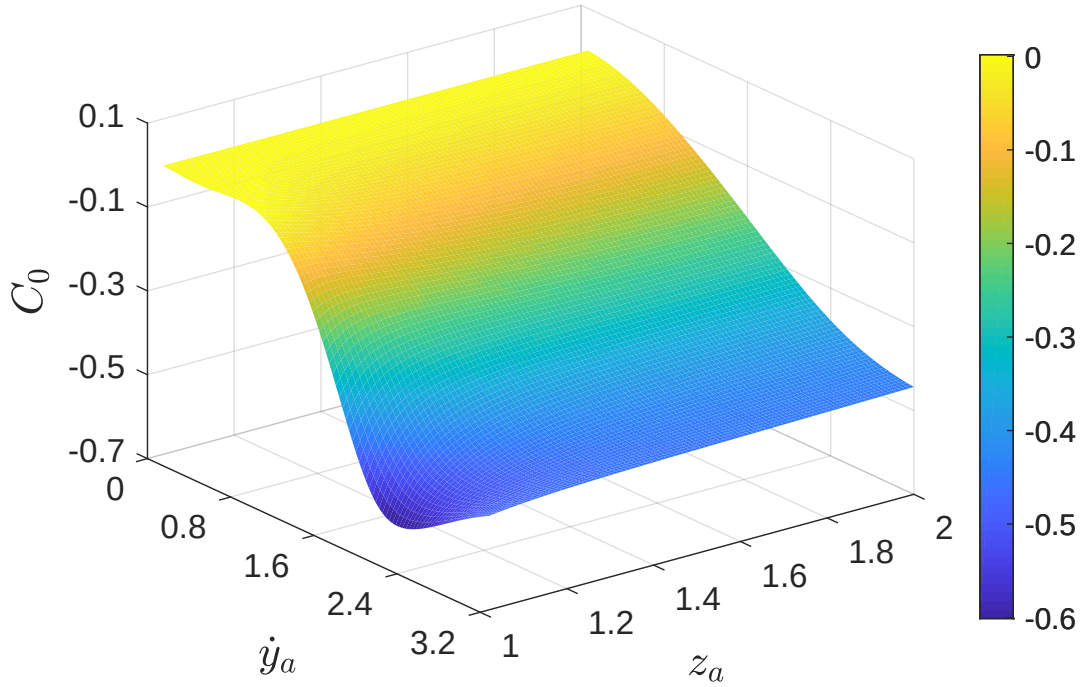

Figure 3.15: Control parameter C_0 of the stable periodic gaits for the MD-SLIP model.

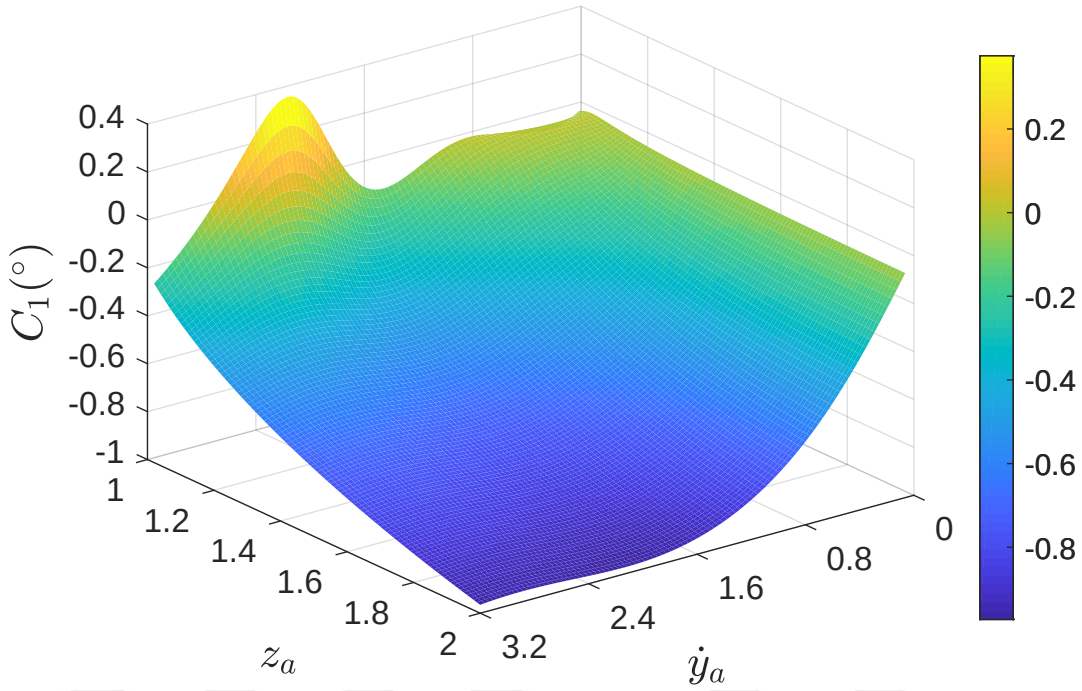

Figure 3.16: Control parameter C_1 of the stable periodic gaits for the MD-SLIP model.

3.3 Performance of MD-SLIP Model on Rough Terrain

3.3.1 Open-Loop Control with Fixed Control Parameters

As stated in Remark 4, one way of evaluating the stability of periodic gaits is to utilize rough terrain simulations, which gives us a measure of robustness of the corresponding periodic motion. In this section, we present various rough terrain simulations to test the robustness of the periodic gaits of three models introduced before, namely SLIP, TD-SLIP and MD-SLIP models. We utilize successful running (i.e. running without falling) rates as a robustness measure, and show that the results obtained in Section 3.2 actually yield sufficiently robust, hence stable, periodic gaits.

Section 3.2 investigates the stability performance of the gaits for the three

Table 3.1: Properties of the Terrains

Terrain	Mean	Variance	Average Power
1	0.00000	0.00000	0.00000
2	-0.01719	0.00552	0.00581
3	-0.03438	0.02207	0.02322
4	0.06568	0.00228	0.00659
5	0.13136	0.00911	0.02636
6	-0.07099	0.00112	0.00616
7	-0.14199	0.00449	0.02465

models, SLIP, TD-SLIP and MD-SLIP, by checking the eigenvalues of the Jacobian matrix around a periodic trajectory. This corresponds to linearizing the dynamics around a periodic motion. In order to have an insight about the region of attraction (validity region for our stability analysis), this section presents the results for stability performance of the three models on rough terrain running experiments. We show that the results obtained in Section 3.2 do not simply yield a local stability but they correspond to gaits that are robust to different rough terrains.

The proposed model, MD-SLIP model, is compared with the TD-SLIP model and the original SLIP model on different terrains, which are depicted in Figure 3.17. Mean, variance and average power of the terrains are given in Table 3.1. Average powers of the terrains are obtained via simple computations (square of the terrain signal integrated over a period normalized by the length of the period) due to the periodicity of the terrains. Additionally, power spectral density of the terrains are illustrated in Figure 3.18 that are computed by the Welch's method [94]. Hence, the intuitive difference between the terrains depicted in Figure 3.17 can be quantitatively observed from Table 3.1 and Figure 3.18.

In order to generalize our results, we performed our tests with various initial conditions, where the dimensionless spring and damping constant were chosen as $k = 36$ and $c = 0.96$, respectively in order to reach optimum performance of the TD-SLIP model for a fair comparison. For the initial conditions, we chose 100 linearly spaced values for $z_a \in [1.01 - 2]$ and 100 linearly spaced values for $\dot{y}_a \in [0.032 - 3.2]$ that yields a total number of 10000 initial condition points.

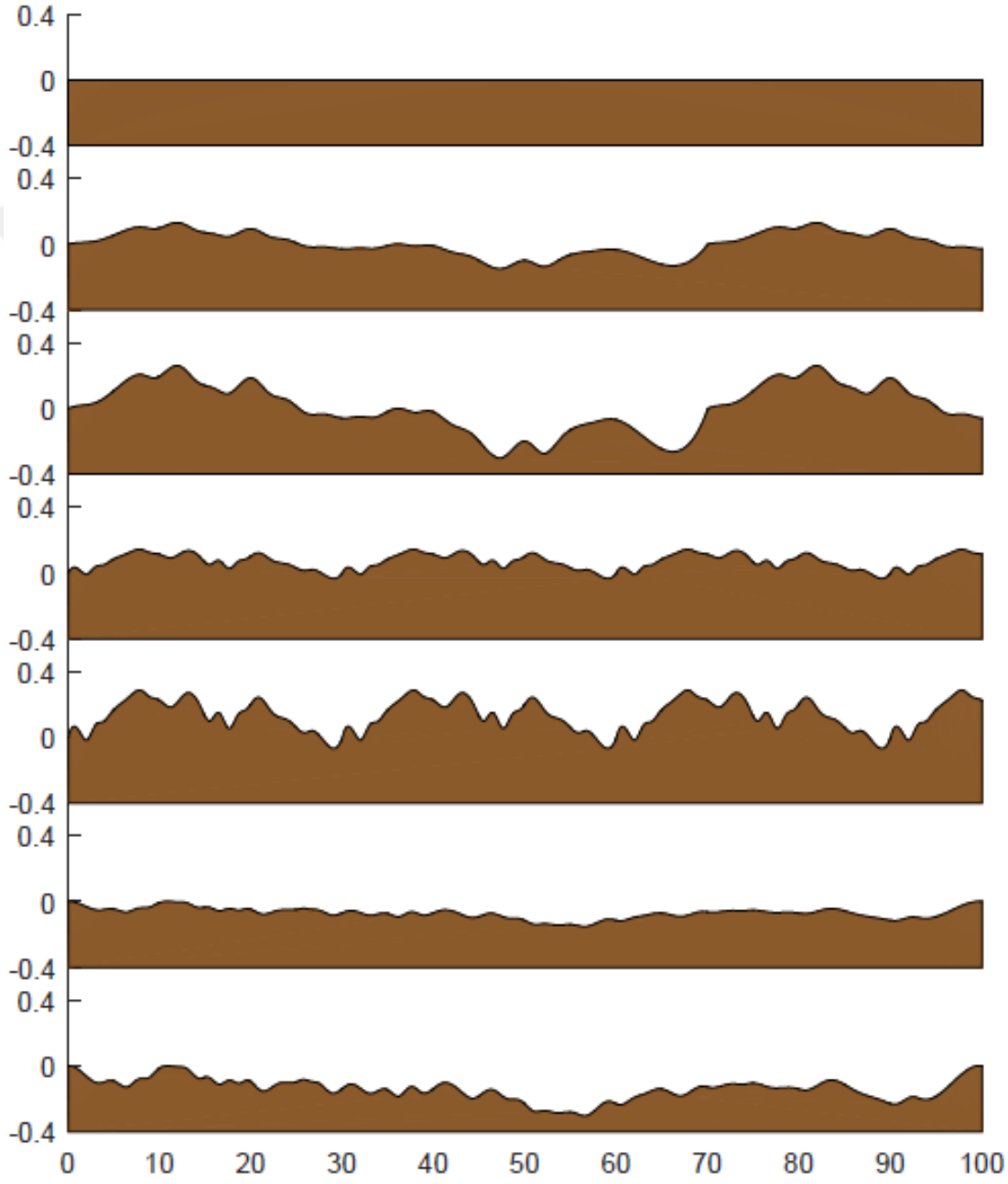

Figure 3.17: Terrains 1-7 used during the simulations. Terrain 1 is the simple flat ground which is used in comparison with the terrains 2-7.

In order to perform our analysis in steady state, we first simulate the models for 1000 steps on the seven terrain models that are depicted in Figure 3.17 and count the successful runs. The step number, 1000, is chosen experimentally to make sure that further increasing the step number does not affect our performance criteria. We note that, we also performed the same simulations for 100 steps. Although the success/failure rates given in Tables 3.2–3.4 changes slightly, the general tendency which indicates that MD-SLIP model outperforms the other SLIP templates remained the same. Further increasing the step size apparently does not change this conclusion. Following these observations, we fixed the step size to 1000 for this section. Also as noted in Remark 4, rough terrain simulations are expected to give an indication on the robustness of stability of periodic gaits; hence from this perspective, we could consider the success/failure rates given in Tables 3.2–3.4 as a measure for stability performance. Table 3.2 lists the percentage failures for the three models on different terrains (Here, a successful run corresponds to a case where the SLIP model completes 1000 steps without falling). As can be seen, MD-SLIP model outperforms the other models with a mean failure error of 21.30% on seven terrains.

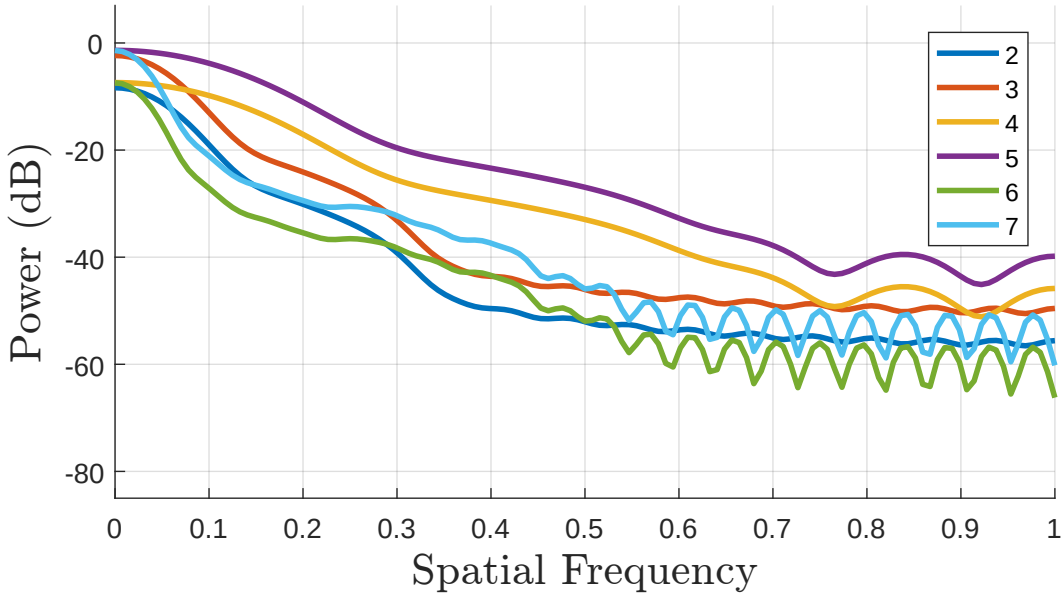

Figure 3.18: Power spectral density for the terrains 2-7

Table 3.2: Percentage of the data points that failed to achieve 1000 steps on the given terrains

	Model		
Terrain	SLIP	TD-SLIP	MD-SLIP
1	77.67	35.29	**2.74**
2	83.35	64.40	**21.20**
3	90.58	71.20	**37.50**
4	90.99	56.67	**20.50**
5	95.81	68.37	**36.21**
6	65.44	40.15	**10.95**
7	77.24	48.19	**20.03**

Having identified the successful runs on rough terrain, we continue to simulate the models for another 1000 steps on flat ground to investigate the robustness of the resulting periodic gaits. Our aim in these simulations is to observe whether the runs which successfully finish 1000 steps in a rough terrain (without falling) would continue to run successfully on a flat ground for another 1000 steps, hence the resulting periodic gait is robust in this sense. Table 3.3 lists the percentage of failure for the three models which could not stand for another 1000 steps on. As can be seen, the MD-SLIP model outperforms the other models in this test.

The final step in our performance observation is to determine whether the initial and final apex states in our simulations for the three models in flat ground following these rough terrains are sufficiently close. If $w_i = (z_a^*, \dot{y}_a^*)$ is the initial apex state and $w_f = (z_{af}, \dot{y}_{af})$ is the final apex state (after 2000 steps in above

Table 3.3: Percentage of the data points that can not stand for additional 1000 steps on the flat ground in addition to the 1000 steps in the given terrains.

	Model		
Terrain	SLIP	TD-SLIP	MD-SLIP
1	78.38	35.37	**2.79**
2	85.96	64.54	**21.26**
3	91.70	71.28	**37.58**
4	90.99	56.67	**20.50**
5	95.81	68.41	**36.21**
6	70.78	41.76	**15.84**
7	82.69	50.11	**26.00**

Table 3.4: Percentage of the data points that are accepted as fixed point periodic gaits.

	Model		
Terrain	SLIP	TD-SLIP	MD-SLIP
1	22.08	17.80	**95.18**
2	14.52	16.69	**78.74**
3	8.86	15.16	**62.42**
4	9.07	17.16	**79.50**
5	4.20	16.21	**63.79**
6	15.85	17.09	**84.16**
7	10.21	16.16	**74.00**

simulations), we consider w_i and w_f to be sufficiently close if $\|w_i - w_f\| < 0.0001$ and we consider the resulting periodic gait as a successful test in this evaluation. The threshold, 0.0001, is also chosen experimentally based on data histogram to consider two states identical at steady state, since obtaining true identical results (corresponds to threshold value of 0) would not be possible in numeric analysis. Table 3.4 illustrates the performance of three models on rough terrains, giving the percentage of successful runs in the sense mentioned above. As seen in Table 3.4, the MD-SLIP model has a better performance in converging to the initial apex state as compared to SLIP and TD-SLIP models.

As can be seen from these simulations as given in Tables 3.2–3.4, the MD-SLIP model outperforms the other models in these tests, which allows us to observe that the periodic gait behaviour of our model is sufficiently robust.

3.3.2 Closed-Loop Control with a Deadbeat Control Strategy

This section investigates the performances of the three models for apex trajectory tracking under closed-loop control. We show that our proposed model yields better tracking performances with a dead-beat controller as compared to other two models.

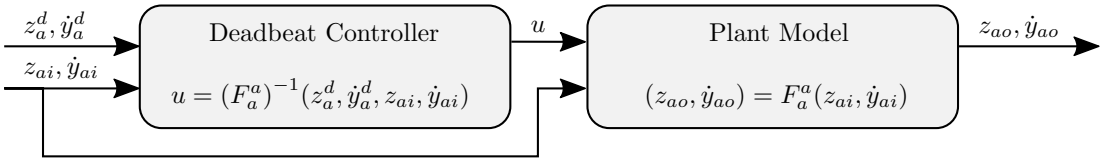

Figure 3.19: Block diagram of the simple deadbeat controller used to compare the closed-loop performance of the models. Here u represents the generic controller output, which is different for different models. $(F_a^a)^{-1}$ is the inverse of the apex map and z_{ao}, $\dot{y}_{ao}$ are the apex height and apex horizontal velocity outputs, respectively.

In order to investigate our statement, we use numeric inverse of the apex return map as the controller in three models. The block diagram of the proposed deadbeat controller scheme is illustrated in Figure 3.19. The inverse map controller takes desired apex state $w^d = (z_a^d, \dot{y}_a^d)$ and current apex state $w_i = (z_{ai}, \dot{y}_{ai})$ as input and calculates the control parameter u to achieve the desired apex state. Note that to have a fair comparison, we apply the same deadbeat controller for all three models. Here u represents the generic controller output, which is different for different models. For instance, in SLIP model, u refers to touchdown angle, θ_{td}, since it is the only control parameter. However, for TD-SLIP model, u represents both the touchdown angle, θ_{td}, and the constant touchdown parameter, α, that is used for determining torque applied to the hip. Finally, in MD-SLIP model, u refers to touchdown angle, θ_{td}, and constant control parameters C_0 and C_1.

Then the system uses this control parameter and achieves an apex state z_{ao}, $\dot{y}_{ao}$. This apex state is used as an input for the next cycle to compute the controller input for the next step.

We define different metrics to evaluate the tracking performance of the proposed closed-loop controller. The apex height tracking performance can be defined as

$$P_z = 100\sqrt{\frac{1}{n}\sum_{i=1}^{n}\left(\frac{z_{ai} - z_a^d}{z_a^d}\right)^2}, \tag{3.34}$$

where n is the total number of apexes, i is the apex index, z_{ai} is apex hight at i^{th} index and z_a^d is the desired apex height. Similarly, apex horizontal velocity

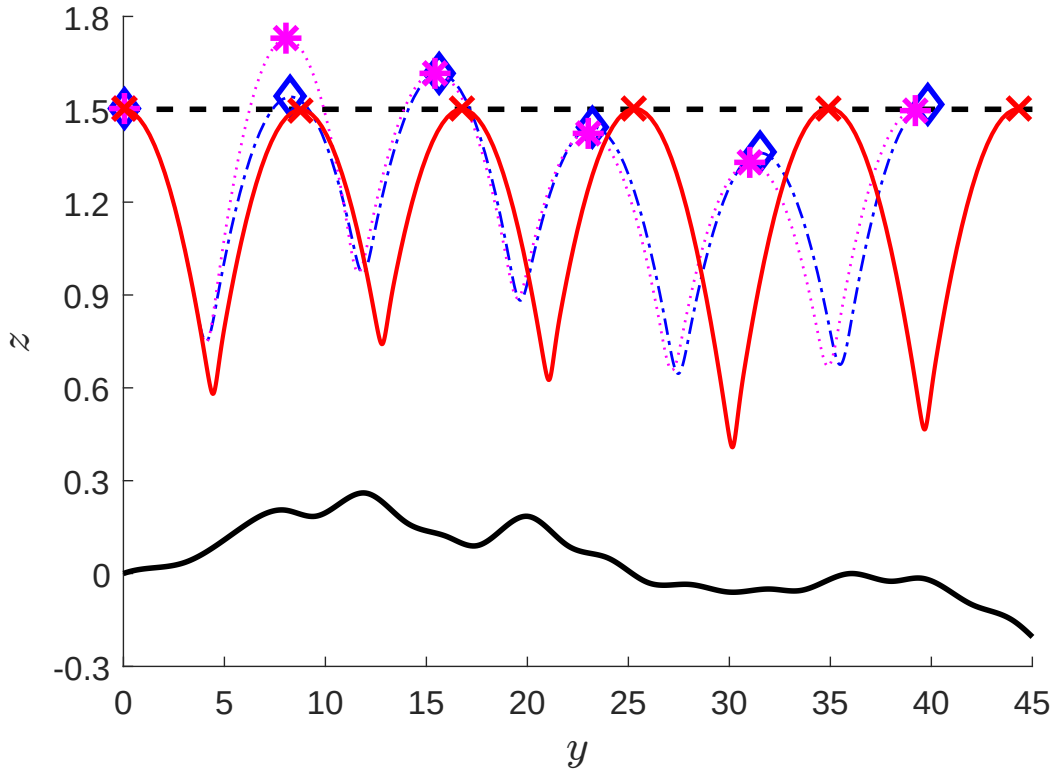

Figure 3.20: During simulation terrain 3 is used and 5 steps are performed. Desired apex height 1.5 and desired apex speed 3.2 are simulated. Black solid line represents the ground. Black dashed line represents the desired apex height. Blue (diamond), magenta (star) and red (cross) points are the apex positions for SLIP, TD-SLIP and MD-SLIP models, respectively. Blue (dot dashed), magenta (dotted) and red (solid) lines are the trajectories that SLIP, TD-SLIP and MD-SLIP models follow, respectively.

tracking performance can be defined as

$$P_{\dot{y}} = 100\sqrt{\frac{1}{n}\sum_{i=1}^{n}\left(\frac{\dot{y}_{ai}-\dot{y}_a^d}{\dot{y}_a^d}\right)^2}, \tag{3.35}$$

where $\dot{y}_{ai}$ is horizontal velocity at i^{th} apex and $\dot{y}_a^d$ is the desired apex horizontal velocity.

Likewise, apex state tracking performance is defined as

$$P_a = 100\sqrt{\frac{1}{n}\sum_{i=1}^{n}\left(\frac{z_{ai}-z_a^d}{z_a^d}\right)^2+\left(\frac{\dot{y}_{ai}-\dot{y}_a^d}{\dot{y}_a^d}\right)^2}. \tag{3.36}$$

Figure 3.20 illustrates a sample run of the three models running at terrain 3 with desired apex height 1.5 and desired apex speed 3.2. It can be clearly observed that MD-SLIP model and the associated closed-loop deadbeat controller preserves the desired apex states with a negligible error when compared to TD-SLIP and SLIP models. In order to generalize our results, we repeated this closed-loop control test for all 10000 initial conditions and computed the mean and standard deviations of the percentage tracking errors in (3.34), (3.35) and (3.36) for terrains $2-7$. The results are listed in Table 3.5. Our results show that MD-SLIP model also outperforms the TD-SLIP and SLIP models when a basic closed-loop controller is used.

The quantities given by (3.34)–(3.36) obviously could be considered as measures to determine the locomotion performance. Indeed they indicate the deviations between the actual trajectory and the (desired) periodic gait during the locomotion over the rough terrains. Table 3.5 indicates that the MD-SLIP model with the proposed controller achieves better locomotion performance over rough terrains. Moreover, as indicated in [93], such mean-variance deviations could also be utilized as a measure for stability performance, or similarly for the robustness performance of the proposed controller. Hence from this perspective, results given in Tables 3.2–3.4 and Table 3.5 are both supporting the conclusion that the MD-SLIP model not only yields better locomotion performance, but also has better stability robustness as compared to the other two SLIP templates.

Table 3.5: Percentage tracking error of apex states in closed-loop system

Model & Metric		Terrain					
		2	3	4	5	6	7
SLIP	P_z	0.694 ± 0.923	1.21 ± 1.58	0.724 ± 0.932	1.27 ± 1.58	0.409 ± 0.551	0.722 ± 0.965
	$P_{\dot{y}}$	0.229 ± 0.125	0.437 ± 0.224	0.267 ± 0.135	0.508 ± 0.246	0.138 ± 0.0719	0.256 ± 0.127
	P_a	0.771 ± 0.899	1.37 ± 1.53	0.826 ± 0.894	1.47 ± 1.51	0.460 ± 0.533	0.820 ± 0.928
TD-SLIP	P_z	1.31 ± 0.948	2.42 ± 1.60	1.40 ± 0.921	2.54 ± 1.53	0.779 ± 0.551	1.48 ± 0.967
	$P_{\dot{y}}$	1.36 ± 1.36	2.88 ± 2.75	1.72 ± 2.13	3.49 ± 4.23	0.870 ± 1.04	1.82 ± 2.11
	P_a	2.24 ± 1.12	4.41 ± 2.20	2.64 ± 1.82	5.08 ± 3.63	1.40 ± 0.894	2.76 ± 1.80
MD-SLIP	P_z	**0.107 ± 0.115**	**0.200 ± 0.166**	**0.122 ± 0.154**	**0.193 ± 0.204**	**0.0699 ± 0.0874**	**0.132 ± 0.142**
	$P_{\dot{y}}$	**0.171 ± 0.0861**	**0.350 ± 0.168**	**0.178 ± 0.0886**	**0.361 ± 0.151**	**0.0925 ± 0.0484**	**0.187 ± 0.0838**
	P_a	**0.215 ± 0.122**	**0.414 ± 0.217**	**0.241 ± 0.143**	**0.438 ± 0.200**	**0.128 ± 0.0835**	**0.246 ± 0.139**

3.4 Discussion: On the Energy Efficiency of Linear and Rotary Actuators

The MD-SLIP model, proposed in this thesis, utilizes a combination of both a linear and rotary actuator. However, when making this kind of choices, energy efficiency of using such actuators and their combinations should be investigated with care, since this is a very important point for a wide range of robotic applications. To investigate this, we first define the *energy consumption/energy loss* as the amount of energy lost due to the damping and spring (in case of early liftoff) components for a single stride, since we need to compensate for the lost energy using our actuators in order to obtain a fixed point. Mathematical expressions are given as special for each of the models when they are presented. Similarly, *energy efficiency* can be defined as losing less energy and hence consuming less energy by the use of our actuators when comparing different models. The energy efficiency of model A compared to model B is defined as

$$\eta_E := \frac{E^B_{loss} - E^A_{loss}}{E^B_{loss}}, \tag{3.37}$$

where E^A_{loss} and E^B_{loss} are the lost energies of the models A and B due to the damping and early liftoff, respectively. To this end, we propose some models as well as associated simulation studies towards analyzing energy efficiency of using such actuators. First of all, we propose two linearly actuated models; one with having a damping term and the other being lossless. The lossy linear actuator SLIP (LA-SLIP) models, their coordinate frames and model parameters are illustrated in Figure 3.21.

Energy injection strategy of the LA-SLIP models is determined as changing the length of the linear actuators with constant speed v_{act} as

$$r_{act} = r_{act,0} + v_{act}t, \tag{3.38}$$

where t represents time duration after touchdown instant. Here, v_{act} values are chosen as to obtain a gait with a fixed-point. Since this model has the ability to retract its leg by using linear actuator, different liftoff conditions can be used.

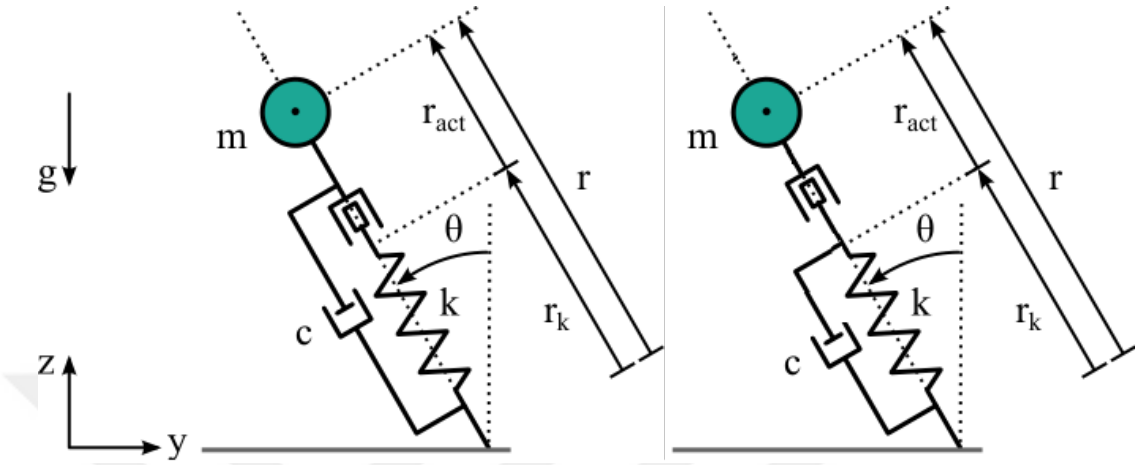

(a) LA1-SLIP Model (b) LA2-SLIP Model

Figure 3.21: Lossy linear actuator SLIP (LA-SLIP) models, coordinate system and model parameters

However, the zero ground reaction force instant

$$k(r_{k,0} - r_k) - c\dot{r} = 0, \tag{3.39}$$

is used for the liftoff condition to avoid using extra energy for retraction and keep the model simple.

The injected energies by the linear actuators in LA1-SLIP and LA2-SLIP models in a single stride are formulated as

$$E_{inj,LA1-SLIP} = \int_{t_{td}}^{t_{lo}} k(r_{k,0} - r_k) v_{act}\, dt, \tag{3.40}$$

$$E_{inj,LA2-SLIP} = \int_{t_{td}}^{t_{lo}} (k(r_{k,0} - r_k) - c\dot{r}_k) v_{act}\, dt, \tag{3.41}$$

respectively. The energy loss due to the damping and early liftoff in LA1-SLIP and LA2-SLIP models in a single stride are given as

$$E_{loss,LA1-SLIP} = \int_{t_{td}}^{t_{lo}} c\dot{r}^2\, dt + \frac{1}{2}k(r_{k,0} - r_{k,lo}), \tag{3.42}$$

$$E_{loss,LA2-SLIP} = \int_{t_{td}}^{t_{lo}} c\dot{r}_k^2\, dt + \frac{1}{2}k(r_{k,0} - r_{k,lo}), \tag{3.43}$$

respectively, where $r_{k,lo}$ is the spring length at liftoff instant. Note that the injected and lost energies should be equal for fixed point gaits.

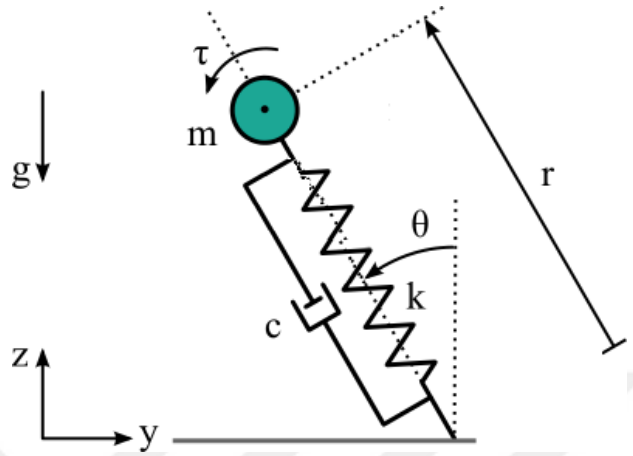

Figure 3.22: Lossy rotary actuator SLIP (RA-SLIP) model, coordinate system and model parameters

Secondly, we defined eight different torque profiles to use with the lossy rotary actuator SLIP (RA-SLIP) model illustrated in Figure 3.22. First four of them use increasing torque profile during different portions of the stance phase as

$$\text{RA1-SLIP} : \tau = Pt, \tag{3.44}$$

$$\text{RA2-SLIP} : \tau = \begin{cases} Pt & \text{if } k(r_{k,0} - r_k) - c\dot{r} > 0 \\ 0 & \text{otherwise} \end{cases}, \tag{3.45}$$

$$\text{RA3-SLIP} : \tau = \begin{cases} Pt & \text{if } \dot{r} \leq 0 \\ 0 & \text{otherwise} \end{cases}, \tag{3.46}$$

$$\text{RA4-SLIP} : \tau = \begin{cases} Pt & \text{if } \theta > 0 \\ 0 & \text{otherwise} \end{cases}, \tag{3.47}$$

where P is a constant that is computed to obtain a gait with a fixed-point. Note that we obtain unique θ_{td} angle that yields fixed point for each initial condition. Here we use ramp torque profile, since we don't need to guess for the liftoff time for increasing ramp torque profiles unlike the decreasing torque used in the literature [37]. Another advantage of ramp torque is that we literally apply no torque at touchdown instant, which reduces the effect of impact collisions. The stopping condition for torque inputs are determined intuitionally to prevent any possible early liftoffs. The different models defined above utilize different stopping conditions to investigate the effect of our choices. The other ones defined below

use constant torque profile during different portions of the stance phase as

$$\text{RA5-SLIP} : \tau = \tau_0 \tag{3.48}$$

$$\text{RA6-SLIP} : \tau = \begin{cases} \tau_0 & \text{if } k(r_{k,0} - r_k) - c\dot{r} > 0 \\ 0 & \text{otherwise} \end{cases} \tag{3.49}$$

$$\text{RA7-SLIP} : \tau = \begin{cases} \tau_0 & \text{if } \dot{r} \leq 0 \\ 0 & \text{otherwise} \end{cases} \tag{3.50}$$

$$\text{RA8-SLIP} : \tau = \begin{cases} \tau_0 & \text{if } \theta > 0 \\ 0 & \text{otherwise} \end{cases} \tag{3.51}$$

where τ_0 is the applied constant torque and it is also computed to obtain a gait with a fixed-point. Similarly, the touchdown leg angle is also unique as the ramp torque case for a given initial condition. Different than ramp torque, constant torque allows injecting same amount of energy by using smaller instantaneous torques. The TD-SLIP model is also used as a decreasing torque profile for comparisons. The following equation is used as liftoff condition for the rotary actuator models

$$(k(r_0 - r) - c\dot{r})\cos\theta - \frac{\tau}{r}\sin\theta = 0, \tag{3.52}$$

which is the boundary condition that makes the ground reaction force zero.

The injected energy by the rotary actuator and energy loss due to the damping and early liftoff in RA-SLIP model in a single stride are formulated as

$$E_{inj,RA-SLIP} = \int_{t_{td}}^{t_{lo}} \tau\dot{\theta}\, dt, \tag{3.53}$$

$$E_{loss,RA-SLIP} = \int_{t_{td}}^{t_{lo}} c\dot{r}^2\, dt + \frac{1}{2}k(r_0 - r_{lo}), \tag{3.54}$$

respectively. Note that the injected and lost energies should be equal for fixed point gaits.

Figure 3.23 illustrates a comparison between the energy consumption of LA1-SLIP and LA2-SLIP models. Energy consumption ratio of model A with respect to model B as percentage is defined as

$$\Delta E = 100\frac{E^A_{loss} - E^B_{loss}}{E^B_{loss}}, \tag{3.55}$$

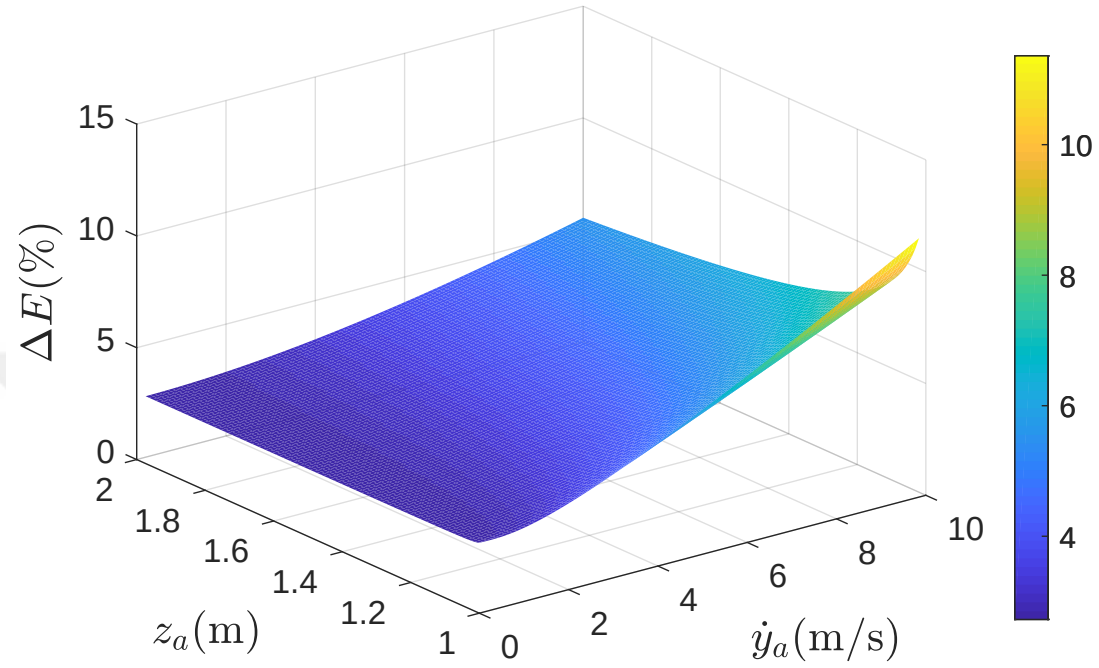

Figure 3.23: Energy consumption ratio of the LA1-SLIP model with respect to LA2-SLIP model as percentage. LA1-SLIP exhibits more energy consumption with respect to LA2-SLIP model.

where E^A_{loss} and E^B_{loss} are the lost energy of the models A and B due to the damping and spring (in case of early liftoff) components, respectively. As seen in Figure 3.23, the LA2-SLIP model is energy efficient with respect to LA1-SLIP. Therefore, we compare the energy efficiency of the rotary models with only LA2-SLIP, since it exhibits a better energy efficiency performance with respect to LA1-SLIP.

Similar to Section 3.3, we performed our simulations by using the values for the dimensionless spring and damping constants as $k = 36$ and $c = 0.96$, respectively. For the initial conditions, we chose 100 linearly spaced values for $z_a \in [1.01 - 2]$ and 100 linearly spaced values for $\dot{y}_a \in [0.032 - 3.2]$ that yields a total number of 10000 initial condition points. The resulting regions are illustrated in Figure 3.24. In the green (horizontally-dashed) region, the LA2-SLIP model is in the mean 10% more energy efficient compared to its closest rivals RA2-SLIP and RA4-SLIP models. RA2-SLIP and RA4-SLIP models are the least energy consuming models

Table 3.6: Mean and standard deviations of the percentage of the energy consumption of the models in a single stride with respect to total energy

Model	Green Region	Red Region	Blue Region
LA1-SLIP	17.0 ± 5.44	23.8 ± 2.70	23.7 ± 3.07
LA2-SLIP	**16.0 ± 5.22**	22.9 ± 2.58	22.9 ± 2.95
RA1-SLIP	17.7 ± 5.14	23.7 ± 1.35	25.8 ± 0.597
RA2-SLIP	17.5 ± 5.10	**22.3 ± 2.53**	18.9 ± 2.84
RA3-SLIP	17.7 ± 5.26	22.9 ± 2.66	15.8 ± 5.53
RA4-SLIP	17.5 ± 5.16	**22.3 ± 2.53**	18.9 ± 2.84
RA5-SLIP	17.6 ± 5.17	23.0 ± 2.07	22.6 ± 1.18
RA6-SLIP	17.6 ± 5.16	22.6 ± 2.55	18.2 ± 3.44
RA7-SLIP	17.7 ± 5.24	22.9 ± 2.65	**12.9 ± 7.34**
RA8-SLIP	17.6 ± 5.20	22.6 ± 2.55	18.2 ± 3.44
TD-SLIP	17.6 ± 5.20	22.8 ± 2.57	15.4 ± 6.36
MD-SLIP	21.1 ± 6.52	24.8 ± 2.92	24.7 ± 3.20

that show similar performance in the red (dotted) region. Their nearest linear actuator competitor is LA2-SLIP model and they have nearly in the mean 3% energy efficiency compared to it. RA7-SLIP is the most efficient model in the blue (vertically-dashed) green region. LA2-SLIP model consumes more energy in this region, so that it is nearly 2 times worse on the average than RA7-SLIP model in that region. Additionally, mean and standard deviations of the percentage of the energy consumption of the models with respect to total energy , that is calculated in a single stride, is given in Table 3.6. Such analysis can be useful for switching between the actuators to obtain optimum energy efficiency for different initial conditions. For example, for the green region in Figure 3.24, the optimum choice would be LA2-SLIP. If the desired fixed point region is somehow switched to a point in the red region, we can switch to RA2-SLIP or RA4-SLIP models, to minimize our energy consumption in this region. Similarly, for the initial conditions in blue region, we can utilize RA7-SLIP model for its energy efficiency.

Finally, we defined three models that includes combination of actuators (CA-SLIP) as illustrated in Figure 3.1 as template with the following torque and linear actuator profiles

$$\text{CA1-SLIP} : \begin{cases} \tau = \tau_0 \\ r_{act} = r_{act,0} + v_{act} t \end{cases} \tag{3.56}$$

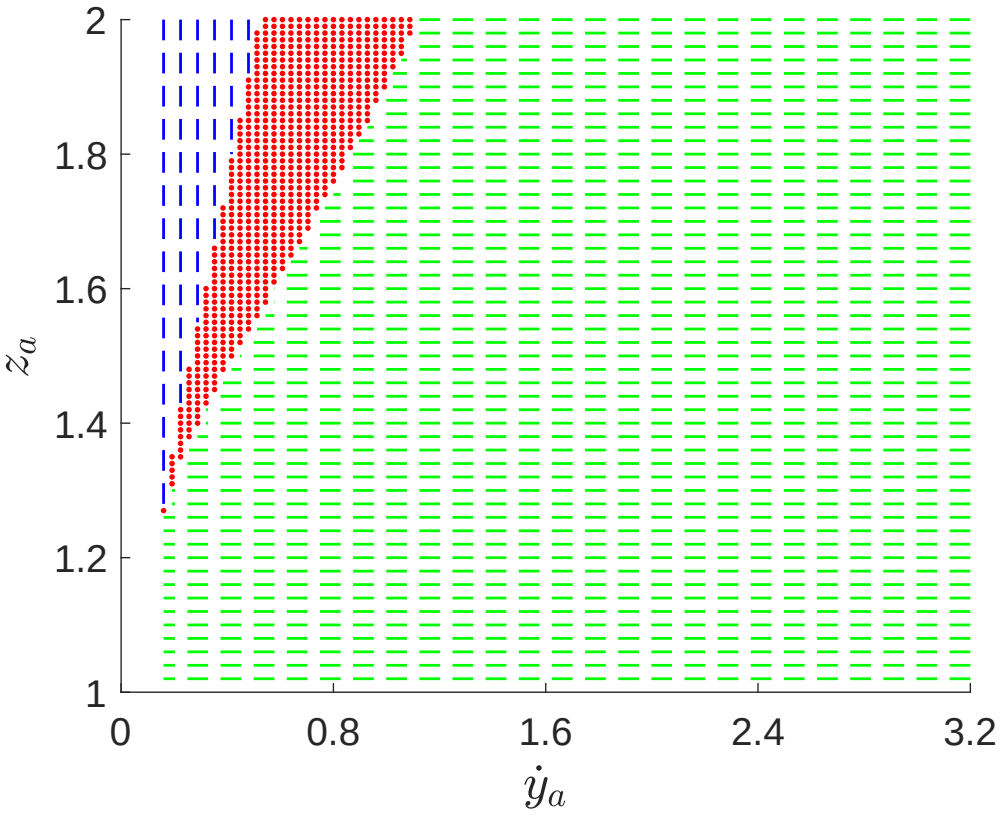

Figure 3.24: The energy efficiency regions for the linear and rotary actuators. Despite a linear actuator model uses less energy in the green (horizontally-dashed) region, both linear actuator models uses more energy in other regions.

$$\text{CA2-SLIP}: \begin{cases} \tau = \begin{cases} \tau_0 & \text{if } k(r_{k,0} - r_k) - c\dot{r} > 0 \\ 0 & \text{otherwise} \end{cases} \\ r_{act} = r_{act,0} + v_{act} t \end{cases} \tag{3.57}$$

$$\text{CA3-SLIP}: \begin{cases} \tau = \begin{cases} \tau_0 & \text{if } \dot{r} \leq 0 \\ 0 & \text{otherwise} \end{cases} \\ r_{act} = \begin{cases} r_{act,0} & \text{if } \dot{r} \leq 0 \\ r_{act,0} + v_{act}\,(t - t_{\dot{r}=0}) & \text{otherwise} \end{cases} \end{cases} \tag{3.58}$$

where $t_{\dot{r}=0}$ is the instant $\dot{r}$ becomes zero. The following equation is used as liftoff condition for the combined actuator models

$$(k(r_{k,0} - r_k) - c\dot{r})\cos\theta - \frac{\tau}{r}\sin\theta = 0, \tag{3.59}$$

which is the boundary condition that makes the ground reaction force zero.

During simulations, we tried to find some balance between τ_0 and v_{act} which minimizes the consumed energy. However, the optimizations resulted in favour to one of them and making other one zero. We observed that, optimizations resulted in $\tau_0 = 0$ in green (horizontally-dashed) region of Figure 3.24 which means it uses only the linear actuator part of the model. Similarly, optimizations resulted in $v_{act} = 0$ in non-green regions of Figure 3.24 which means it uses only the rotary actuator part of the model. By analyzing these results, we concluded that, CA-SLIP models (at least three models that we defined above) are not better than their single actuated counterparts in the sense of energy efficiency. However, as compared its advantages such as enforcing exact analytical solutions to its stance dynamics, we prefer to use MD-SLIP model in our analysis.

Chapter 4

Multi-Actuated Dissipative Bipedal SLIP (MDB-SLIP) Model

The goal of this chapter is to extend the proposed multi-actuated dissipative locomotion model as well as the associated partial feedback linearization strategy to bipedal legged locomotion models. To achieve this, we first give a brief discussion on the existing bipedal legged locomotion models in the literature and then give our approach which includes assigning two multi-actuated dissipative SLIP (MD-SLIP) model corresponding to each leg in the bipedal legged locomotion model. We then show how the partial feedback linearization theory can be utilized to enforce exact analytical solutions to the trajectories of each leg.

4.1 Background: Bipedal SLIP Models

Geyer et al. [76] studied the bipedal SLIP (B-SLIP) model to describe the walking mechanics/dynamics of human locomotion. They showed that compliant legs and double support phase (where two legs touch ground) are two essential features

of walking. The model they proposed shows similar characteristics with human walking in terms of small vertical oscillations and ground reaction forces. They showed that the model presents a successful template especially for walking and running gaits. Although some recent studies directly use the B-SLIP model [82], some prefer embedding its behavior in a higher level model [85]. The studies of [87, 88] such as modeling walking dynamics and developing approximate analytical solutions to its originally non-integrable stance dynamics show the promising nature of the proposed model for future investigations.

In this section, we will give some brief introduction and some terminology regarding the bipedal SLIP models. Then we continue with some recent studies from literature related to our work.

4.1.1 Dissipative Bipedal SLIP Model

The dissipative bipedal spring-loaded inverted pendulum (B-SLIP) model is actually like the combination of two dissipative SLIP models that are explained in detail in Section 2.1.1. For the sake of simplicity, the body has been modeled as a point mass (as in Section 2.1.1) connected to two massless lossy springy legs. The model is illustrated in Figure 4.1.

The dissipative B-SLIP model has hybrid system dynamics by nature of the SLIP models. However, different than classical SLIP models, the B-SLIP model alternates between three main phases during its locomotion. One of these phases is the flight phase in which none of the legs is in contact with the ground. The second one is the single support phase (SS) in which one of the legs is in contact with the ground but the other one is on the fly. Finally, the third phase is the double support phase (DS) where both legs are in contact with the ground. This locomotion behaviour characterizes the running gait of B-SLIP model. As opposed to the running gait, during the walking gait, the model consecutively switches between SS and DS phases as illustrated in Figure 4.2. Hence the basic B-SLIP model captures both the running and walking behaviours. However, in sequel we will mainly focus on the walking behaviour.

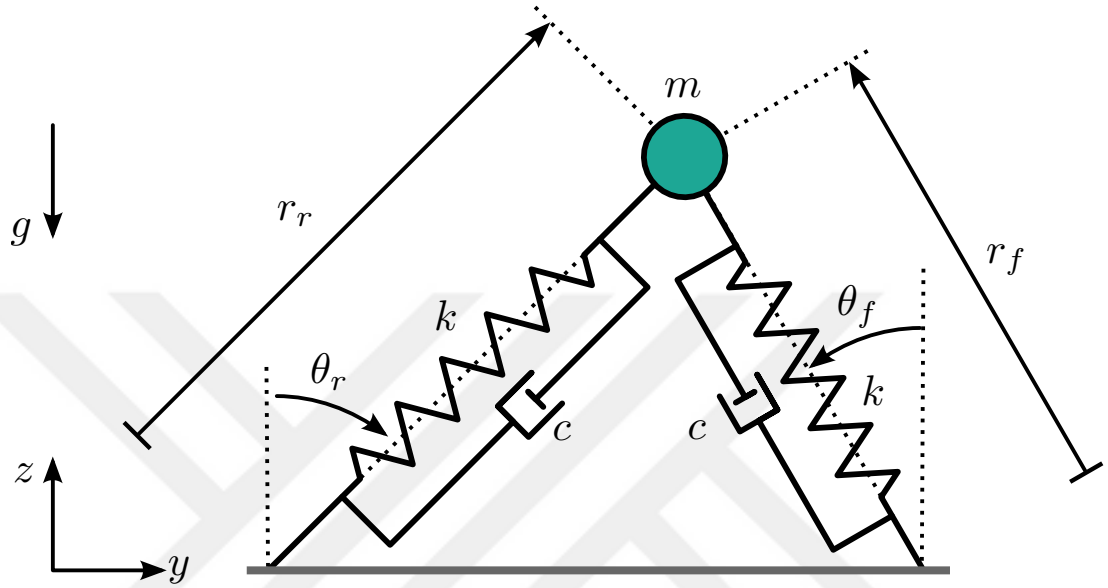

Figure 4.1: The dissipative B-SLIP model, coordinate system and model parameters

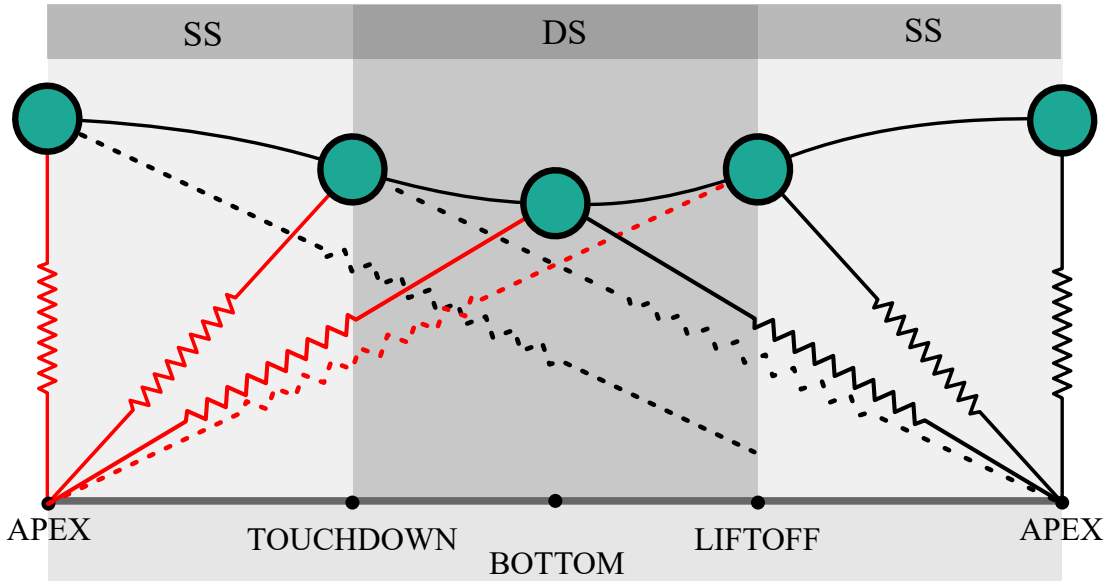

Figure 4.2: The phases of locomotion of the B-SLIP model during walking

The phases of the locomotion is separated by some events that are triggered by pre-determined boundary conditions. Let the model first start with an *apex* state where the point mass has no vertical speed and the vertical acceleration is downwards. Then the *touchdown* event occurs when the front leg touches to the ground as the name implies and the transition from the single support phase to double support phase occurs. During double support phase, *bottom* event occurs when the point mass has the minimum height and the vertical speed changes its direction. At the end of the double support phase, the rear leg loses contact with the ground and the *liftoff* event occurs which changes the phase to the single support phase. Finally, the point mass reaches a maximum height which triggers the *apex* event and the locomotion reaches the state where it started.

A sample *stride* for the B-SLIP model, which is the trajectory between two subsequent apexes are illustrated in Figure 4.2. The term *stride*, walking gait or simply gait will be used interchangeably. The path that the point mass follows during this locomotion will be called as a trajectory. Then we can define the locomotion of B-SLIP as subsequent recursion of gaits illustrated in Figure 4.2. A motion where initial and final apex states are equal is called as periodic gait and the resultant locomotion called as periodic locomotion.

One of the goals of this chapter is to examine the existence of the periodic gaits of the B-SLIP model and determine stability characteristics of such periodic gaits. Stable periodic gaits are important, because they could be used as steady state control targets during locomotion. As such, deviations from these steady state targets while walking on noisy terrain could be used as a performance metric of a controller.

Dimensionless formulation described in Section 2.1.1 will also be used in this chapter to generalize our solutions for a general class of legged locomotion systems. As a reminder, time and length will be scaled with $\sqrt{r_0/g}$ and leg rest length r_0, respectively, to have dimensionless quantities. Table 2.1 has the equations to transform the physical quantities (which are represented by variables with bars) to corresponding non-dimensional ones. In addition to Table 2.2,

Table 4.1: Additional notation for B-SLIP model

B-SLIP Parameters	
r_f, θ_f	Front leg length and angle
r_r, θ_r	Rear leg length and angle
$\dot{r}_f, \dot{r}_r$	Front and rear leg compression rates
$y_{toe,f,a}, y_{toe,r,a}$	Apex front and rear leg toe horizontal positions

some notations specific to B-SLIP model are given in Table 4.1. Note that all relationships below use the non-dimensional parameter formulation described above unless otherwise specified.

System dynamics of the dissipative B-SLIP model during its single support phase has the same equations of motion for the stance phase of the dissipative SLIP model as in (2.5) and (2.6). As stated in Section 2.1.1, (2.5) and (2.6) are non-integrable [48] and hence no exact solution is available.

In the non-dimensional formulation, Lagrangian and Rayleigh dissipation functions of the double support dynamics for the B-SLIP model can be obtained as

$$L = \frac{1}{2}\left(\dot{z}^2 + \dot{y}^2\right) - \frac{k}{2}(1 - r_f)^2 - \frac{k}{2}(1 - r_r)^2 - z, \tag{4.1}$$

$$D = \frac{c}{2}\left(\dot{r}_f^2 + \dot{r}_r^2\right), \tag{4.2}$$

respectively. By using the classical Lagrange's equation

$$\frac{d}{dt}\left(\frac{\partial L}{\partial \dot{q}_j}\right) - \frac{\partial L}{\partial q_j} + \frac{\partial D}{\partial \dot{q}_j} = 0, \tag{4.3}$$

with $q_1 = y$, $q_2 = z$, $\partial r_f/\partial y = -\sin\theta_f$, $\partial r_r/\partial y = -\sin\theta_r$, $\partial r_f/\partial z = \cos\theta_f$ and $\partial r_r/\partial z = \cos\theta_r$, we obtain the following equations of motion for the double support phase of the B-SLIP model as

$$\ddot{y} = -\left(k\left(1 - r_f\right) - c\dot{r}_f\right)\sin\theta_f - \left(k\left(1 - r_r\right) - c\dot{r}_r\right)\sin\theta_r, \tag{4.4}$$

$$\ddot{z} = -1 + \left(k\left(1 - r_f\right) - c\dot{r}_f\right)\cos\theta_f + \left(k\left(1 - r_r\right) - c\dot{r}_r\right)\cos\theta_r, \tag{4.5}$$

in Cartesian coordinates. Similar to the single support phase dynamics, double support dynamics of the B-SLIP model has also no exact solution [87]. However, stance trajectories can still be obtained by using numerical integration. On

the other hand, this option is not feasible for online computations, e.g., online optimization of controller parameters. Some researchers proposed analytical approximate solutions to the otherwise non-integrable double support dynamics of the B-SLIP model [87, 88]. We will continue with the approximations proposed in [87, 88] for the double support phase of this model.

4.1.2 Axial-torsional SLIP (AT-SLIP) Model

Shahbazi et al. [87] studied the B-SLIP model to unify the walking, running and transitions between each other for bipedal locomotion and also provided an approximation to the double support phase by introducing an auxiliary template called as axial-torsional SLIP (AT-SLIP) model. This model has a virtual leg that represents the characteristics of two legs at the double support phase as illustrated in Figure 4.3.

The single virtual leg is used to approximate the behaviors of real legs by a virtual axial and a virtual torsional spring. This virtual leg is located between point mass and midpoint of the ground contact of the actual legs. The torsional spring is located at the toe of the virtual leg. The spring constant of the axial spring and the rest length of it are defined as k_a and l_{r_0}, respectively. Similarly,

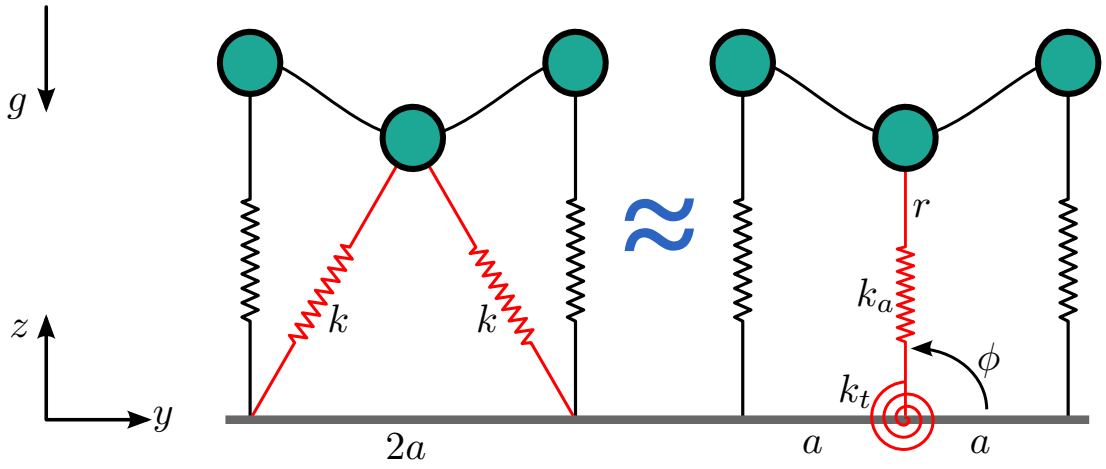

Figure 4.3: Axial-torsional SLIP (AT-SLIP) Model, coordinate system and model parameters

the spring constant and the zero torque angle of the torsional spring are defined as k_t and ϕ_0. Here the zero torque angle corresponds to the angle of the torsional spring when there is no compression or decompression on the torsional spring. The equations of motion for the AT-SLIP model in DS phase is given as:

$$m\begin{bmatrix}\ddot{y}\\ \ddot{z}\end{bmatrix} = m\begin{bmatrix}0\\ -g\end{bmatrix} + \begin{bmatrix}\cos\phi & -\sin\phi\\ \sin\phi & \cos\phi\end{bmatrix}\begin{bmatrix}k_a\left(l_{r_0}-r\right)\\ k_t\left(\phi_0-\phi\right)/r\end{bmatrix}, \tag{4.6}$$

in Cartesian coordinates [87]. The equilibrium point of the B-SLIP model is calculated by equating both equations, (4.4) and (4.5), to zero. As a result of symmetry, zero torque angle becomes $\phi_0 = \pi/2$. The length of the actual legs at the equilibrium point l_{eq} can be found by solving the equation

$$l_{eq}^4 - 2l_0 l_{eq}^3 + (l_0^2 - a^2 - (mg/k)^2/4)l_{eq}^2 + 2a^2 l_0 l_{eq} - a^2 l_0^2 = 0. \tag{4.7}$$

By substituting l_{eq} in

$$z_{eq} = \sqrt{l_{eq}^2 - a^2}, \tag{4.8}$$

the height of the equilibrium point z_{eq} can be found. By assuming small angular span and small spring compression as in [51], approximate values for axial spring constant $\bar{k}_a$, axial spring rest length $\bar{l}_{r_0}$ and torsional spring constant $\bar{k}_t$ can be derived as

$$\bar{k}_a = \frac{mg}{\sqrt{l_0^2 - a^2} - z_{eq}}, \tag{4.9}$$

$$\bar{l}_{r_0} = \frac{mg}{\bar{k}_a} + z_{eq}, \tag{4.10}$$

$$\bar{k}_t = \frac{2ka^2 l_0 \bar{l}_{r_0}^2}{\left(a^2 + \bar{l}_{r_0}^2\right)^{3/2}}. \tag{4.11}$$

Following and extending the approaches used in [51] and [52], the approximate analytical solution to the equations of motion for the double support phase of the B-SLIP model is derived. These derivations and more details can be found in [87].

4.1.3 Lossy Axial-torsional SLIP (LAT-SLIP) Model

Shahbazi et al. [88] also worked on the lossy B-SLIP model and named the model as Lossy Axial-torsional SLIP (LAT-SLIP) model. They used a similar virtual leg approach to approximate the double support dynamics. This model is illustrated in Figure 4.4.

To approximate the losses on both legs, the axial and torsional springs are replaced with their lossy counterparts. The damping coefficients of the virtual axial and torsional springs are defined as c_a and c_t, respectively. The equations of motion for the LAT-SLIP model in DS phase is given as:

$$m\begin{bmatrix}\ddot{y}\\ \ddot{z}\end{bmatrix} = m\begin{bmatrix}0\\ -g\end{bmatrix} + \begin{bmatrix}-\sin\theta & \cos\theta\\ \cos\theta & \sin\theta\end{bmatrix}\begin{bmatrix}k_a\left(l_{r_0}-r\right)-c_a\dot{r}\\ k_t\left(\theta_0-\theta\right)/r - c_t\dot{\theta}/r\end{bmatrix}, \tag{4.12}$$

in Cartesian coordinates [88]. Instead of using equilibrium point as in AT-SLIP model, the approximations are made at the point where the legs have rest length. This does not change the zero torque angle which is $\theta_0 = 0$. However, axial spring rest length r_{rest} is changed as

$$r_{rest} = \sqrt{l_{rest}^2 - a^2}. \tag{4.13}$$

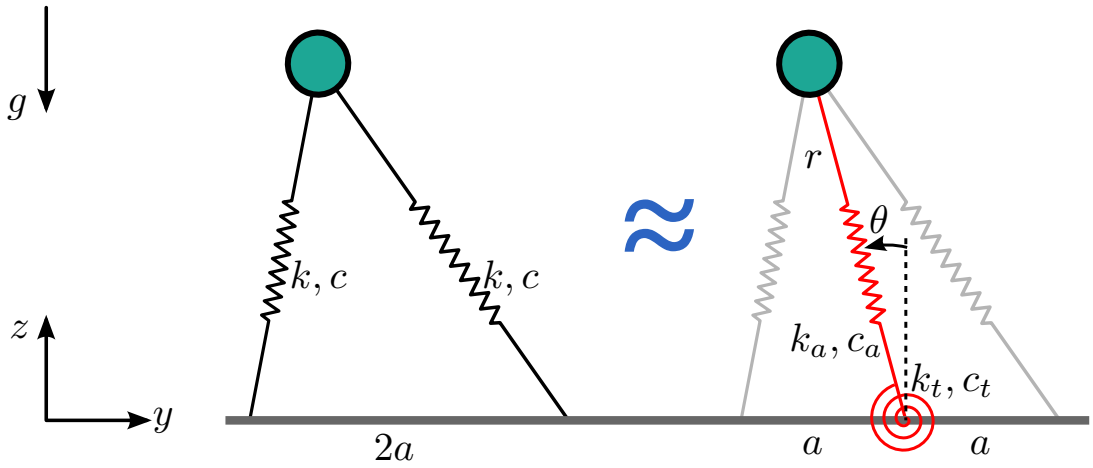

Figure 4.4: Lossy Axial-torsional SLIP (LAT-SLIP) Model, coordinate system and model parameters

This approach also changes the approximated axial and torsional spring coefficients as

$$k_a = 2\left(r_{rest}/l_{rest}\right)^2 k, \tag{4.14}$$

$$k_t = 2a^2\left(r_{rest}/l_{rest}\right)^2 k. \tag{4.15}$$

Newly added axial and torsional spring damping constants are approximated as

$$c_a = 2\left(r_{rest}/l_{rest}\right)^2 c, \tag{4.16}$$

$$c_t = 2a^2\left(r_{rest}/l_{rest}\right)^2 c. \tag{4.17}$$

A detailed analysis including the complete derivations of the above equations can be found in [88].

4.2 Multi-Actuated Dissipative Bipedal SLIP Model

4.2.1 Model and Dynamics

Multi-actuated dissipative bipedal SLIP (MDB-SLIP) model is actually a point mass attached to two legs, which are modeled as the MD-SLIP model. The proposed model includes two linear and two rotational actuators that can be utilized during the locomotion. In the original MD-SLIP model, we used a single linear and a single rotational actuator to ensure and enforce exact analytical solutions to model dynamics. Here, in the MDB-SLIP model, we utilize a similar principle to obtain exact analytical solutions for the double support dynamics as well. The proposed model can be seen in Figure 4.5 with the coordinate system, model parameters as well the actuators on it.

Note that our additional actuators do not violate or change the assumptions on the original B-SLIP model such as point mass, massless legs, etc. However, addition of new actuators changes the double support dynamics, since now we are

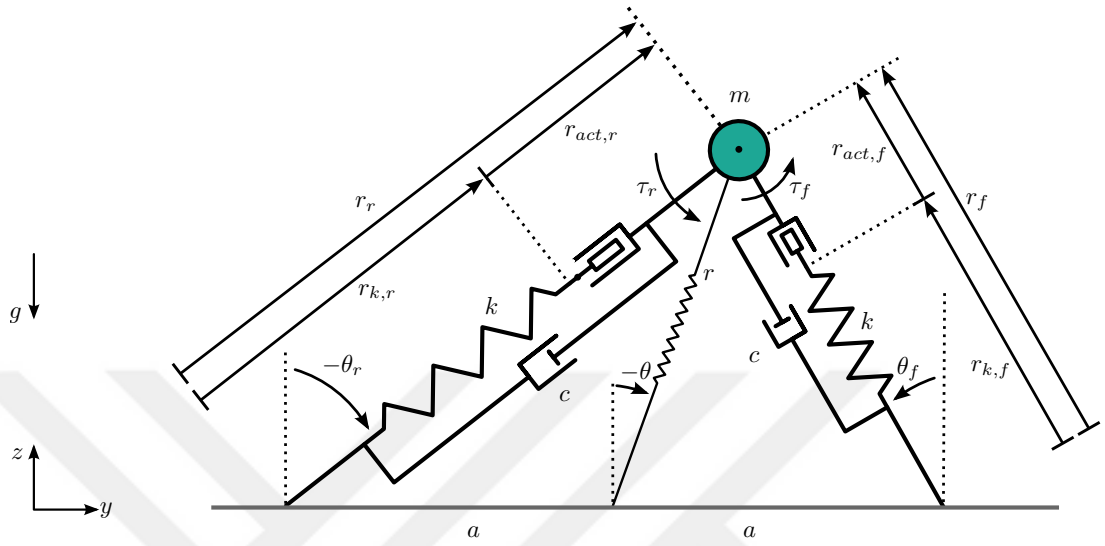

Figure 4.5: Multi-actuated dissipative bipedal SLIP model, coordinate system and model parameters. The difference of this model with the dissipative B-SLIP model (illustrated in Figure 4.1) is the addition of the linear and the rotary actuators.

capable of injecting and removing energy from the system during double support phase by using our additional actuators. Therefore, the modified double support dynamics for the multi-actuated dissipative bipedal SLIP (MDB-SLIP) model can be obtained by using the corresponding Lagrangian and Rayleigh dissipation functions

$$L = \frac{1}{2}\left(\dot{z}^2 + \dot{y}^2\right) - \frac{k}{2}(1 - r_f + \Delta r_{act,f})^2 - \frac{k}{2}(1 - r_r + \Delta r_{act,r})^2 - z, \tag{4.18}$$

$$D = \frac{c}{2}\left(\dot{r}_f^2 + \dot{r}_r^2\right), \tag{4.19}$$

respectively. By using the classical Lagrange's equation

$$\frac{d}{dt}\left(\frac{\partial L}{\partial \dot{q}_j}\right) - \frac{\partial L}{\partial q_j} + \frac{\partial D}{\partial \dot{q}_j} = Q_j, \tag{4.20}$$

with $q_1 = y$, $q_2 = z$, $\partial r_f/\partial y = -\sin\theta_f$, $\partial r_r/\partial y = -\sin\theta_r$, $\partial r_f/\partial z = \cos\theta_f$, $\partial r_r/\partial z = \cos\theta_r$ and external forces

$$Q_1 = -\tau_r/r_r \cos\theta_r - \tau_f/r_f \cos\theta_f, \tag{4.21}$$

$$Q_2 = -\tau_r/r_r \sin\theta_r - \tau_f/r_f \sin\theta_f, \tag{4.22}$$

we obtain the following equations of motion for the double support phase of the MDB-SLIP model

$$\begin{bmatrix} \ddot{y} \\ \ddot{z} \end{bmatrix} = \begin{bmatrix} 0 \\ -1 \end{bmatrix} + \begin{bmatrix} -\sin\theta_r & -\cos\theta_r \\ \cos\theta_r & -\sin\theta_r \end{bmatrix} \begin{bmatrix} F_{r,r} \\ F_{a,r} \end{bmatrix} + \begin{bmatrix} -\sin\theta_f & -\cos\theta_f \\ \cos\theta_f & -\sin\theta_f \end{bmatrix} \begin{bmatrix} F_{r,f} \\ F_{a,f} \end{bmatrix} \quad (4.23)$$

in Cartesian coordinates. Here radial rear leg force $F_{r,r}$ and radial front leg force $F_{r,f}$ are defined as

$$F_{r,r} = k\left(1 - r_r + \Delta r_{act,r}\right) - c\dot{r}_r, \quad (4.24)$$

$$F_{r,f} = k\left(1 - r_f + \Delta r_{act,f}\right) - c\dot{r}_f, \quad (4.25)$$

where $\Delta r_{act,r} = r_{act,r} - r_{act,0}$ and $\Delta r_{act,f} = r_{act,f} - r_{act,0}$. Similarly, the angular forces $F_{a,r}$ for the rear leg and $F_{a,f}$ for the front leg are defined as

$$F_{a,r} = \tau_r / r_r, \quad (4.26)$$

$$F_{a,f} = \tau_f / r_f, \quad (4.27)$$

respectively, with τ_r and τ_f are the torque applied by the rear and front rotary actuators, respectively.

We note that, all time-dependent functions in Section 4.2 use touchdown time as reference for the sake of simplicity.

4.2.2 Adjusting MD-SLIP Stance Dynamics for MDB-SLIP Single Support Dynamics

Section 3.1.2 details our investigations on the stance dynamics of the MD-SLIP. Note that the resulting solutions for the equations of motion from Section 3.1.2 can actually be used for the single support phase of the MDB-SLIP model. However, we need to update the boundary conditions for the MDB-SLIP model.

The equation (3.9) is modified to obtain the solution for the radial dynamics for the single support phase of the MDB-SLIP model as

$$r(t) = A_3 + A_4 \sin(\omega t) + A_5 \cos(\omega t) \quad (4.28)$$

where $w = \sqrt{k}$. By using the following boundary conditions

$$r(0) = r_b, \tag{4.29}$$

$$\dot{r}(0) = \dot{r}_b, \tag{4.30}$$

$$\theta(0) = \theta_b, \tag{4.31}$$

$$\dot{\theta}(0) = \dot{\theta}_b, \tag{4.32}$$

one can compute the unknowns in (4.28) as

$$A_3 = \frac{\cos\theta_b - r_b\dot{\theta}_b^2}{k} + \Delta r_{act,b} + 1, \tag{4.33}$$

$$A_4 = \frac{\dot{r}_b}{w}, \tag{4.34}$$

$$A_5 = r_b - A_3, \tag{4.35}$$

where r_b, $\dot{r}_b$, θ_b, $\dot{\theta}_b$ and $\Delta r_{act,b}$ is the leg length, radial velocity, leg angle, angular velocity and linear actuator displacement at the instant between the transition of single support and double support phases, respectively.

The equation (3.10) for the angular velocity of the MD-SLIP model is modified for the single support phase of the MDB-SLIP model as

$$\dot{\theta} = C_2\cos(\theta) + B_4, \tag{4.36}$$

where C_2 is a free control parameter and $B_4 = \dot{\theta}_b - C_2\cos(\theta_b)$. Then, the solution for the leg angle can be obtained as

$$\theta(t) = \frac{\pi}{2} + 2\text{atan}\left(\frac{C_2 - B_5\tanh\left(\frac{B_5 t}{2} + B_6\right)}{B_4}\right), \tag{4.37}$$

where B_5 and B_6 are defined as

$$B_5 := \sqrt{C_2^2 - B_4^2}, \tag{4.38}$$

$$B_6 := \text{atanh}\left(\frac{C_2 - B_4\tan\left(\frac{\theta_b - \frac{\pi}{2}}{2}\right)}{B_5}\right). \tag{4.39}$$

Remark 5. *Note that in MD-SLIP model we have extra control parameters C_0 in (3.9) and C_1 in (3.10). Here in MDB-SLIP model we choose not to utilize*

these control parameters since we have other free control parameters available to control the locomotion. However, obviously these parameters could also be utilized in (4.28) and (4.36), if desired. This point requires and deserves further analysis and is left as a future work. ■

4.2.3 Solving Double Support Dynamics

As in single support dynamics, double support dynamics also have no exact analytical solution due to non-integrability of the equations of motion. Choosing appropriate function for $\Delta r_{act,r}$, $\Delta r_{act,f}$, τ_r and τ_f in (4.24)-(4.27) may result exact analytical solutions. Similar to the approach presented in Chapter 3, we will utilize partial feedback linearization concept to solve the equations of motion in (4.23) by cancelling some nonlinear terms and enforcing some desired trajectory for point mass body to follow.

First, we start by deriving the equations of motion in polar coordinates, which is centered at the midpoint of the two leg's contact points with the ground (illustrated in Figure 4.5). The radial and angular accelerations can be obtained as

$$\begin{aligned}\ddot{r} =& -2kr + r\dot{\theta}^2 - \cos\theta + \frac{\tau_r a\cos\theta}{r^2+a^2-2ar\sin\theta} - \frac{\tau_f a\cos\theta}{r^2+a^2+2ar\sin\theta} \\ &+ \frac{k\left(1+\Delta r_{act,r} - \dfrac{c}{k}\dfrac{r\dot{r} - a\dot{r}\sin\theta - ar\dot{\theta}\cos\theta}{\sqrt{r^2+a^2-2ar\sin\theta}}\right)(r - a\sin\theta)}{\sqrt{r^2+a^2-2ar\sin\theta}} \\ &+ \frac{k\left(1+\Delta r_{act,f} - \dfrac{c}{k}\dfrac{r\dot{r} + a\dot{r}\sin\theta + ar\dot{\theta}\cos\theta}{\sqrt{r^2+a^2+2ar\sin\theta}}\right)(r + a\sin\theta)}{\sqrt{r^2+a^2+2ar\sin\theta}},\end{aligned} \tag{4.40}$$

$$
\begin{aligned}
r\ddot{\theta} = &-2\dot{r}\dot{\theta} + \sin\theta + \frac{\tau_r\left(r - a\sin\theta\right)}{r^2 + a^2 - 2ar\sin\theta} + \frac{\tau_f\left(r + a\sin\theta\right)}{r^2 + a^2 + 2ar\sin\theta} \\
&- \frac{k\left(1 + \Delta r_{act,r} - \dfrac{c}{k}\dfrac{r\dot{r} - a\dot{r}\sin\theta - ar\dot{\theta}\cos\theta}{\sqrt{r^2 + a^2 - 2ar\sin\theta}}\right)a\cos\theta}{\sqrt{r^2 + a^2 - 2ar\sin\theta}} \\
&+ \frac{k\left(1 + \Delta r_{act,f} - \dfrac{c}{k}\dfrac{r\dot{r} + a\dot{r}\sin\theta + ar\dot{\theta}\cos\theta}{\sqrt{r^2 + a^2 + 2ar\sin\theta}}\right)a\cos\theta}{\sqrt{r^2 + a^2 + 2ar\sin\theta}},
\end{aligned}
\tag{4.41}
$$

respectively. Here a is the half of the distance between the two toes' contact points as illustrated in Figure 4.5.

To simplify the equations (4.40) and (4.41), rear and front leg linear actuator displacements are chosen as

$$
\Delta r_{act,r} = \left(\frac{r\dot{r} - a\dot{r}\sin\theta - ar\dot{\theta}\cos\theta}{\sqrt{r^2 + a^2 - 2ar\sin\theta}} - \dot{r}_{r,td}\right)\frac{c}{k} + \Delta r_{act,r,td}, \tag{4.42}
$$

$$
\Delta r_{act,f} = \left(\frac{r\dot{r} + a\dot{r}\sin\theta + ar\dot{\theta}\cos\theta}{\sqrt{r^2 + a^2 + 2ar\sin\theta}} - \dot{r}_{f,td}\right)\frac{c}{k} + \Delta r_{act,f,td}, \tag{4.43}
$$

respectively, where td subscripted variables are the values at touchdown instant.

By substituting equations (4.42) and (4.43) in (4.40) and (4.41) the radial and angular acceleration become

$$
\begin{aligned}
\ddot{r} = -2kr + r\dot{\theta}^2 - \cos\theta &+ \frac{\tau_r a\cos\theta}{r^2 + a^2 - 2ar\sin\theta} - \frac{\tau_f a\cos\theta}{r^2 + a^2 + 2ar\sin\theta} \\
&+ \frac{\left(k\left(1 + \Delta r_{act,r,td}\right) - c\dot{r}_{r,td}\right)\left(r - a\sin\theta\right)}{\sqrt{r^2 + a^2 - 2ar\sin\theta}} \\
&+ \frac{\left(k\left(1 + \Delta r_{act,f,td}\right) - c\dot{r}_{f,td}\right)\left(r + a\sin\theta\right)}{\sqrt{r^2 + a^2 + 2ar\sin\theta}},
\end{aligned}
\tag{4.44}
$$

$$
\begin{aligned}
r\ddot{\theta} = -2\dot{r}\dot{\theta} + \sin\theta &+ \frac{\tau_r\left(r - a\sin\theta\right)}{r^2 + a^2 - 2ar\sin\theta} + \frac{\tau_f\left(r + a\sin\theta\right)}{r^2 + a^2 + 2ar\sin\theta} \\
&- \frac{\left(k\left(1 + \Delta r_{act,r,td}\right) - c\dot{r}_{r,td}\right)a\cos\theta}{\sqrt{r^2 + a^2 - 2ar\sin\theta}} \\
&+ \frac{\left(k\left(1 + \Delta r_{act,f,td}\right) - c\dot{r}_{f,td}\right)a\cos\theta}{\sqrt{r^2 + a^2 + 2ar\sin\theta}},
\end{aligned}
\tag{4.45}
$$

respectively.

Similar to the approach used in the MD-SLIP model, we propose to use the following equation for the radial dynamics

$$r(t) = A_6 + A_7 \sin(w_{DS} t) + C_3 \cos(w_{DS} t), \tag{4.46}$$

where C_3 is a free control parameter, $w_{DS} := \sqrt{2k}$, $A_6 = r_{td} - C_3$ and $A_7 = \dot{r}_{td}/w_{DS}$. Here the parameters A_6 and A_7 are calculated by using the following boundary conditions

$$r(0) = r_{td}, \tag{4.47}$$

$$\dot{r}(0) = \dot{r}_{td}, \tag{4.48}$$

$$\theta(0) = \theta_{td}, \tag{4.49}$$

$$\dot{\theta}(0) = \dot{\theta}_{td}. \tag{4.50}$$

Note that one can ensure that (4.46) form an exact solution for (4.40) via appropriate selection of τ_r and τ_f. Different than the MD-SLIP model, we set $C_0 = 0$, since the free control parameter C_3 is sufficient for solving double support dynamics, see Remark 5. Similarly, the angular velocity is chosen as

$$\dot{\theta} = C_4 \cos\theta + B_7, \tag{4.51}$$

where C_4 is a free control parameter and B_7 is calculated by using the boundary conditions (4.49) and (4.50) as $B_7 = \dot{\theta}_{td} - C_4 \cos\theta_{td}$.

Solving the angular velocity equation (4.51) for the angular position results in

$$\theta(t) = \frac{\pi}{2} + 2\text{atan}\left(\frac{C_4 - B_8 \tanh\left(\frac{B_8 t}{2} + B_9\right)}{B_7}\right), \tag{4.52}$$

where B_8 and B_9 are defined as

$$B_8 := \sqrt{C_4^2 - B_7^2}, \tag{4.53}$$

$$B_9 := \text{atanh}\left(\frac{C_4 - B_7 \tan\left(\frac{\theta_{td} - \frac{\pi}{2}}{2}\right)}{B_8}\right). \tag{4.54}$$

The required torque inputs τ_r and τ_f can be calculated by solving equations

(4.44) and (4.45) by using the solutions of (4.46) and (4.52) as

$$\begin{aligned}\tau_r = &\frac{r_r^2}{2r}\left(2\dot{r}\dot{\theta} - C_5 r\dot{\theta}\sin\theta - \sin\theta\right)\\ &+ \frac{r_r^2\,(r + a\sin\theta)}{2ar\cos\theta}\left(2kr_{td} - 2C_3k - r\dot{\theta}^2 + \cos\theta\right)\\ &- \frac{r_r^2 r_f}{2ar\cos\theta}\left(k\left(1 + \Delta r_{act,f,td}\right) - c\dot{r}_{f,td}\right)\\ &- \frac{r_r(r^2 - a^2)}{2ar\cos\theta}\left(k\left(1 + \Delta r_{act,r,td}\right) - c\dot{r}_{r,td}\right),\end{aligned} \tag{4.55}$$

$$\begin{aligned}\tau_f = &\frac{r_f^2}{2r}\left(2\dot{r}\dot{\theta} - C_5 r\dot{\theta}\sin\theta - \sin\theta\right)\\ &- \frac{r_f^2\,(r - a\sin\theta)}{2ar\cos\theta}\left(2kr_{td} - 2C_3k - r\dot{\theta}^2 + \cos\theta\right)\\ &+ \frac{r_f^2 r_r}{2ar\cos\theta}\left(k\left(1 + \Delta r_{act,r,td}\right) - c\dot{r}_{r,td}\right)\\ &+ \frac{r_f(r^2 - a^2)}{2ar\cos\theta}\left(k\left(1 + \Delta r_{act,f,td}\right) - c\dot{r}_{f,td}\right),\end{aligned} \tag{4.56}$$

respectively, where the variables r_r and r_f are defined as

$$r_r := \sqrt{r^2 + a^2 - 2ar\sin\theta}, \tag{4.57}$$

$$r_f := \sqrt{r^2 + a^2 + 2ar\sin\theta}, \tag{4.58}$$

respectively. Note that (4.52) is an exact solution of (4.41). Different than the MD-SLIP model, we set $C_1 = 0$, since the free control parameter C_4 is sufficient for solving double support dynamics, see Remark 5.

To determine the end of the double support phase, the liftoff condition needs to be determined. The liftoff occurs when the rear leg loses the ground contact, which means the ground reaction force becomes zero. The ground reaction force of the rear leg, $F_{GRF,r}$, is given as

$$F_{GRF,r} = F_{r,r}\cos\theta_r - F_{a,r}\sin\theta_r, \tag{4.59}$$

where rear leg radial and angular forces $F_{r,r}$ and $F_{a,r}$ are given by (4.24) and (4.26), respectively. Finding an analytical expression for the solution of (4.59) is challenging due to its highly nonlinear nature. This led us to solve it numerically to determine the end of the double support phase.

4.2.4 Apex to Apex Return Map

As mentioned earlier, the locomotion of the MDB-SLIP model is divided into consecutively repeating subphases of locomotion. In our analysis, we will use the apex point as the starting point which means we will perform the analysis from apex to apex map. Therefore, we need to construct the apex to apex map of the MDB-SLIP model. The state variables of the initial apex are defined as initial apex height z_{a0}, initial apex horizontal velocity $\dot{y}_{a0}$, initial apex rear leg linear actuator displacement $\Delta r_{act,r,a0}$ and initial apex rear leg toe horizontal displacement $\Delta y_{toe,r,a0} := y_{toe,r,a} - y_a$. After locomotion starts from an initial apex position, the point mass follows the trajectory defined by the equations (3.1) and (3.2), which are solved as (3.9) and (3.17), until front leg toe touches to the ground. Hence the function for the single support phase can be written as

$$(r_{r,td}, \dot{r}_{r,td}, \theta_{r,td}, \dot{\theta}_{r,td}) = G_a^{td}(z_{a0}, \dot{y}_{a0}, \Delta r_{act,r,a0}, \Delta y_{toe,r,a0}), \tag{4.60}$$

where the subscript td indicates the touchdown and G_a^{td} is the apex to touchdown map, respectively. Note that the map G_a^{td} depends on θ_{td}, $\Delta r_{act,td}$ and C_2 which are considered as control parameters.

After the front leg toe touches the ground, the point mass starts to follow the double support dynamics (4.40) and (4.41) which are solved as (4.46) and (4.52). The function for the double support phase can be written as

$$(r_{lo}, \dot{r}_{lo}, \theta_{lo}, \dot{\theta}_{lo}) = G_{td}^{lo}(r_{td}, \dot{r}_{td}, \theta_{td}, \dot{\theta}_{td}), \tag{4.61}$$

where the subscript lo indicates the liftoff and G_{td}^{lo} is the touchdown to liftoff map. Note that the map G_{td}^{lo} depends on the control parameters θ_{td}, $\Delta r_{act,td}$, C_3 and C_4, see (4.46) and (4.52).

The liftoff event occurs, when the rear leg toe loses ground contact. After this instant the point mass follows the single support phase again until apex point. This phase can be represented as

$$(z_{a1}, \dot{y}_{a1}, \Delta r_{act,f,a1}, \Delta y_{toe,f,a1}) = G_{lo}^{a}(r_{f,lo}, \dot{r}_{f,lo}, \theta_{f,lo}, \dot{\theta}_{f,lo}), \tag{4.62}$$

where G^a_{lo} is the liftoff to apex map. Note that the map depends on the control parameter C_2.

After describing necessary functions for the phases of the locomotion, the apex to apex map can be written as

$$G^a_a = G^a_{lo} \circ W_{lo} \circ G^{lo}_{td} \circ W_{td} \circ G^{td}_a, \tag{4.63}$$

where G^a_a represents apex to apex return map. The functions W_{lo} and W_{td} are the required transformations to jump from one coordinate frame to the next one.

The next apex state can be determined by using the apex to apex map and the current apex state as

$$(z_{a1}, \dot{y}_{a1}, \Delta r_{act,f,a1}, \Delta y_{toe,f,a1}) = G^a_a(z_{a0}, \dot{y}_{a0}, \Delta r_{act,r,a0}, \Delta y_{toe,r,a0}), \tag{4.64}$$

where z_{a1}, $\dot{y}_{a1}$, $\Delta r_{act,f,a1}$ and $\Delta y_{toe,f,a1}$ stands for apex height, apex horizontal velocity, apex front leg linear actuator displacement and apex front leg toe horizontal displacement, respectively. At this point, the rear leg sets its angle to θ_{td} and becomes front leg. As such, the locomotion continues by consecutive activation of the apex to apex map. The apex to apex map G^a_a depends on the control parameters θ_{td}, $\Delta r_{act,td}$, C_2, C_3 and C_4. The next step will be choosing these parameters appropriately to obtain stable gait patterns.

Remark 6. *As noted in Remark 5, in MD-SLIP model we utilized control parameters C_0 and C_1 in (3.9) and (3.10), respectively, but we choose not to utilize these parameters in MDB-SLIP model. If we choose to use these parameters as well, the resulting apex to apex map G^a_a given in (4.64) would depend on these parameters as well. This approach would increase the free parameters from 5 (θ_{td}, $\Delta r_{act,td}$, C_2, C_3, C_4) to 7, which obviously increases the computational complexity. Hence, to reduce the computational complexity, we choose not to utilize these parameters in MDB-SLIP model. However, as noted in Remark 5, these parameters could also be utilized and their effect on the stability of fixed points could also be investigated by using the approach presented in this chapter. This approach is left as a future work.* ■

4.3 Periodic Gaits and Their Stability in MDB-SLIP Model

The fixed points of the map G_a^a result periodic gaits for the MDB-SLIP model. The state of the fixed point is defined as $(z_a^*, \dot{y}_a^*, \Delta r_{act,a}^*, \Delta y_{toe,a}^*)$ and it is the solution of the equation

$$(z_a^*, \dot{y}_a^*, \Delta r_{act,a}^*, \Delta y_{toe,a}^*) = G_a^a(z_a^*, \dot{y}_a^*, \Delta r_{act,a}^*, \Delta y_{toe,a}^*). \tag{4.65}$$

We will use the Jacobian matrix analysis to determine the stability of the locomotion. The eigenvalues of the Jacobian matrix of the apex to apex map G_a^a will be evaluated at the fixed point. The Jacobian matrix for G_a^a is defined as

$$J_{MDB-SLIP} := \begin{bmatrix} \frac{\partial z_{a1}}{\partial z_{a0}} & \frac{\partial z_{a1}}{\partial \dot{y}_{a0}} & \frac{\partial z_{a1}}{\partial \Delta r_{act,a0}} & \frac{\partial z_{a1}}{\partial \Delta y_{toe,a0}} \\ \frac{\partial \dot{y}_{a1}}{\partial z_{a0}} & \frac{\partial \dot{y}_{a1}}{\partial \dot{y}_{a0}} & \frac{\partial \dot{y}_{a1}}{\partial \Delta r_{act,a0}} & \frac{\partial \dot{y}_{a1}}{\partial \Delta y_{toe,a0}} \\ \frac{\partial \Delta r_{act,a1}}{\partial z_{a0}} & \frac{\partial \Delta r_{act,a1}}{\partial \dot{y}_{a0}} & \frac{\partial \Delta r_{act,a1}}{\partial \Delta r_{act,a0}} & \frac{\partial \Delta r_{act,a1}}{\partial \Delta y_{toe,a0}} \\ \frac{\partial \Delta y_{toe,a1}}{\partial z_{a0}} & \frac{\partial \Delta y_{toe,a1}}{\partial \dot{y}_{a0}} & \frac{\partial \Delta y_{toe,a1}}{\partial \Delta r_{act,a0}} & \frac{\partial \Delta y_{toe,a1}}{\partial \Delta y_{toe,a0}} \end{bmatrix}. \tag{4.66}$$

Since other bipedal SLIP models do not have actuators on them, the Jacobian matrix is different for them and it is defined as

$$J_{B-SLIP} := \begin{bmatrix} \frac{\partial z_{a1}}{\partial z_{a0}} & \frac{\partial z_{a1}}{\partial \dot{y}_{a0}} & \frac{\partial z_{a1}}{\partial \Delta y_{toe,a0}} \\ \frac{\partial \dot{y}_{a1}}{\partial z_{a0}} & \frac{\partial \dot{y}_{a1}}{\partial \dot{y}_{a0}} & \frac{\partial \dot{y}_{a1}}{\partial \Delta y_{toe,a0}} \\ \frac{\partial \Delta y_{toe,a1}}{\partial z_{a0}} & \frac{\partial \Delta y_{toe,a1}}{\partial \dot{y}_{a0}} & \frac{\partial \Delta y_{toe,a1}}{\partial \Delta y_{toe,a0}} \end{bmatrix}. \tag{4.67}$$

Since we do not have an analytic solution to the apex to apex maps of the locomotion of the models, we need to approximate the Jacobian matrices and solve them numerically. We started by using a simple approximation as defined

in Section 3.2. However, we observed that, the results are not satisfactory. As a result, we decided to use a numerical Jacobian matrix calculation approach based on Romberg extrapolation [95] rather than previously used simple approximation.

The non-dimensional values used for parameters and initial conditions during simulations are $z_a \in [0.900 - 0.995]$, $\dot{y}_a \in [0.16 - 0.64]$ and $k \in [12.75 - 51.00]$.

Remark 7. *Note that the ranges defined for parameters and initial conditions in order to simulate MD-SLIP model in Section 3.2 and MDB-SLIP model show different characteristics. Since the hopping behaviour of the MD-SLIP model is investigated, the apex height is greater than leg length and apex speed can have greater values. However, in MDB-SLIP model, the walking behaviour is examined, which limits the height of the body mass as well as the apex height to leg length and limits the apex speed to velocities that are possible to walk.* ■

4.3.1 Optimizing Control Parameters for Minimizing Magnitude of Eigenvalues of Jacobian Matrix

The goal of this section is to investigate the stability of the periodic motion for the proposed MDB-SLIP model. In order to begin stability analysis, fixed points of the corresponding Poincaré map should be extracted. To obtain periodic gaits, we can use control parameters θ_{td}, $\Delta r_{act,td}$, C_2, C_3 and C_4. However, the solution that gives fixed point is not unique for a given initial state. Therefore, we need to minimize the solutions by an appropriate optimization.

When we examine the eigenvalues of the Jacobian matrix of the apex to apex map, we observed that one of the eigenvalues is on the unit circle, which is a characteristic property for the periodic motion, see e.g. [90]. Therefore, we use the magnitudes of the other eigenvalues to determine the stability of the gaits. Magnitude of the maximum eigenvalue will be used as a stability measure. More precisely, let λ_1, λ_2, λ_3 and λ_4 be the eigenvalues of the Jacobian matrix where $|\lambda_1| = 1$. Then the optimization problem considered in this section is given as

$$\min_{\theta_{td},\Delta r_{act,td},C_2,C_3,C_4} \max\{|\lambda_2|, |\lambda_3|, |\lambda_4|\}. \tag{4.68}$$

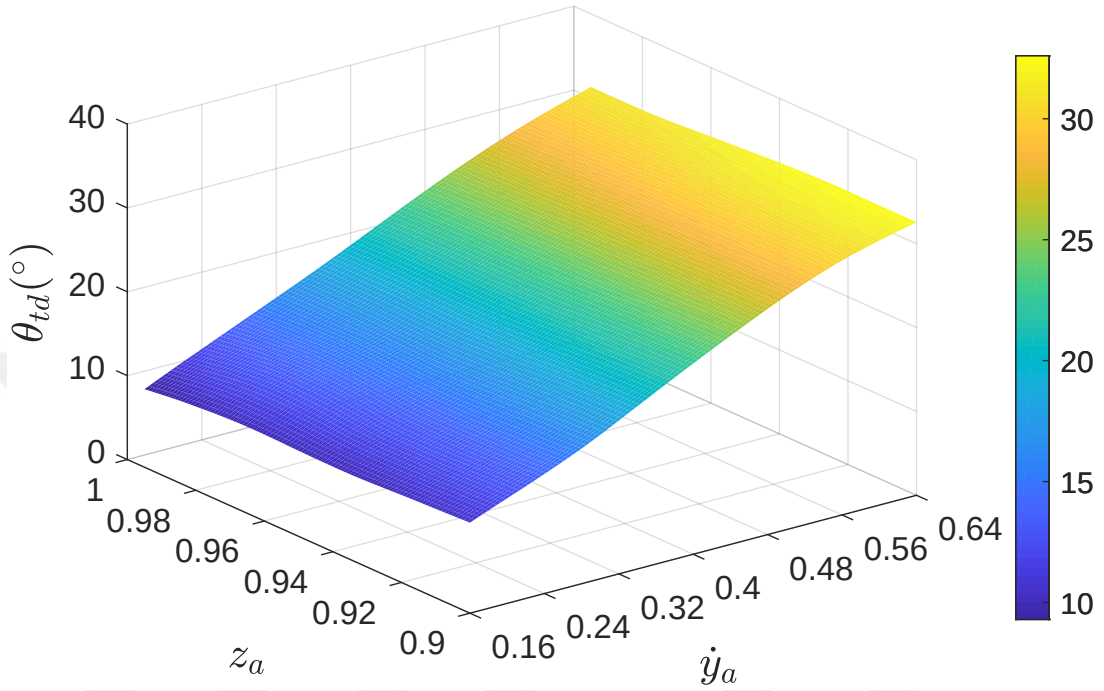

Figure 4.6: Touchdown leg angle that results minimal eigenvalues for MDB-SLIP model.

As a result we obtained stable fixed point manifolds for the apex to apex map. The resultant θ_{td} and $\Delta r_{act,td}$ are illustrated in Figure 4.6 and Figure 4.7, respectively. An important observation is that the touchdown angle θ_{td} that results in periodic motion is also more or less proportional to the apex horizontal velocity $\dot{y}_a$ as in Figure 4.6. Note that this property is also observed in the original SLIP template and [1] designed touchdown angle controllers to regulate apex horizontal velocity based on this principle. Another important observation is that the linear actuator displacement $\Delta r_{act,td}$ is shortening while the point mass has lower heights. This makes the toe height more or less same across all initial points. Similarly, smooth affine dependence of $\Delta r_{act,td}$ to the initial height and initial horizontal velocity allows designing simple controllers.

The result of (4.68) is illustrated in Figure 4.8. It is observed that, the magnitudes of the eigenvalues of the Jacobian matrix of the periodic gaits of the MDB-SLIP model result values smaller that 0.2. This means we have a model whose gaits are stable all over the region we made simulations. This shows us

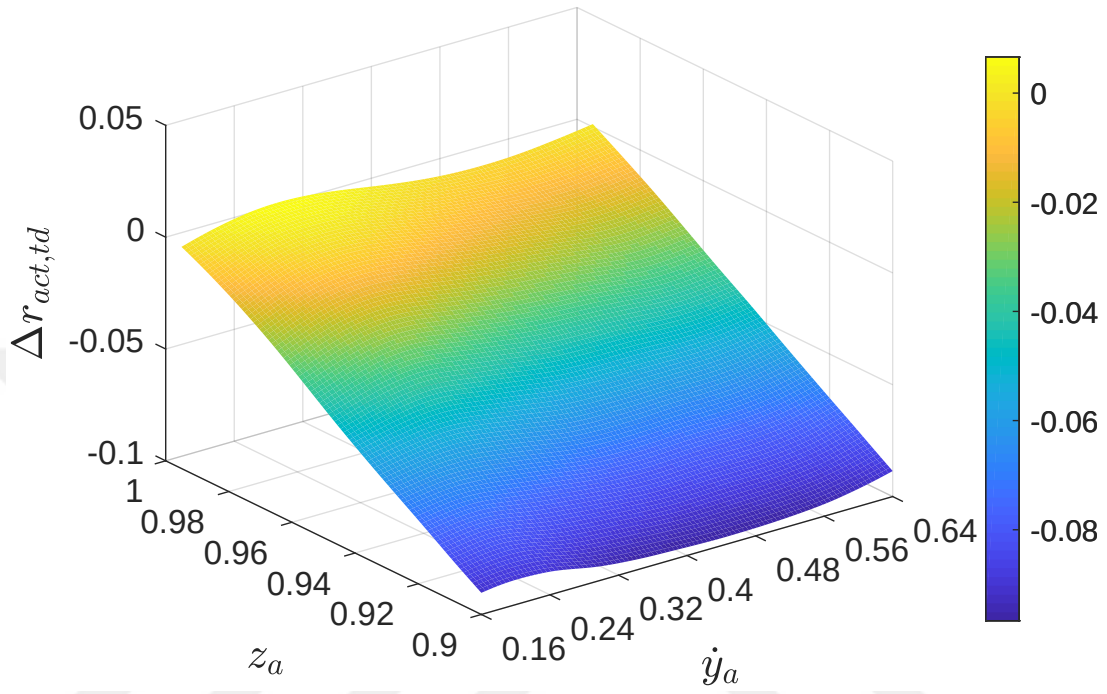

Figure 4.7: Touchdown linear actuator displacement that results minimal eigenvalues for MDB-SLIP model.

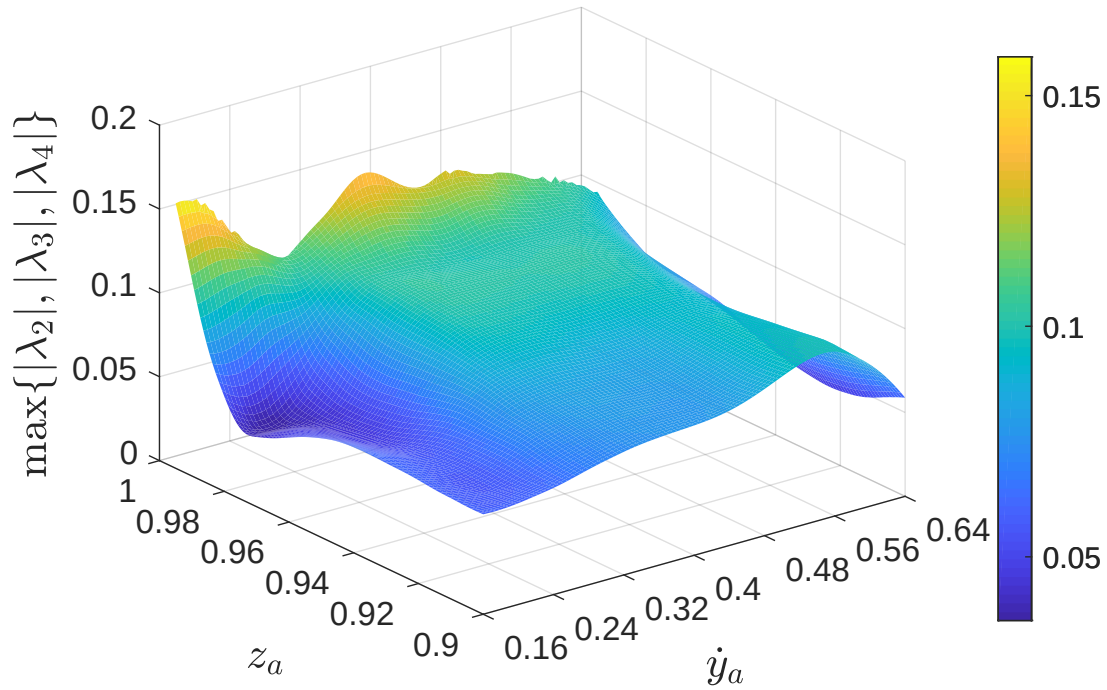

Figure 4.8: Touchdown linear actuator displacement that results minimal eigenvalues for MDB-SLIP model.

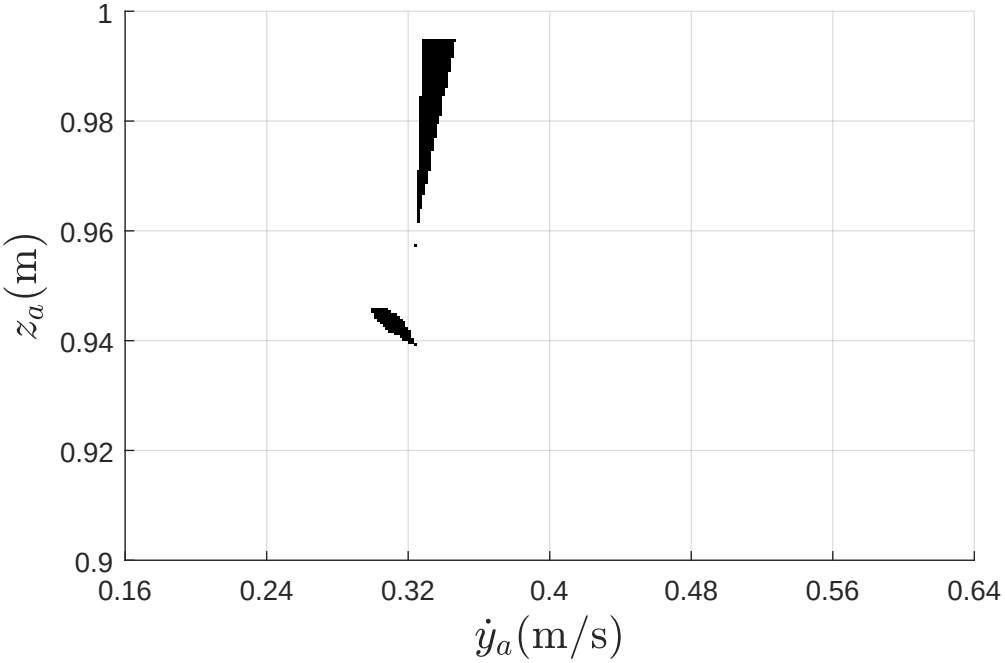

Figure 4.9: The stable periodic gaits of the B-SLIP model is illustrated with black colored region.

that we also have some margin for other variables to optimize.

Note that investigating the fixed points of periodic gaits requires the conservation of energy. In our model, we can compensate for energy losses using our actuators. However, for the case of B-SLIP, such a compensation may not be possible. Therefore, for the sake of obtaining a fair comparison of stability characteristics, we choose damping to be zero for the B-SLIP model. Hence, we can obtain the fixed points and observe their stability. Similarly, we can find the fixed point for the AT-SLIP and LAT-SLIP models as well. However, our investigations showed that B-SLIP model outperforms the AT-SLIP and LAT-SLIP models, so we compare our MDB-SLIP model only with the B-SLIP model.

Figure 4.9 illustrates the region of stability for the B-SLIP model. Note that as seen in Figure 4.8, our MDB-SLIP model is stable on the whole desired range. However, the B-SLIP model is stable only in a small portion of the desired range. Hence, the MDB-SLIP model exhibits much better stability characteristics as

compared to other models especially due to the availability of our actuators.

Remark 8. *Note that there are some existing studies which aims to achieve minimal control of bipedal legged locomotion in a two-step strategy [96]. Actually, this study shows that it is not possible to generate arbitrary fixed points in a single stride for a bipedal legged locomotion model [96]. However, utilizing such a method, with a two-step control strategy yields period-2 stability characteristics. On the contrary, the goal of this study is to investigate stability characteristics of bipedal locomotion for period-1 gaits. Therefore, we first show the stability regions for the period-1 motion for the bipedal legged locomotion models in the literature and then design period-1 deadbeat controllers. However, we need to note that if the sole goal is to obtain larger stability regions for bipedal legged locomotion models, considering higher period motions as well, one may need to utilize the two-step analysis and control methods as proposed in [96] to consider period-2 motion of the associated models. This point requires and deserves further investigation. Since our main aim is to analyze period-1 motions, this point is left as a possible future research topic.* ■

4.3.2 Optimizing Control Parameters for Robustness to Parametric Uncertainty

Our goal in this section is to optimize our control parameters towards obtaining a stable gait, which is robust to parametric uncertainty in initial conditions. Here we consider "successful walking gait" as our desired gait of interest for which we seek to maximize the robustness to parametric uncertainty.

To achieve this we first define what we mean by "successful walking gait" to make our problem definition more clear. A "successful walking gait" should have the following properties

- The point mass should not collide with the ground.
- The simulation results should be compatible with physical laws such as any

of toes should not go inside the ground, the leg length should not result in a negative value, etc.

- The gait should not switch to running gait, which requires both legs to lose contact with the ground simultaneously.

Having defined the requirements for "successful walking gait", now we need to define our robustness criteria. Let the walking gait start from an initial condition

$$x_0 = \begin{bmatrix} z_{a0} \\ \dot{y}_{a0} \\ \Delta r_{act,r,a0} \\ \Delta y_{toe,r,a0} \end{bmatrix} \tag{4.69}$$

and assume that it continues its locomotion as a "successful walking gait". Our problem of interest is to find maximum perturbation values we can add to this initial conditions as

$$\tilde{x}_0 = \begin{bmatrix} z_{a0} \\ \dot{y}_{a0} \\ \Delta r_{act,r,a0} \\ \Delta y_{toe,r,a0} \end{bmatrix} \pm \underbrace{\begin{bmatrix} \delta_z \\ \delta_{\dot{y}} \\ \delta_{\Delta r_{act}} \\ \delta_{\Delta y_{toe}} \end{bmatrix}}_{\delta x_0} \tag{4.70}$$

such that we will still have a "successful walking gait". Now the optimization problem is to choose optimum control parameters, θ_{td}, $\Delta r_{act,td}$, C_2, C_3, C_4 such that norm of δx_0 is maximized. In a mathematical sense, the optimization problem is

$$\max_{\theta_{td},\Delta r_{act,td},C_2,C_3,C_4} \{\|\delta x_0\| \,|\, \max\{|\lambda_2|,|\lambda_3|,|\lambda_4|\} < 0.9\}. \tag{4.71}$$

ensuring that maximum of the eigenvalues is less than 0.9 to guarantee stability with a safety margin of 0.1.

The resulting bounds of state variables for parametric uncertainty are illustrated in Figure 4.10, Figure 4.11, Figure 4.12 and Figure 4.13. These figures illustrate how well our model can preserve stability for the computed perturbation ranges of the initial conditions. The perturbations ranges computed in this part is capable of handling small noisy perturbations either in our measurements

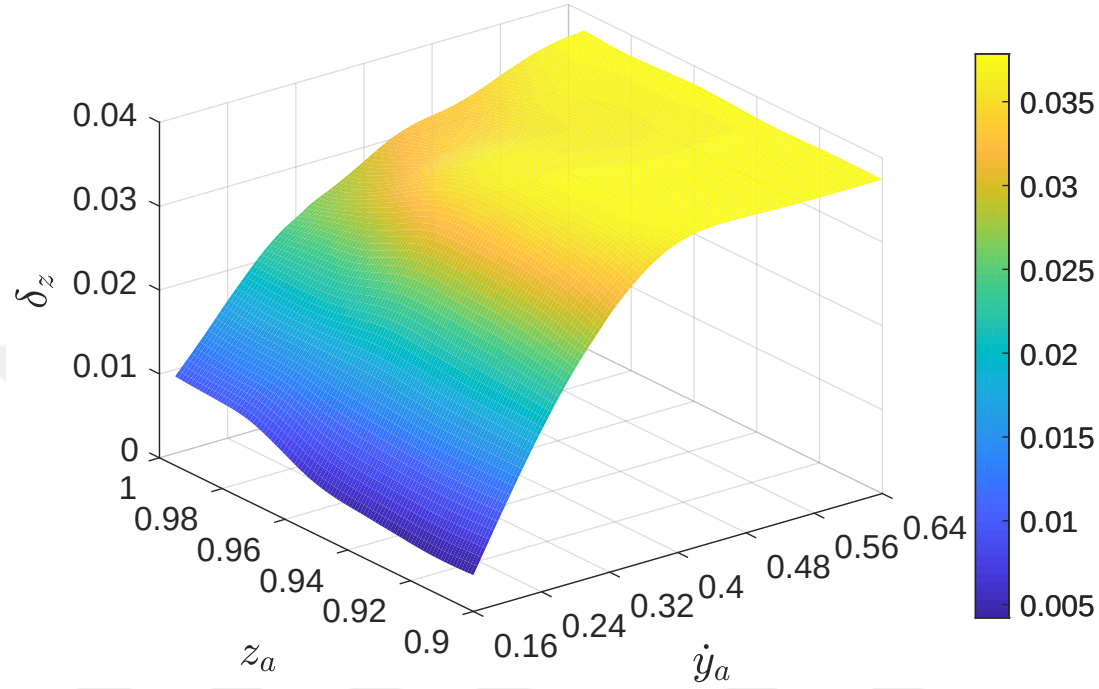

Figure 4.10: Maximal δ_z bound obtained through optimization for the MDB-SLIP model.

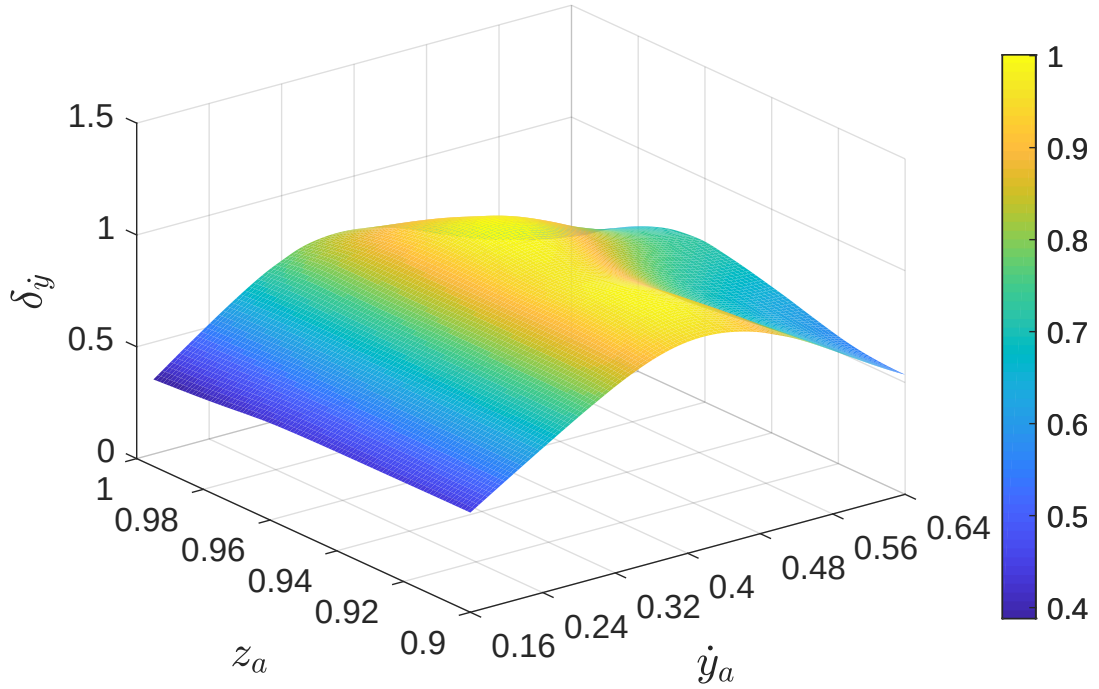

Figure 4.11: Maximal $\delta_{\dot{y}}$ bound obtained through optimization for the MDB-SLIP model.

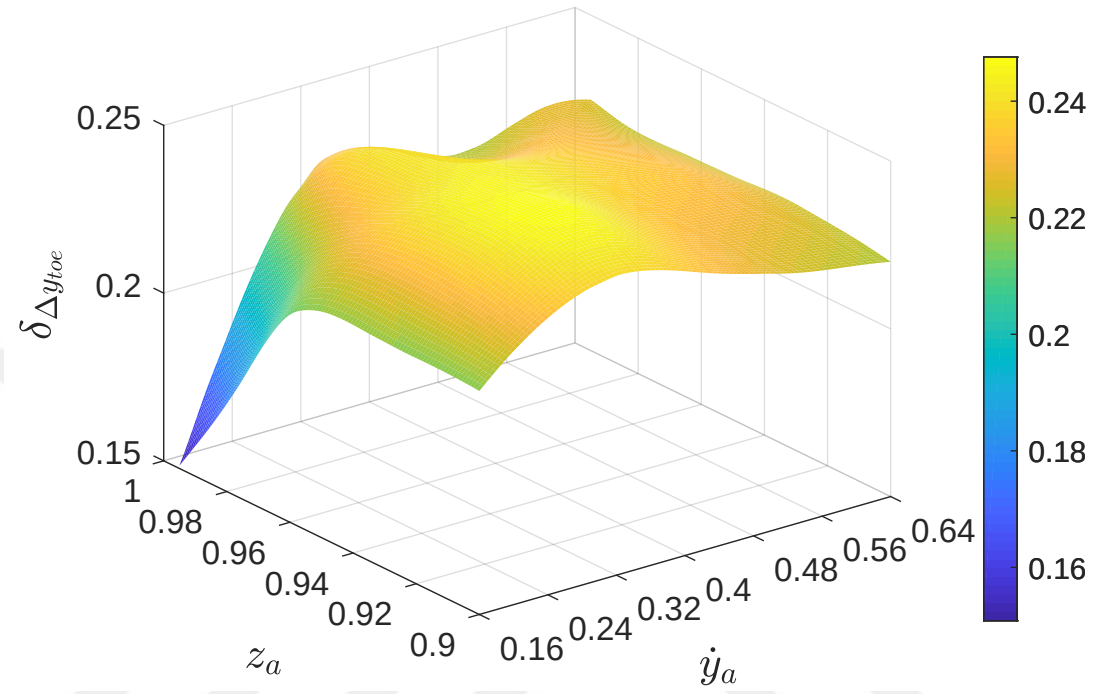

Figure 4.12: Maximal $\delta_{\Delta r_{act}}$ bound obtained through optimization for the MDB-SLIP model.

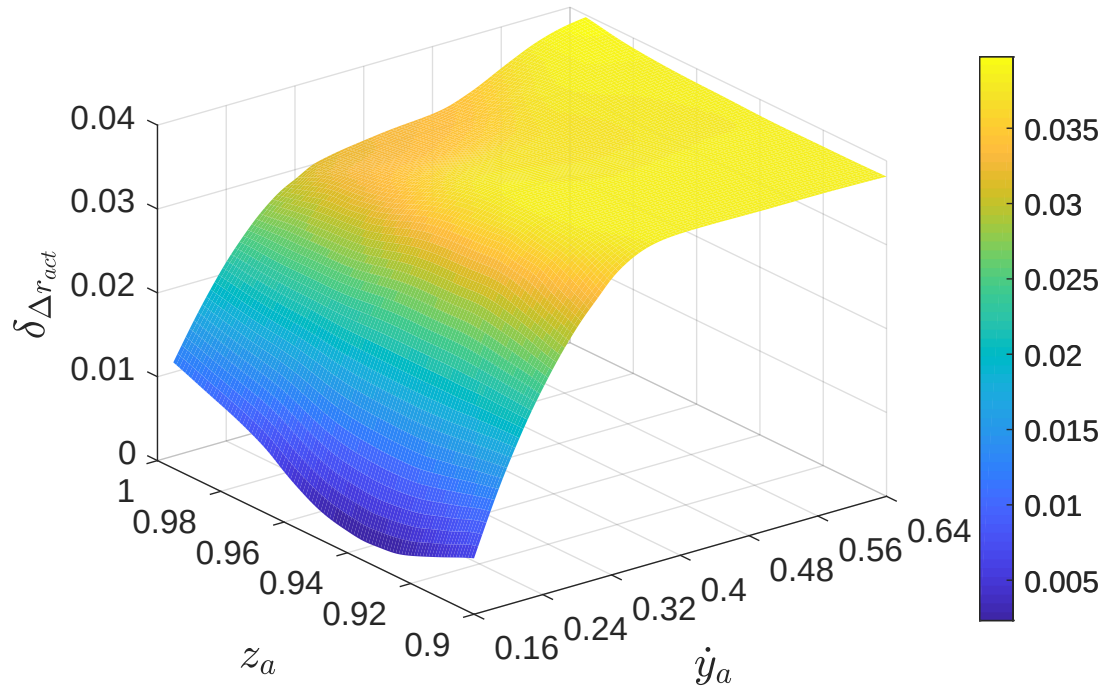

Figure 4.13: Maximal $\delta_{\Delta y_{toe}}$ bound obtained through optimization for the MDB-SLIP model.

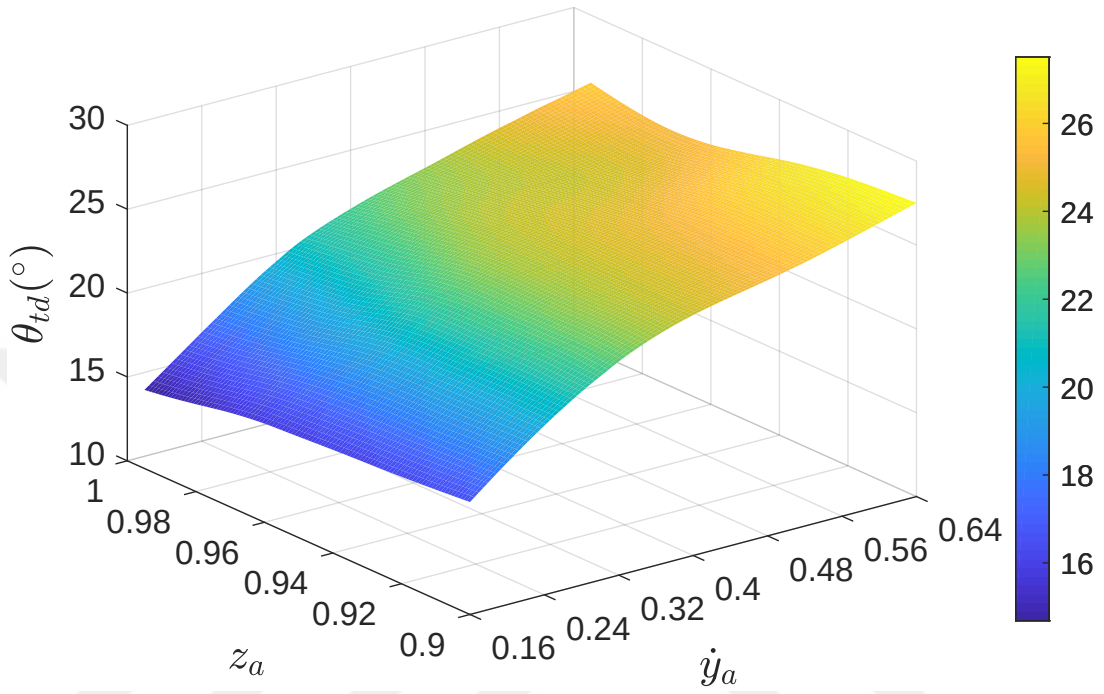

Figure 4.14: Touchdown leg angle that results maximal bounds for MDB-SLIP model.

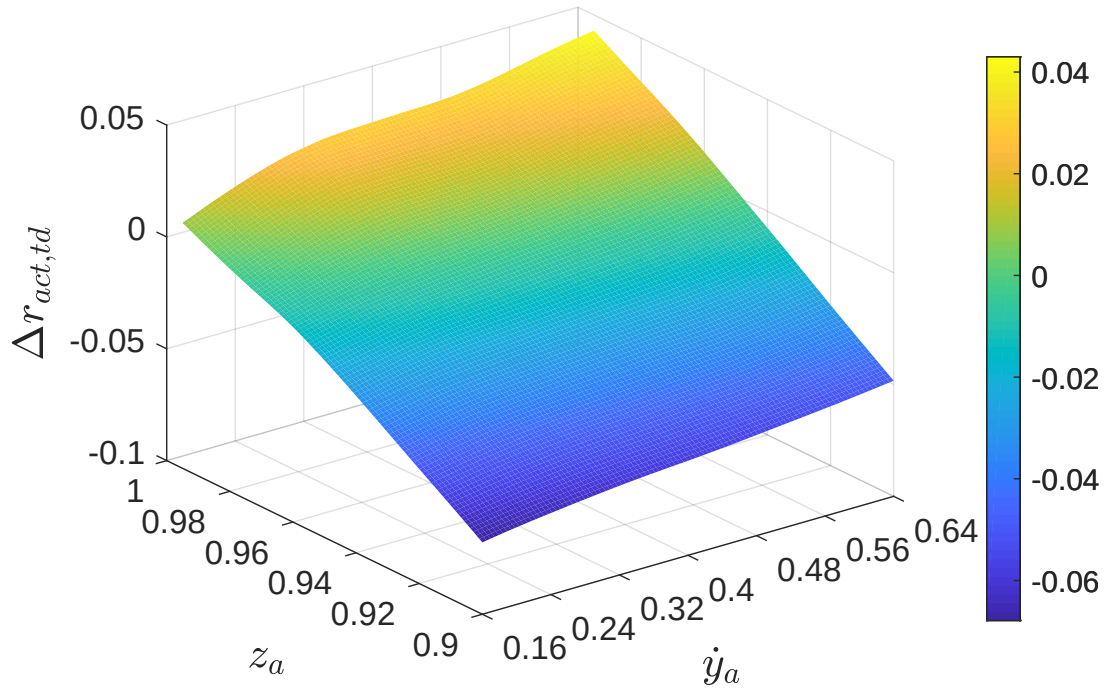

Figure 4.15: Touchdown linear actuator displacement that results maximal bounds for MDB-SLIP model.

or in the ground profile where the robot is walking on. The bounds are quite satisfactory for noisy perturbations, since we assume that our measurement errors will stay well below these bounds.

On the other hand, Figure 4.14 and Figure 4.15 illustrates the touchdown leg angle and the touchdown linear actuator displacement that results the maximal bounds for perturbations. Note that these parameters also exhibit almost affine dependence on initial height and initial horizontal velocity. Hence, we can also build simple predictors to compute touchdown leg angle and the linear actuator displacement based on given initial conditions.

Chapter 5

Performance of MDB-SLIP Model on Different Terrains

This chapter is devoted to performance analysis of different bipedal locomotion models on various terrain types such as sloped and noisy ground simulations. The models we are interested in are the B-SLIP, AT-SLIP, LAT-SLIP and MDB-SLIP models, which are introduced in Chapter 4. Note that the other models except the MDB-SLIP are recent studies used from literature for comparison purposes. To accomplish this goal, we first derive the equations of motion for the double support (DS) dynamics of the MDB-SLIP model on sloped ground. Then, considering our solution methodology for the standard MDB-SLIP model on flat ground, we propose similar solution strategies for the sloped ground case. In addition to open-loop locomotion analysis, we also present comparative investigations for the closed-loop walking performance on various rough terrains.

5.1 Solving Double Support Dynamics of MDB-SLIP Model for Sloped Ground

In this section, we explain the details of our solutions for the double support dynamics of the MDB-SLIP model for sloped ground. The proposed model and parameters on a sloped ground are illustrated in Figure 5.1 with the associated coordinate system. The double support dynamics for the sloped ground case (as the flat ground case) have no exact analytical solutions due to non-integrability of the equations of motion. Hence, similar to Chapter 4, we utilize partial feedback linearization to solve equations of motion by canceling nonlinear terms and enforcing desired body trajectories.

Our analysis starts by deriving the equations of motion in polar coordinates, whose center is virtually placed at the midpoint of the two leg's contact points with the ground as illustrated in Figure 5.1. Hence, the radial and angular

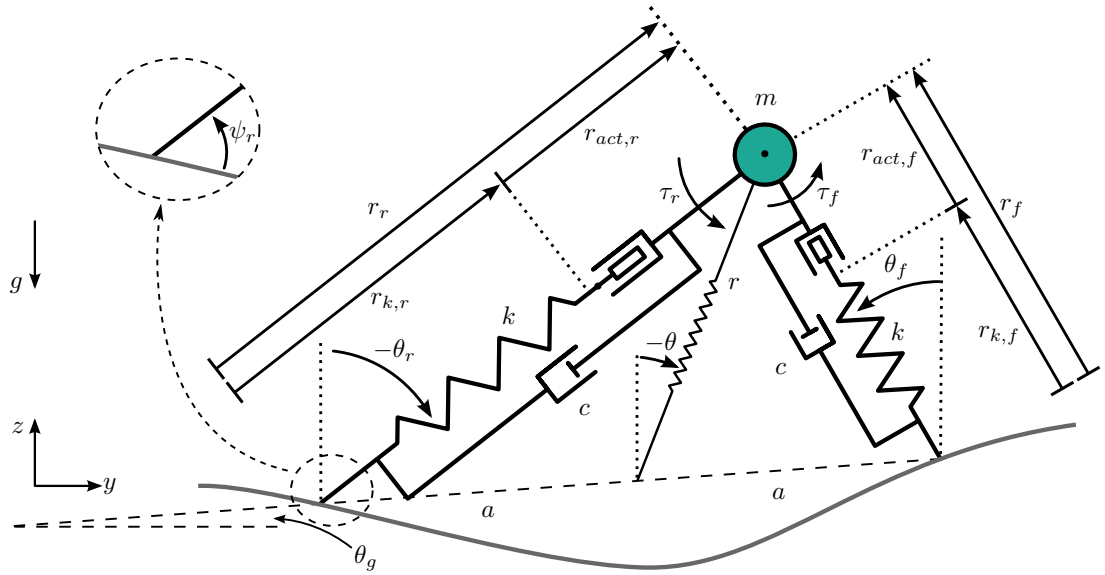

Figure 5.1: Multi-actuated dissipative bipedal SLIP model, coordinate system and model parameters for sloped ground. Different than the flat ground case (illustrated in Figure 4.5), we now give the necessary variables to solve the equations of motion for sloped ground.

accelerations can be obtained as

$$\begin{aligned}\ddot{r} =& -2kr + r\dot{\theta}^2 - \cos\theta + \frac{\tau_r a\cos(\theta-\theta_g)}{r^2+a^2-2ar\sin(\theta-\theta_g)} - \frac{\tau_f a\cos(\theta-\theta_g)}{r^2+a^2+2ar\sin(\theta-\theta_g)} \\ &+ \frac{k\left(1+\Delta r_{act,r} - \frac{c}{k}\frac{r\dot{r} - a\dot{r}\sin(\theta-\theta_g) - ar\dot{\theta}\cos(\theta-\theta_g)}{\sqrt{r^2+a^2-2ar\sin(\theta-\theta_g)}}\right)(r - a\sin(\theta-\theta_g))}{\sqrt{r^2+a^2-2ar\sin(\theta-\theta_g)}} \\ &+ \frac{k\left(1+\Delta r_{act,f} - \frac{c}{k}\frac{r\dot{r} + a\dot{r}\sin(\theta-\theta_g) + ar\dot{\theta}\cos(\theta-\theta_g)}{\sqrt{r^2+a^2+2ar\sin(\theta-\theta_g)}}\right)(r + a\sin(\theta-\theta_g))}{\sqrt{r^2+a^2+2ar\sin(\theta-\theta_g)}},\end{aligned} \tag{5.1}$$

$$\begin{aligned}r\ddot{\theta} =& -2\dot{r}\dot{\theta} + \sin\theta + \frac{\tau_r(r - a\sin(\theta-\theta_g))}{r^2+a^2-2ar\sin(\theta-\theta_g)} + \frac{\tau_f(r + a\sin(\theta-\theta_g))}{r^2+a^2+2ar\sin(\theta-\theta_g)} \\ &- \frac{k\left(1+\Delta r_{act,r} - \frac{c}{k}\frac{r\dot{r} - a\dot{r}\sin(\theta-\theta_g) - ar\dot{\theta}\cos(\theta-\theta_g)}{\sqrt{r^2+a^2-2ar\sin(\theta-\theta_g)}}\right)a\cos(\theta-\theta_g)}{\sqrt{r^2+a^2-2ar\sin(\theta-\theta_g)}} \\ &+ \frac{k\left(1+\Delta r_{act,f} - \frac{c}{k}\frac{r\dot{r} + a\dot{r}\sin(\theta-\theta_g) + ar\dot{\theta}\cos(\theta-\theta_g)}{\sqrt{r^2+a^2+2ar\sin(\theta-\theta_g)}}\right)a\cos(\theta-\theta_g)}{\sqrt{r^2+a^2+2ar\sin(\theta-\theta_g)}},\end{aligned} \tag{5.2}$$

respectively. The a terms here refers to the half distance between the two toes' contact points and θ_g represents the angle of the slope of the ground as shown in Figure 5.1.

To clarify (and simplify) the equations (5.1) and (5.2), we choose the rear and front leg linear actuator displacements as

$$\Delta r_{act,r} = \left(\frac{r\dot{r} - a\dot{r}\sin(\theta-\theta_g) - ar\dot{\theta}\cos(\theta-\theta_g)}{\sqrt{r^2+a^2-2ar\sin(\theta-\theta_g)}} - \dot{r}_{r,td}\right)\frac{c}{k} + \Delta r_{act,r,td}, \tag{5.3}$$

$$\Delta r_{act,f} = \left(\frac{r\dot{r} + a\dot{r}\sin(\theta-\theta_g) + ar\dot{\theta}\cos(\theta-\theta_g)}{\sqrt{r^2+a^2+2ar\sin(\theta-\theta_g)}} - \dot{r}_{f,td}\right)\frac{c}{k} + \Delta r_{act,f,td}, \tag{5.4}$$

respectively, where variables with subscript td corresponds to their values at the touchdown instant.

Plugging the equations (5.3) and (5.4) into (5.1) and (5.2), the radial and angular acceleration equations take the form

$$\begin{aligned}\ddot{r} = -2kr + r\dot{\theta}^2 - \cos\theta &+ \frac{\tau_r a\cos(\theta-\theta_g)}{r^2+a^2-2ar\sin(\theta-\theta_g)} - \frac{\tau_f a\cos(\theta-\theta_g)}{r^2+a^2+2ar\sin(\theta-\theta_g)} \\ &+ \frac{\left(k\left(1+\Delta r_{act,r,td}\right) - c\dot{r}_{r,td}\right)\left(r - a\sin(\theta-\theta_g)\right)}{\sqrt{r^2+a^2-2ar\sin(\theta-\theta_g)}} \\ &+ \frac{\left(k\left(1+\Delta r_{act,f,td}\right) - c\dot{r}_{f,td}\right)\left(r + a\sin(\theta-\theta_g)\right)}{\sqrt{r^2+a^2+2ar\sin(\theta-\theta_g)}},\end{aligned} \tag{5.5}$$

$$\begin{aligned}r\ddot{\theta} = -2\dot{r}\dot{\theta} + \sin\theta &+ \frac{\tau_r\left(r - a\sin(\theta-\theta_g)\right)}{r^2+a^2-2ar\sin(\theta-\theta_g)} + \frac{\tau_f\left(r + a\sin(\theta-\theta_g)\right)}{r^2+a^2+2ar\sin(\theta-\theta_g)} \\ &- \frac{\left(k\left(1+\Delta r_{act,r,td}\right) - c\dot{r}_{r,td}\right)a\cos(\theta-\theta_g)}{\sqrt{r^2+a^2-2ar\sin(\theta-\theta_g)}} \\ &+ \frac{\left(k\left(1+\Delta r_{act,f,td}\right) - c\dot{r}_{f,td}\right)a\cos(\theta-\theta_g)}{\sqrt{r^2+a^2+2ar\sin(\theta-\theta_g)}},\end{aligned} \tag{5.6}$$

respectively.

In order to reduce the complexity of our solutions, we keep the radial dynamics of the sloped ground case same with the flat ground case. For the sake of clarity, we will repeat the exact analytical solution of (5.1) for radial dynamics as given below

$$r(t) = A_6 + A_7\sin(w_{DS}t) + C_3\cos(w_{DS}t). \tag{5.7}$$

However, we choose a new angular velocity solution form as

$$\dot{\theta} = C_5\cos(\theta-\theta_g) + B_{10}, \tag{5.8}$$

where C_5 is a free control parameter and B_{10} is calculated as $B_{10} = \dot{\theta}_{td} - C_5\cos(\theta_{td}-\theta_g)$ by using the boundary conditions $\theta(0) = \theta_{td}$ and $\dot{\theta}(0) = \dot{\theta}_{td}$.

Furthermore, we can solve the angular velocity equation (5.8) to obtain the angular position as

$$\theta(t) = \frac{\pi}{2} + \theta_g + 2\text{atan}\left(\frac{C_5 - B_{11}\tanh\left(\frac{B_{11}t}{2} + B_{12}\right)}{B_{10}}\right), \tag{5.9}$$

where B_{11} and B_{12} are defined as

$$B_{11} := \sqrt{C_5^2 - B_{10}^2}, \tag{5.10}$$

$$B_{12} := \operatorname{atanh}\left(\frac{C_5 - B_{10}\tan\left(\frac{\theta_{td}-\theta_g-\frac{\pi}{2}}{2}\right)}{B_{11}}\right). \tag{5.11}$$

At this point, the required torque inputs τ_r and τ_f can be computed by solving the equations (5.5) and (5.6) via the solutions of (5.7) and (5.9) as

$$\begin{aligned}\tau_r = &\frac{r_{r,s}^2}{2r}\left(2\dot{r}\dot{\theta} - C_5 r\dot{\theta}\sin(\theta-\theta_g) - \sin\theta\right)\\ &+ \frac{r_{r,s}^2(r + a\sin\theta)}{2ar\cos\theta}\left(2kr_{td} - 2C_3k - r\dot{\theta}^2 + \cos\theta\right)\\ &- \frac{r_{r,s}^2 r_{f,s}}{2ar\cos(\theta-\theta_g)}\left(k\left(1+\Delta r_{act,f,td}\right) - c\dot{r}_{f,td}\right)\\ &- \frac{r_{r,s}(r^2-a^2)}{2ar\cos(\theta-\theta_g)}\left(k\left(1+\Delta r_{act,r,td}\right) - c\dot{r}_{r,td}\right),\end{aligned} \tag{5.12}$$

$$\begin{aligned}\tau_f = &\frac{r_{f,s}^2}{2r}\left(2\dot{r}\dot{\theta} - C_5 r\dot{\theta}\sin(\theta-\theta_g) - \sin\theta\right)\\ &- \frac{r_{f,s}^2(r - a\sin\theta)}{2ar\cos\theta}\left(2kr_{td} - 2C_3k - r\dot{\theta}^2 + \cos\theta\right)\\ &+ \frac{r_{f,s}^2 r_{r,s}}{2ar\cos(\theta-\theta_g)}\left(k\left(1+\Delta r_{act,r,td}\right) - c\dot{r}_{r,td}\right)\\ &+ \frac{r_{f,s}(r^2-a^2)}{2ar\cos(\theta-\theta_g)}\left(k\left(1+\Delta r_{act,f,td}\right) - c\dot{r}_{f,td}\right),\end{aligned} \tag{5.13}$$

respectively, where the variables $r_{r,s}$ and $r_{f,s}$ are defined as

$$r_{r,s} := \sqrt{r^2 + a^2 - 2ar\sin(\theta-\theta_g)}, \tag{5.14}$$

$$r_{f,s} := \sqrt{r^2 + a^2 + 2ar\sin(\theta-\theta_g)}. \tag{5.15}$$

A final step is to determine the liftoff event by defining a valid liftoff condition for the double support phase. The liftoff occurs when the rear leg takes off from the ground, which can be mathematically defined as the instant when the ground reaction force on the toe becomes zero. Hence, we define the ground reaction force of the rear leg, $F_{GRF,r}$, as

$$F_{GRF,r} = F_{r,r}\sin\psi_r + F_{a,r}\cos\psi_r, \tag{5.16}$$

where ψ_r is the small angle measured counter-clockwise from the tangent line to the ground at rear toe contact point as illustrated in Figure 5.1. Besides, rear leg radial and angular forces $F_{r,r}$ and $F_{a,r}$ are given by (4.24) and (4.26), respectively. Since the exact analytical solution is very challenging and makes the solutions much more complex than already they are, we prefer to use simple numerical solution for the determination of liftoff instant based on the above principles.

5.2 Performance of MDB-SLIP Model on Sloped Ground

This section presents our analysis for the performance of the MDB-SLIP for walking gait on sloped ground. To accomplish this goal, we perform extensive simulation studies by using 620 initial condition points that are selected from the range $z_a \in [0.900 - 0.995]$ and $\dot{y}_a \in [0.16 - 0.64]$ with non-dimensional spring constant k of 12.75. Our success criteria in these simulations was to observe 1000 steps of walking gait behaviors. Hence, if the model falls down or transits to running behavior (both legs are on the fly), we consider the test as failed.

Here we define two virtual models as sub-models of the original MDB-SLIP. In the first model, MDB1-SLIP, we compute the fixed points via optimizing the control parameters that minimizes the magnitude of the eigenvalues of the Jacobian matrix defined in Section 4.3.1. On the other hand, for the MDB2-SLIP model, we compute the fixed points via optimizing the control parameters that maximizes the robustness to the parametric uncertainty as defined in Section 4.3.2.

To present our analysis, we first define the simulations and the success rate we are considering in this part. We run both the MDB1-SLIP and MDB2-SLIP solutions on a sloped ground for 1000 steps with all initial conditions that are defined above. The ground slope can both be negative and positive corresponding to going downwards and upwards, respectively in the range $[-0.1, 0.1]$ of slope. The slope is defined as $\arctan(\theta_g)$, which corresponds to the amount of change

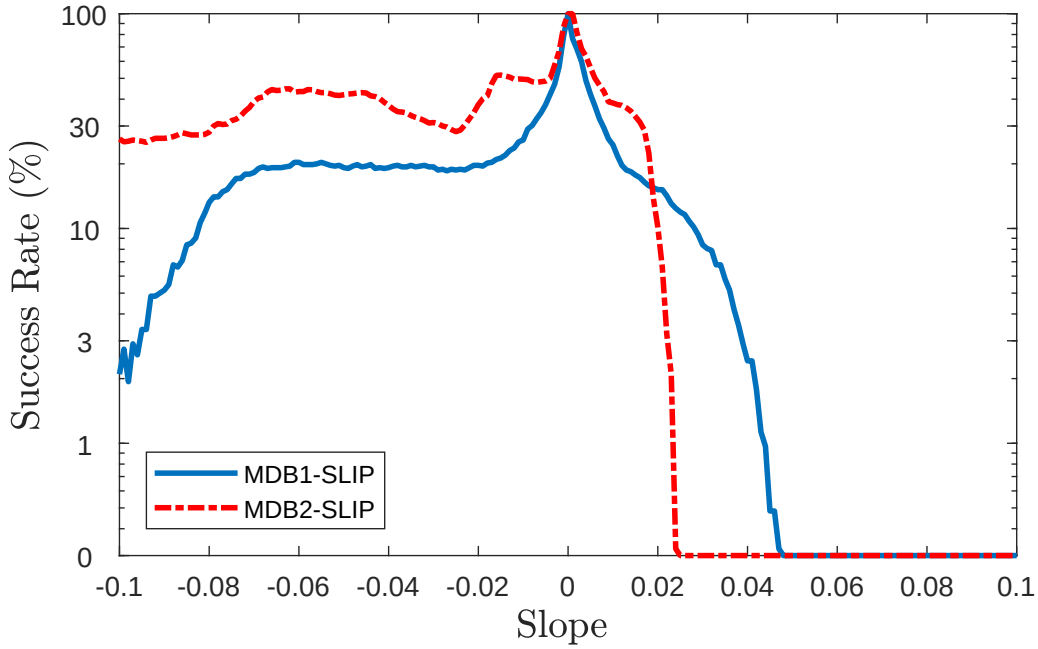

Figure 5.2: Percentage success rate of MBD1-SLIP and MDB2-SLIP models on sloped ground. MDB2-SLIP model performs better than the MDB1-SLIP model in terms of successfully completing the 1000 steps.

in z that corresponds to a unit change in y. The success rate is defined as the percentage of tests that completed 1000 successful walking steps. Figure 5.2 illustrates the results for both the MBD1-SLIP and MDB2-SLIP solutions with respect to 201 different ground slopes that are chosen equidistantly in the range $[-0.1, 0.1]$. Note that both models exhibit 100% success rate for flat ground case (with zero slope) as expected. The key observation here is that MDB2-SLIP model exhibits better performance for going downwards than the MDB1-SLIP model. However, both models are poor while going upwards due to increased demand of energy to climb upwards. Note that the success rate axis for Figure 5.2 is in log scale but we manually added the 0% value to indicate that some tests result in 0% success while going upwards. A final note here is that fixed point solutions are obtained from flat ground but tested on sloped ground. If one can measure the ground profile and compute the fixed points considering the slope of the ground, we expect the solutions to be more successful. However, the goal of this study is to investigate the performance of our flat ground solutions on

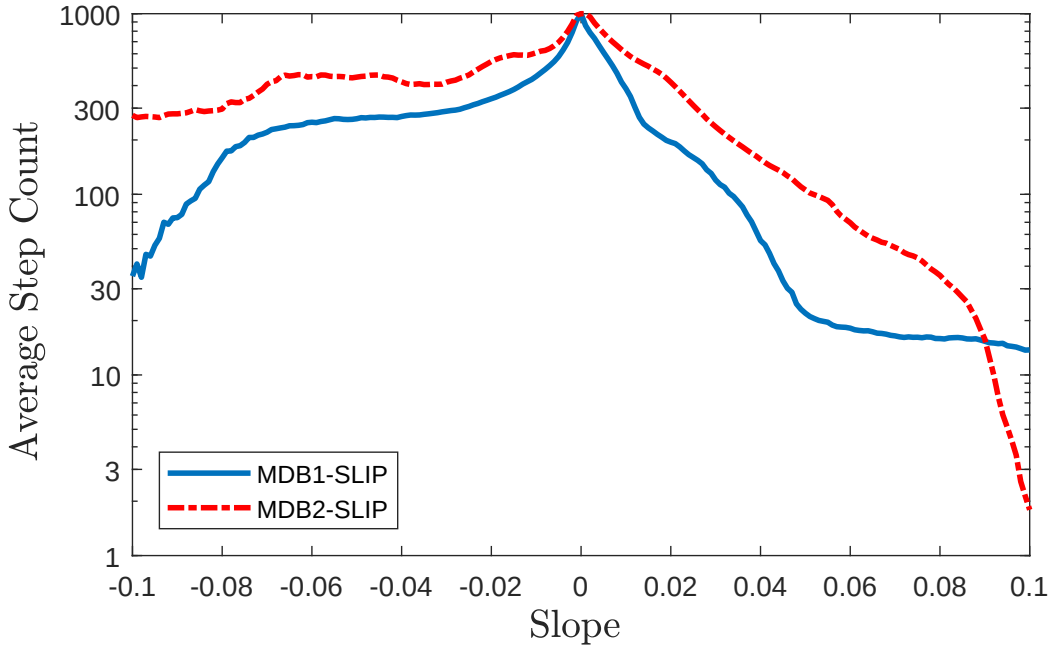

Figure 5.3: The average number of successful walking gait steps before failure for the MDB1-SLIP and MDB2-SLIP models on sloped ground. MDB2-SLIP model exhibits better performance in terms of average number of steps before failure.

sloped ground, hence this part is left out of the scope of current study as a future research direction.

In addition, we report the average number of successful steps before failure for each ground slope value. Figure 5.3 illustrates the comparative analysis that are obtained from MDB1-SLIP and MDB2-SLIP models. Similarly, MDB2-SLIP model exhibits better performance in terms of average number of successful steps criteria. We believe that the main reason behind this is that MDB2-SLIP model is designed to maximize robustness and hence it shows better performance on unmeasured sloped grounds.

5.3 Performance of MDB-SLIP Model on Different Noisy Terrains

This section investigates the performance of the MDB-SLIP model and its variants on different noisy rough terrains. Note that ability to perform a gait is an important measure of robustness for a periodic motion. Hence, we evaluate the stability of periodic gaits via numerical simulations on different terrains to investigate their stability characteristics.

In previous sections, we presented two variants of MDB-SLIP model as MDB1-SLIP and MDB2-SLIP models based on the way their fixed points are generated. In addition to these proposed model, we investigate B-SLIP, AT-SLIP and LAT-SLIP models from the literature for comparison purposes. Our robustness or success measure is the successful completion of walking gait without falling or transiting to a different gait. The analysis in this section show that our results obtained in Section 4.3 are indeed robust, stable periodic gaits.

In Chapter 4, we investigated stability performance of the gaits for the four models; B-SLIP, AT-SLIP, LAT-SLIP and MDB-SLIP by checking the eigenvalues of the Jacobian matrix around a periodic trajectory. However, this stability analysis gives us information about the stability characteristics of the equilibrium points. In order to investigate the stability properties of the gait for a region around such equilibrium points (validity region for our stability analysis), we present our analysis for investigating their stability characteristics on rough terrain simulations. The analysis presented in this section demonstrates that the stability results obtained in Section 4.3 are not simple equilibrium point stabilities but they have a considerable region of attraction around them in which they can preserve their stability. We also propose comparative analysis by investigating the similar characteristics of the models from the literature; B-SLIP, AT-SLIP and LAT-SLIP.

Here we first give a brief implementation details about generating the noisy rough terrain for our simulations. The ground profiles we use in this section

are generated depending on two main variables, Υ and Ω. We create a ground profile consisting of m points that are evenly separated from each other by Υ non-dimensional length. Let (y_n, z_n) be a pair of numbers for each discrete point on the ground profile for $\forall n \in 0, 1, \ldots, m-1$. Here, y_n refers to horizontal position of the point, while z_n corresponds to height of the specific point. Note that the horizontal distance among two points are defined by Υ and they are fixed, so we can define the horizontal position for each point using

$$y_0 = 0, \tag{5.17}$$

$$y_n = y_{n-1} + \Upsilon \qquad \forall n \in 1, 2, ..., m-1, \tag{5.18}$$

In order to generate noise for the height, we use a truncated normal distribution $\mathcal{N}^T$ and set the height of each point by using the following equations

$$z_0 = 0, \tag{5.19}$$

$$d_n = \mathcal{N}^T(0, 1, \Omega/10) \qquad \text{for } n = 1, 2, ..., m-1, \tag{5.20}$$

$$z_n = z_{n-1} + d_n \qquad \text{for } n = 1, 2, ..., m-1, \tag{5.21}$$

Note that Ω determines the noise level for each ground segment, whose lengths are determined by Υ. Hence, these two parameters define a mathematical formulation for the rough terrain profiles used in this thesis. The procedure is repeated if the resulting z_n values are not in the range of $\pm\Omega$. In order to have a continuous definition of the ground profile (to generate the inter point values), we use cubic spline interpolation [97] and can generate height values for any ground point.

The average length of each step used in our models are around 0.5 in non-dimensional units. We repeated our analysis for different Υ values that are chosen as integer multiples of the average step length as 1, 2 and 4. In addition, we performed the tests with various initial conditions with a non-dimensional spring constant of $k = 12.75$. The initial conditions are chosen as 20 equidistant values for $z_a \in [0.900 - 0.995]$ and 31 equidistant values for $\dot{y}_a \in [0.16 - 0.64]$, which correspond to 620 initial condition points.

5.3.1 Open-Loop Control with Fixed Control Parameters

The open-loop simulations aim to run the models for 1000 steps on a randomly generated terrain to count the successful runs. The successful run means preserving the walking gait without falling or transitioning to running behavior. The number of steps, 1000, is chosen big enough to ensure that further increasing the step number does not affect the results and hence our analysis.

We also mentioned that rough terrain simulations can be used as a metric to investigate robustness of the stability of the periodic gaits. Hence, the results we obtained from these simulation experiments, illustrated in Figures 5.4–5.9, will be used a measure for stability performance. Among these results, Figure 5.4, Figure 5.6 and Figure 5.8 illustrate the percentage rate of successful runs for the five different models we aim to compare here. In contrast, Figure 5.5, Figure 5.7 and Figure 5.9 represents the average number of steps that are performed for each experiment on different ground noise levels. The extensive comparative analysis with a wide range of initial conditions and noise levels demonstrate that the MDB-SLIP models variants outperform the models in the literature in terms of robustness in an open-loop rough terrain analysis.

Figure 5.4, Figure 5.6 and Figure 5.8 correspond to percentage success rate of the experiments for the five models with respect to noise levels for $\Upsilon = 0.5$, $\Upsilon = 1$ and $\Upsilon = 2$, respectively. Note that the success rate axes for Figure 5.4, Figure 5.6 and Figure 5.8 are in log scale but we manually added the 0% value to indicate that some tests result in 0% success for increasing Ω values. The first thing we need to mention about these plots is that as Υ becomes bigger, the roughness of the ground profile becomes smoother. Hence, the methods become more successful for larger Υ values. A simple observation of the results presented in Figure 5.4, Figure 5.6 and Figure 5.8 demonstrates that our proposed models MDB1-SLIP and MDB2-SLIP outperform the available methods in the literature in a non-negligible way. Actually, the percentage success rate of the methods B-SLIP, AT-SLIP and LAT-SLIP are well below 3% in our noise level range, which is a very poor performance for locomotion. On the other hand, the proposed

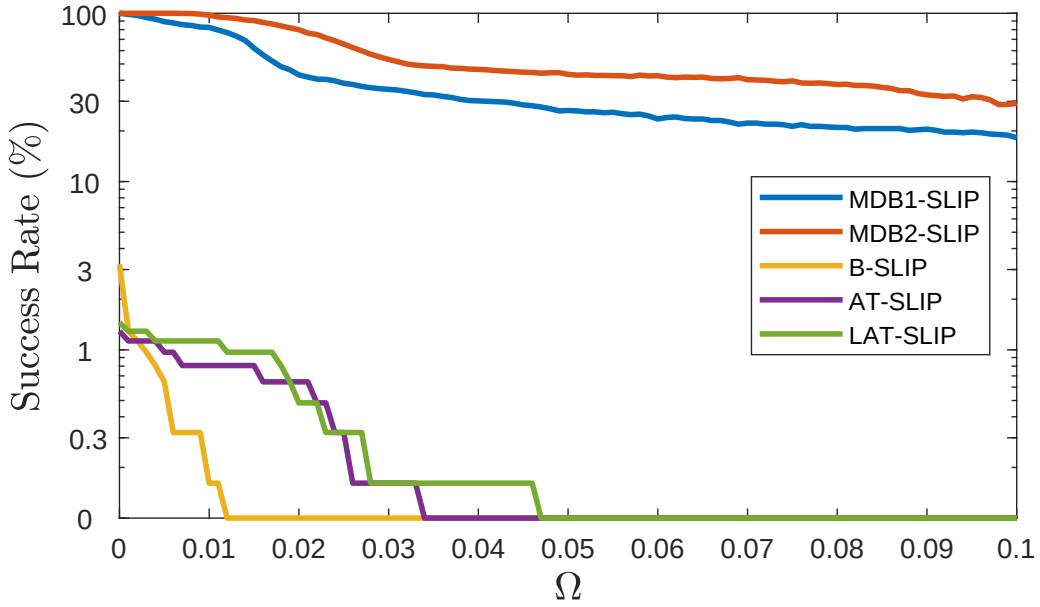

Figure 5.4: Percentage success rate of five models on noisy ground. MDB1-SLIP and MDB2-SLIP models outperform the B-SLIP, AT-SLIP and LAT-SLIP in terms of successfully completing the 1000 steps for $\Upsilon = 0.5$.

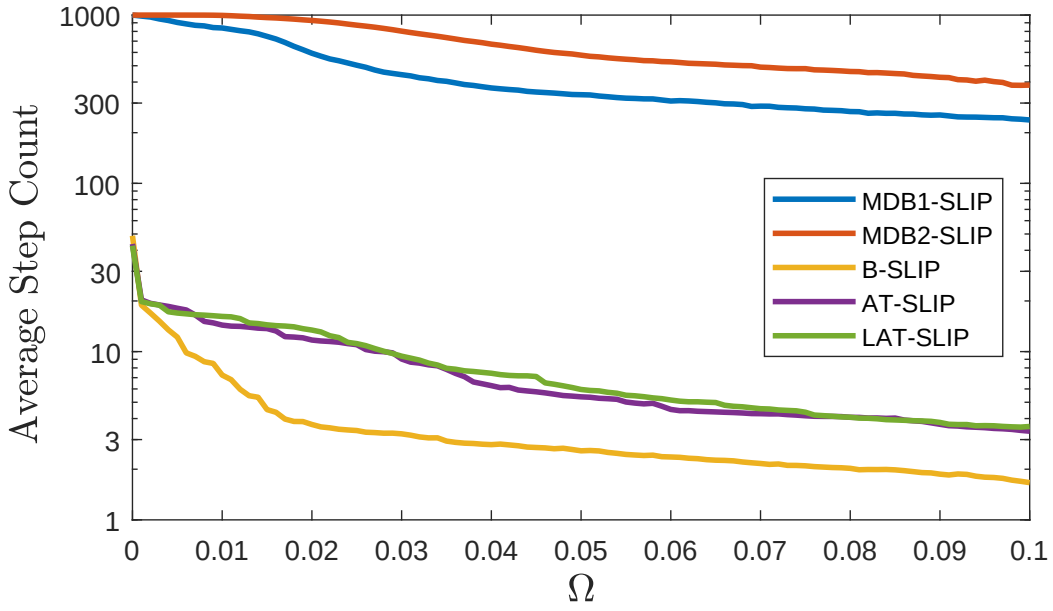

Figure 5.5: The average number of successful walking gait steps before failure for the five models on noisy ground. MDB1-SLIP and MDB2-SLIP models exhibit better performance in terms of average number of steps before failure for $\Upsilon = 0.5$.

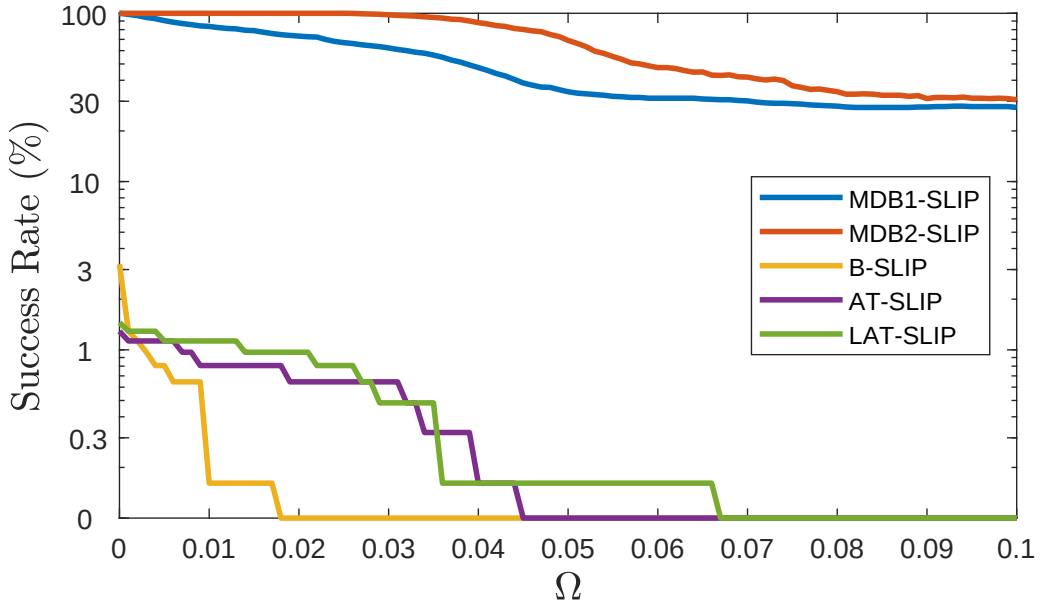

Figure 5.6: Percentage success rate of five models on noisy ground. MDB1-SLIP and MDB2-SLIP models outperform the B-SLIP, AT-SLIP and LAT-SLIP in terms of successfully completing the 1000 steps for $\Upsilon = 1$.

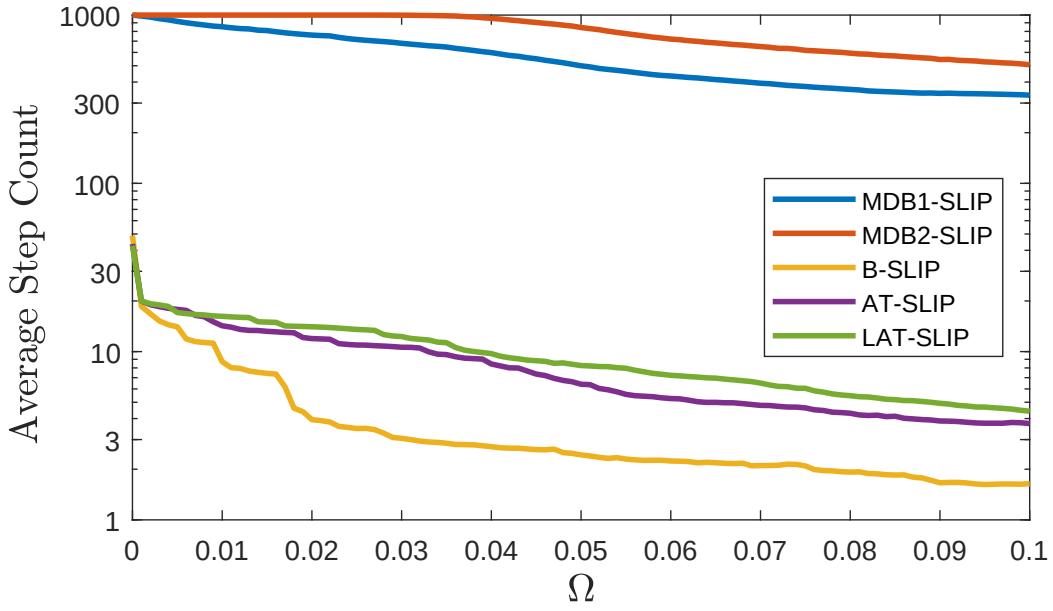

Figure 5.7: The average number of successful walking gait steps before failure for the five models on noisy ground. MDB1-SLIP and MDB2-SLIP models exhibit better performance in terms of average number of steps before failure for $\Upsilon = 1$.

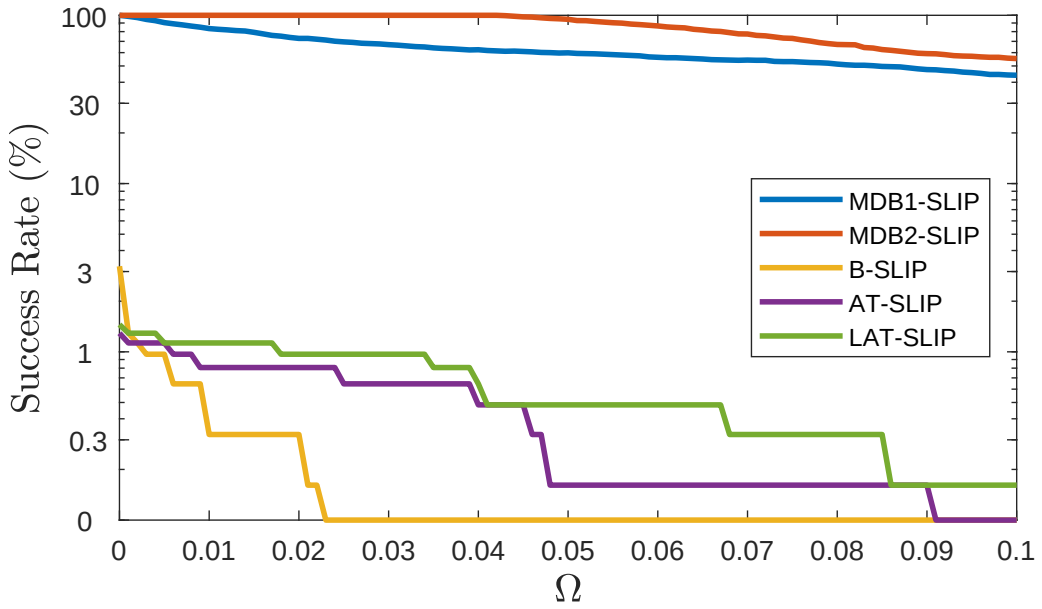

Figure 5.8: Percentage success rate of five models on noisy ground. MDB1-SLIP and MDB2-SLIP models outperform the B-SLIP, AT-SLIP and LAT-SLIP in terms of successfully completing the 1000 steps for $\Upsilon = 2$.

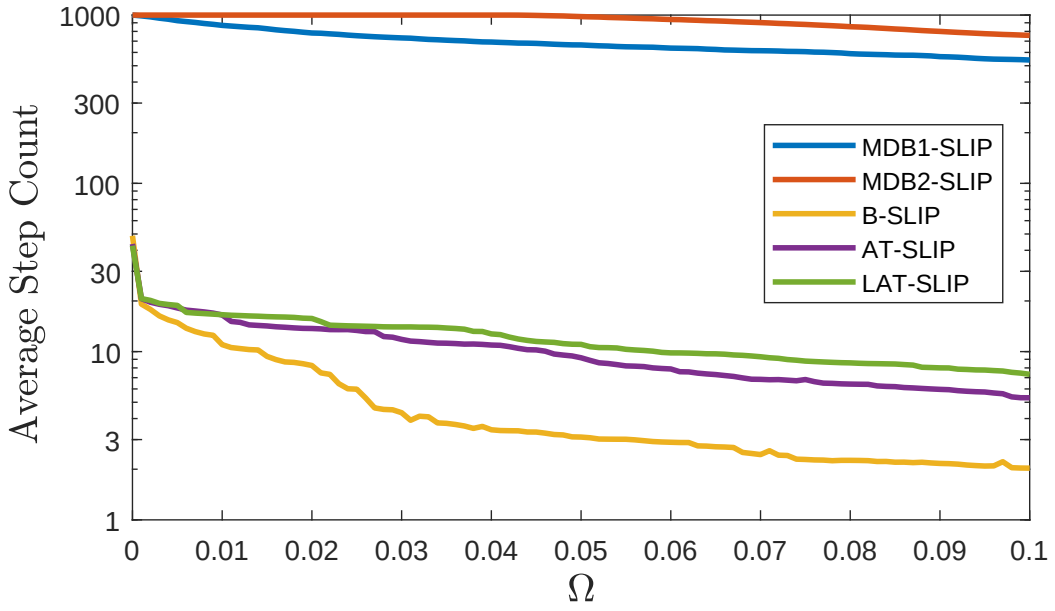

Figure 5.9: The average number of successful walking gait steps before failure for the five models on noisy ground. MDB1-SLIP and MDB2-SLIP models exhibit better performance in terms of average number of steps before failure for $\Upsilon = 2$.

methods MDB1-SLIP and MDB2-SLIP are above 30% even with the smallest (most difficult) Υ value with the largest ground noise level. A final comment that needs to be given here is that MDB2-SLIP model is better than MDB1-SLIP model in almost all scenarios in terms of robustness. This is mainly because the MDB2-SLIP model is designed to ensure maximum performance by carefully choosing the fixed points.

Figure 5.5, Figure 5.7 and Figure 5.9 correspond to average number of steps that are achieved for the five different models for a wide range of ground noise levels and for $\Upsilon = 0.5$, $\Upsilon = 1$ and $\Upsilon = 2$, respectively. These plots also give similar performance results with the percentage success rate. The proposed MDB1-SLIP and MDB2-SLIP are more successful than the other models B-SLIP, AT-SLIP and LAT-SLIP in terms of the average number of steps that can accomplish, since our models are able to complete the 1000 step experiments for a great percentage of the experiments. Similar to previous results, MDB2-SLIP model would be the optimal choice for robustness to achieve successful rough terrain locomotion in an open-loop manner.

5.3.2 Closed-Loop Control with a Deadbeat Control Strategy

In the previous sections, we investigated the stability characteristics of the five models on sloped and noisy ground profiles in an open-loop manner. This section is devoted to investigate the apex trajectory tracking performance of these five models under closed-loop control paradigm. The extensive analysis we performed in this section show that the proposed models exhibit better tracking performance with a dead-beat controller as compared to other models.

The control strategy we use in this part is based on numerical inversion of the apex to apex return map as the deadbeat controller for the models. We utilized the controller strategy defined in Section 3.3.2, whose representative block diagram is given in Figure 3.19. The inverse map based controller takes desired

Table 5.1: Percentage tracking errors of apex states P_a for $\Upsilon = 0.5$ in closed-loop system.

	Models				
Ω	MDB1-SLIP	MDB2-SLIP	AT-SLIP	LAT-SLIP	B-SLIP
0.005	**0.156 ± 0.138**	**0.180 ± 0.158**	0.999 ± 2.67	1.52 ± 3.35	5.79 ± 9.58
0.015	**0.503 ± 0.454**	**0.589 ± 0.513**	1.94 ± 4.64	3.40 ± 7.34	5.76 ± 8.39
0.025	**0.858 ± 0.762**	**1.05 ± 1.00**	2.65 ± 4.54	4.05 ± 7.45	6.72 ± 9.50
0.035	**1.22 ± 1.10**	**1.67 ± 2.37**	3.05 ± 4.84	5.25 ± 9.69	7.57 ± 9.69
0.045	**1.63 ± 1.54**	**2.19 ± 2.21**	3.64 ± 6.00	5.53 ± 9.05	8.31 ± 10.1
0.055	**2.09 ± 2.00**	**2.77 ± 2.57**	4.13 ± 6.82	6.39 ± 9.92	9.14 ± 11.8
0.065	**2.73 ± 4.17**	**3.51 ± 4.22**	4.36 ± 7.83	7.04 ± 10.3	10.1 ± 11.9
0.075	**3.39 ± 6.51**	**4.13 ± 4.18**	4.71 ± 8.01	7.21 ± 10.9	9.88 ± 10.5
0.085	**3.92 ± 4.96**	**4.88 ± 5.77**	4.84 ± 8.36	7.93 ± 12.2	9.83 ± 9.79
0.095	**4.29 ± 4.92**	**5.27 ± 5.64**	5.00 ± 8.56	7.92 ± 11.2	9.89 ± 10.1

apex state $w^d = (z_a^d, \dot{y}_a^d)$ and current apex state $w_i = (z_{ai}, \dot{y}_{ai})$ as its input and tries to compute the optimal control parameters u to achieve the desired apex state from the current apex state. In order to make a fair comparison, the same controller logic is applied for all five models used in our analysis. However, one should note that the control parameters defined under the control signal vector u may differ for each of the five models by definition. For instance, in B-SLIP, AT-SLIP and LAT-SLIP models, u includes the touchdown angle, θ_{td} only, since it is the sole control parameter used for these three models. However, for our proposed models, MD1-SLIP and MDB2-SLIP models, the input signal u includes touchdown angle, θ_{td}, touchdown linear actuator displacement $\Delta r_{act,td}$, and constant control parameters C_2, C_3 and C_4.

In order to generalize our results, the experiments are repeated for all 620 initial conditions under closed-loop control and mean and standard deviations of the percentage tracking errors (3.34), (3.35) and (3.36) are computed for randomly generated noisy terrains. Table 5.1, Table 5.2 and Table 5.3 presents the apex state tracking error for $\Upsilon = 0.5$, $\Upsilon = 1$ and $\Upsilon = 2$, respectively. The error metric we use is based on (3.36), which measures percentage apex tracking error. The results indicate the MDB1-SLIP and MDB2-SLIP models perform better locomotion on rough terrain under closed-loop control with respect to B-SLIP, AT-SLIP

Table 5.2: Percentage tracking errors of apex states P_a for $\Upsilon = 1$ in closed-loop system.

	Models				
Ω	MDB1-SLIP	MDB2-SLIP	AT-SLIP	LAT-SLIP	B-SLIP
0.005	**0.0845 ± 0.0701**	**0.103 ± 0.0887**	0.496 ± 1.09	0.880 ± 1.87	2.07 ± 4.82
0.015	**0.264 ± 0.219**	**0.375 ± 1.12**	1.35 ± 2.51	2.17 ± 3.38	3.51 ± 6.00
0.025	**0.458 ± 0.384**	**0.569 ± 0.467**	2.09 ± 5.74	4.24 ± 8.97	4.56 ± 7.57
0.035	**0.659 ± 0.545**	**0.863 ± 0.814**	2.81 ± 6.06	4.31 ± 8.57	5.27 ± 7.57
0.045	**0.886 ± 0.729**	**1.22 ± 1.48**	3.18 ± 5.85	4.53 ± 8.22	5.61 ± 8.13
0.055	**1.15 ± 1.09**	**1.63 ± 2.22**	3.72 ± 6.59	5.41 ± 8.85	6.08 ± 8.04
0.065	**1.47 ± 1.47**	**1.81 ± 1.44**	3.96 ± 6.70	6.01 ± 9.82	5.92 ± 7.59
0.075	**1.81 ± 1.93**	**2.39 ± 2.82**	4.59 ± 7.86	6.04 ± 9.33	6.57 ± 9.13
0.085	**2.23 ± 2.34**	**2.79 ± 2.99**	4.42 ± 6.77	6.17 ± 8.91	6.81 ± 8.16
0.095	**2.61 ± 2.72**	**3.02 ± 3.14**	4.51 ± 6.71	6.31 ± 9.26	7.80 ± 9.90

Table 5.3: Percentage tracking errors of apex states P_a for $\Upsilon = 2$ in closed-loop system.

	Models				
Ω	MDB1-SLIP	MDB2-SLIP	AT-SLIP	LAT-SLIP	B-SLIP
0.005	**0.0451 ± 0.0372**	**0.0541 ± 0.0523**	0.313 ± 1.24	0.475 ± 0.981	1.49 ± 3.48
0.015	**0.139 ± 0.113**	**0.166 ± 0.142**	1.08 ± 3.05	1.92 ± 4.16	3.17 ± 5.90
0.025	**0.238 ± 0.193**	**0.294 ± 0.317**	1.62 ± 3.59	2.87 ± 5.59	3.68 ± 6.66
0.035	**0.340 ± 0.270**	**0.432 ± 0.399**	2.07 ± 4.17	3.62 ± 6.99	4.40 ± 8.09
0.045	**0.446 ± 0.359**	**0.569 ± 0.484**	2.42 ± 5.38	3.86 ± 7.26	5.00 ± 8.99
0.055	**0.566 ± 0.504**	**0.744 ± 0.897**	2.81 ± 5.72	3.86 ± 6.39	5.37 ± 8.72
0.065	**0.711 ± 0.698**	**0.860 ± 0.743**	2.85 ± 4.44	4.46 ± 7.82	5.31 ± 7.75
0.075	**0.853 ± 0.855**	**1.067 ± 1.07**	3.25 ± 5.67	5.00 ± 8.65	5.97 ± 9.58
0.085	**1.08 ± 1.21**	**1.215 ± 1.12**	3.29 ± 4.76	5.41 ± 8.55	5.77 ± 8.46
0.095	**1.31 ± 1.53**	**1.443 ± 1.56**	3.82 ± 5.81	5.09 ± 7.00	6.17 ± 8.90

and LAT-SLIP models. Moreover, in terms of mean-variance deviations, as indicated as a stability metric in [93], we show that the MDB1-SLIP and MDB2-SLIP models exhibit better locomotion performance with a better robustness in stability. The main difference of closed-loop experiments is that now MDB1-SLIP model performs better than the MDB2-SLIP models under closed-loop control although MDB2-SLIP model was better in open-loop experiments. The quantitative details can be found in Table 5.1, Table 5.2 and Table 5.3. There are some very minor cases where the other models exhibit a better performance but for a majority of the cases, the MDB1-SLIP and MDB2-SLIP models yield better tracking accuracy.

5.4 Discussion

In this chapter, we explained the details of our investigations for performance analysis of the proposed model with respect to some recent prominent models in the literature. We performed extensive simulation experiments to investigate how these models perform on noisy rough terrain with different noise levels. Our analysis concluded that the proposed model, together with its additional actuators, performs better in terms of stability and robustness with respect to the models in the literature. One can simply think that this is an expected result, since we utilize more actuation in our models. However, the goal of this section is to illustrate how we can develop solutions for these kind of complex models using partial feedback linearization and use them in very complicated cases as a legged locomotion model. Actual, the punch line here is that we show how effective use of actuators yield more stable and robust legged locomotion models that also perform better in closed-loop under a dedicated control strategy.

Chapter 6

Conclusions and Future Work

In the first part of this thesis, we started by considering an actuator-enhanced model of the standard spring-loaded inverted pendulum (SLIP) model that is a widely used tool for capturing and studying legged locomotion. The model we consider, which we call as Multi-Actuated Dissipative SLIP (MD-SLIP) model, contains a linear force actuator in leg and a rotational torque actuator at the hip. We showed partial feedback linearization technique can be used to obtain analytical solutions to the stance trajectories of the MD-SLIP model, which were originally non-integrable for basic SLIP models. In addition, we also show how the controlled system possess stable periodic gaits in a wide range of initial conditions. Besides, we showed MD-SLIP model exhibits quite successful results in terms of stability and robustness in rough terrain.

In the following parts, we considered using similar actuations for bipedal locomotion. Fortunately, analysis and control of bipedal legged locomotion have received considerable attention from the robotics community and hence there were a lot of successful results in the literature. However, the non-integrability problem of the basic SLIP model also prevents analytical solutions for the SLIP-based bipedal legged locomotion models. Another problem with the models in current literature was that their stability properties and robustness have not yet been investigated in a systematic way, leaving the practicality of their use on

rough terrain as an open problem. To this end, we first formulated an actuator-enhanced bipedal legged locomotion model called, Multi-Actuated Dissipative Bipedal Spring-Loaded Inverted Pendulum (MDB-SLIP) model. Now, both legs have their own linear actuators and torque actuators yielding two linear and two torque actuators for the MDB-SLIP model. Fortunately, we were able to present a similar feedback linearization strategy to obtain analytical solutions for the trajectories of the MDB-SLIP model as well. In order to characterize its performance, we presented detailed simulation studies illustrating how the MDB-SLIP model can be used to obtain periodic locomotion exhibiting a great stability and robustness performance. For a deeper discussion, we also implemented three recent studies from literature and presented a comparative analysis for the MDB-SLIP against these models in terms of stability and robustness both in an open-loop and closed-loop manner. The results showed that MDB-SLIP model is quite successful in terms of open-loop walking performance on rough terrain as well as desired trajectory tracking performance under closed-loop control.

An important comment that needs to be given about this thesis is that we do not only consider new models and demonstrate their properties but we include a detailed background, where we explain various legged locomotion models for both one-legged and bipedal cases. In addition, we present extensive simulation studies to compare the performance of these models with the ones that are already in the literature. We believe that the extensive analysis results presented in this thesis will serve as a guide in literature that will help future researches for their comparative analysis. We also give implementation details and parameters used in our analysis.

To summarize, the main contributions of this thesis can be listed as follows:

- We demonstrated simulation studies on investigating stability characteristics of a variety of SLIP-based legged locomotion models.
- We considered a multi-actuated SLIP model, called MD-SLIP, to enhance the stability region of the SLIP-based models in the literature. The MD-SLIP model includes a linear actuator to compress leg spring as well as a

rotary actuator to inject torque inputs to the system.

- We utilized partial feedback linearization theory to obtain exact analytical solutions of the proposed MD-SLIP model. Besides, the way we utilize the partial feedback linearization also allows enforcing specified trajectories for the equations of MD-SLIP model.

- Another contribution of this thesis was the extension of our multi-actuated SLIP model for bipedal legged locomotion models, which is called as MDB-SLIP model. We presented how the multi-actuated structure for each leg can be utilized to increase stability of bipedal legged locomotion models. Besides, we can also utilize the partial feedback linearization to enforce some desired locomotion trajectories.

- Finally, we showed the stability and robustness performance of the proposed models (as well as the partial feedback linearization strategy) on various noisy terrain locomotion simulations via a dead-beat control strategy.

The results presented in this thesis could be improved in various directions. Partial feedback linearization proves that it is possible to obtain analytical solutions for the SLIP model by the use of accurately chosen control laws. Hence, one can design different, maybe application-based control laws, that will generate analytical solutions for the SLIP model, which radically simplifies the analysis and control of such models. The proposed control laws can also be utilized for motion planning due to its computational advantage as a result of its analytical nature. In addition, the applications like adjusting best foothold placement for optimizing stability and energy efficiency can be better satisfied when an analytical tool is available to describe the trajectories of a legged locomotion model.

Another future direction about the bipedal legged locomotion part would be including a torso in the model. An interesting study would be designing the torque inputs considering their effects both on the body mass trajectory as well as the motions and stability of the torso. We believe that the dynamic legged locomotion models are fundamental for developing bipedal robots that move like animals do in nature.

Bibliography

[1] M. H. Raibert, *Legged Robots That Balance*. The MIT Press, Cambridge, MA, USA, 1986.

[2] P. Holmes, R. J. Full, D. E. Koditschek, and J. Guckenheimer, "The dynamics of legged locomotion: Models, analyses, and challenges," *SIAM Review*, vol. 48, pp. 207–304, May 2006.

[3] U. Saranli, M. Buehler, and D. E. Koditschek, "RHex: A simple and highly mobile hexapod robot," *The International Journal of Robotics Research*, vol. 20, pp. 616–631, July 2001.

[4] M. H. Dickinson, C. T. Farley, R. J. Full, M. A. R. Koehl, R. Kram, and S. Lehman, "How animals move: An integrative view," *Science*, vol. 288, pp. 100–106, Apr. 2000.

[5] H. Fang, S. Li, K. W. Wang, and J. Xu, "Phase coordination and phase–velocity relationship in metameric robot locomotion," *Bioinspiration & Biomimetics*, vol. 10, no. 6, p. 066006, 2015.

[6] D. Wooden, M. Malchano, K. Blankespoor, A. Howardy, A. A. Rizzi, and M. Raibert, "Autonomous navigation for BigDog," in *2010 IEEE International Conference on Robotics and Automation (ICRA)*, pp. 4736–4741, May 2010.

[7] S. Seok, A. Wang, M. Y. Chuah, D. Otten, J. Lang, and S. Kim, "Design principles for highly efficient quadrupeds and implementation on the mit cheetah robot," in *2013 IEEE International Conference on Robotics and Automation*, pp. 3307–3312, May 2013.

[8] J. A. Grimes and J. W. Hurst, "The design of ATRIAS 1.0 a unique monopod, hopping robot," in *Proceedings of the 2012 International Conference on Climbing and Walking Robots and the Support Technologies for Mobile Machines*, pp. 548–554, 2012.

[9] M. Raibert, K. Blankespoor, G. Nelson, and R. Playter, "BigDog, the rough-terrain quadruped robot," *IFAC Proceedings Volumes*, vol. 41, no. 2, pp. 10822–10825, 2008. 17th IFAC World Congress.

[10] S. Feng, X. Xinjilefu, C. G. Atkeson, and J. Kim, "Optimization based controller design and implementation for the atlas robot in the darpa robotics challenge finals," in *2015 IEEE-RAS 15th International Conference on Humanoid Robots (Humanoids)*, pp. 1028–1035, Nov. 2015.

[11] S. Dubey, M. Prateek, and M. Saxena, "Robot locomotion - a review," *International Journal of Applied Engineering Research*, vol. 10, no. 3, pp. 7357–7369, 2015.

[12] S. Kajita and B. Espiau, *Legged Robots*, pp. 361–389. Berlin, Heidelberg: Springer Berlin Heidelberg, 2008.

[13] U. Saranlı, Ö. Arslan, M. M. Ankaralı, and Ö. Morgül, "Approximate analytic solutions to non-symmetric stance trajectories of the passive spring-loaded inverted pendulum with damping," *Nonlinear Dynamics*, vol. 62, no. 4, pp. 729–742, 2010.

[14] H. Fang, S. Li, K. W. Wang, and J. Xu, "A comprehensive study on the locomotion characteristics of a metameric earthworm-like robot. part a: Modeling and gait generation," *Multibody System Dynamics*, vol. 34, pp. 391–413, Aug. 2015.

[15] H. Yu, M. Li, P. Wang, and H. Cai, "Approximate perturbation stance map of the SLIP runner and application to locomotion control," *Journal of Bionic Engineering*, vol. 9, no. 4, pp. 411–422, 2012.

[16] I. Uyanik, *Identification of legged locomotion via model-based and data-driven approaches*. PhD thesis, Bilkent University, 2017.

[17] W. C. Martin, A. Wu, and H. Geyer, "Experimental evaluation of deadbeat running on the ATRIAS biped," *IEEE Robotics and Automation Letters*, vol. 2, no. 2, pp. 1085–1092, 2017.

[18] A. Wu, *The Theory, Implementation, and Evaluation of Spring Mass Running on ATRIAS, a Bipedal Robot*. PhD thesis, Carnegie Mellon University, 2017.

[19] I. Uyanik, M. M. Ankarali, N. J. Cowan, Ö. Morgül, and U. Saranli, "Toward data-driven models of legged locomotion using harmonic transfer functions," in *Proceedings of the IEEE International Conference on Advanced Robotics*, pp. 357–362, IEEE, 2015.

[20] I. Uyanik, M. M. Ankarali, N. J. Cowan, U. Saranli, and Ö. Morgül, "Identification of a vertical hopping robot model via harmonic transfer functions," *Transactions of the Institute of Measurement and Control*, vol. 38, no. 5, pp. 501–511, 2016.

[21] S. A. Burden and S. S. Sastry, "Reduction and identification for hybrid dynamical models of terrestrial locomotion," in *SPIE Defense, Security, and Sensing*, vol. 8725, pp. 87251B–87251B–10, International Society for Optics and Photonics, 2013.

[22] D. Logan, T. Kiemel, and J. J. Jeka, "Using a system identification approach to investigate subtask control during human locomotion," *Frontiers in Computational Neuroscience*, vol. 10, 2016.

[23] E. Kuzucu Hıdır, "Identification, stability analysis and control of linear time periodic systems via harmonic transfer functions," Master's thesis, Bilkent University, Aug. 2017.

[24] I. Uyanik, U. Saranli, M. M. Ankarali, and Ö. Morgül, "Frequency domain subspace identification of linear time periodic (LTP) systems," *IEEE Transactions on Automatic Control*, 2017. Under Review.

[25] I. Uyanik, U. Saranli, Ö. Morgül, and M. M. Ankarali, "Parametric identification of hybrid linear-time-periodic systems," *IFAC-PapersOnLine*, vol. 49, no. 9, pp. 7–12, 2016.

[26] C. M. A. Pinto, "Stability of quadruped robots' trajectories subjected to discrete perturbations," *Nonlinear Dynamics*, vol. 70, no. 3, pp. 2089–2094, 2012.

[27] M. Golubitsky, I. Stewart, P.-L. Buono, and J. Collins, "Symmetry in locomotor central pattern generators and animal gaits," *Nature*, vol. 401, no. 6754, pp. 693–695, 1999.

[28] J. J. Collins and I. N. Stewart, "Coupled nonlinear oscillators and the symmetries of animal gaits," *Journal of Nonlinear Science*, vol. 3, pp. 349–392, Dec. 1993.

[29] B. Andrews, B. Miller, J. Schmitt, and J. E. Clark, "Running over unknown rough terrain with a one-legged planar robot," *Bioinspiration & Biomimetics*, vol. 6, p. 026009, May 2011.

[30] R. M. Alexander, "Three uses for springs in legged locomotion," *International Journal of Robotics Research*, vol. 9, no. 2, pp. 53–61, 1990.

[31] R. Blickhan and R. J. Full, "Similarity in multilegged locomotion: Bouncing like a monopode," *Journal of Comparative Physiology A: Neuroethology, Sensory, Neural, and Behavioral Physiology*, vol. 173, pp. 509–517, Nov. 1993.

[32] C. T. Farley and D. P. Ferris, "Biomecahnics of Walking and Running: Center of Mass Movements to Muscle Action," *Excercise and Sport Science Reviews*, vol. 26, pp. 253–283, 1998.

[33] P. Gregorio, M. Ahmadi, and M. Buehler, "Design, control, and energetics of an electrically actuated legged robot," *Transactions on Systems, Man, and Cybernetics*, vol. 27, pp. 626–634, Aug. 1997.

[34] G. Zeglin, *The bow leg hopping robot*. PhD thesis, Carnegie Mellon University, 1999.

[35] A. Sato and M. Buehler, "A planar hopping robot with one actuator: design, simulation, and experimental results," in *2004 IEEE/RSJ International Conference on Intelligent Robots and Systems (IROS) (IEEE Cat. No.04CH37566)*, vol. 4, pp. 3540–3545, Sept. 2004.

[36] J. W. Hurst, J. E. Chestnutt, and A. A. Rizzi, "Design and philosophy of the bimasc, a highly dynamic biped," in *2007 IEEE International Conference on Robotics and Automation (ICRA)*, pp. 1863–1868, 2007.

[37] M. M. Ankarali and U. Saranli, "Stride-to-stride energy regulation for robust self-stability of a torque-actuated dissipative spring-mass hopper," *Chaos: An Interdisciplinary Journal of Nonlinear Science*, vol. 20, no. 3, p. 033121, 2010.

[38] R. J. Full and D. E. Koditschek, "Templates and anchors: neuromechanical hypotheses of legged locomotion on land," *Journal of Experimental Biology*, vol. 202, no. 23, pp. 3325–3332, 1999.

[39] B. Han, X. Luo, Q. Liu, B. Zhou, and X. Chen, "Hybrid control for SLIP-based robots running on unknown rough terrain," *Robotica*, vol. 32, no. 7, pp. 1065–1080, 2014.

[40] B. Dadashzadeh, H. R. Vejdani, and J. Hurst, "From template to anchor: A novel control strategy for spring-mass running of bipedal robots," in *2014 IEEE/RSJ International Conference on Intelligent Robots and Systems*, pp. 2566–2571, Sept. 2014.

[41] H. Yu, H. Gao, Z. Fan, Z. Deng, and L. Zhang, "Dual-slip model based galloping gait control for quadruped robot: A task-space formulation," in *2017 American Control Conference (ACC)*, pp. 191–197, May 2017.

[42] K. A. Hamed, N. Sadati, W. A. Gruver, and G. A. Dumont, "Exponential stabilisation of periodic orbits for running of a three-dimensional monopedal robot," *IET Control Theory Applications*, vol. 5, pp. 1304–1320, July 2011.

[43] J. wen Luo, Y. li Fu, and S. guo Wang, "3d stable biped walking control and implementation on real robot," *Advanced Robotics*, vol. 31, pp. 634–649, Apr. 2017.

[44] K. A. Hamed and J. W. Grizzle, "Robust event-based stabilization of periodic orbits for hybrid systems: Application to an underactuated 3d bipedal robot," in *2013 American Control Conference*, pp. 6206–6212, June 2013.

[45] Y. Liu, P. M. Wensing, D. E. Orin, and Y. F. Zheng, "Dynamic walking in a humanoid robot based on a 3D actuated dual-SLIP model," in *2015 IEEE International Conference on Robotics and Automation (ICRA)*, pp. 5710–5717, May 2015.

[46] S. G. Carver, N. J. Cowan, and J. M. Guckenheimer, "Lateral stability of the spring-mass hopper suggests a two-step control strategy for running," *Chaos: An Interdisciplinary Journal of Nonlinear Science*, vol. 19, no. 2, p. 026106, 2009.

[47] W. J. Schwind and D. E. Koditschek, "Approximating the stance map of a 2-DOF monoped runner," *Journal of Nonlinear Science*, vol. 10, pp. 533–568, Oct. 2000.

[48] P. Holmes, "Poincaré, celestial mechanics, dynamical-systems theory and "chaos"," *Physics Reports*, vol. 193, pp. 137–163, Sept. 1990.

[49] O. Arslan and U. Saranli, "Reactive planning and control of planar spring-mass running on rough terrain," *IEEE Transactions on Robotics*, vol. 28, pp. 567–579, June 2012.

[50] I. Uyanik, U. Saranli, and Ö. Morgül, "Adaptive control of a spring-mass hopper," in *2011 IEEE International Conference on Robotics and Automation (ICRA)*, pp. 2138–2143, 2011.

[51] H. Geyer, A. Seyfarth, and R. Blickhan, "Spring-mass running: simple approximate solution and application to gait stability," *Journal of Theoretical Biology*, vol. 232, no. 3, pp. 315–328, 2005.

[52] O. Arslan, U. Saranli, and O. Morgul, "An approximate stance map of the spring mass hopper with gravity correction for nonsymmetric locomotions," in *2009 IEEE International Conference on Robotics and Automation*, pp. 2388–2393, May 2009.

[53] I. Uyanik, Ö. Morgül, and U. Saranli, "Experimental validation of a feedforward predictor for the spring-loaded inverted pendulum template," *IEEE Transactions on Robotics*, vol. 31, pp. 208–216, Feb. 2015.

[54] M. Shahbazi, R. Babuška, and G. A. Lopes, "Analytical approximation for the double-stance phase of a walking robot," in *Proceedings of the IEEE International Conference on Robotics and Automation*, pp. 5754–5760, IEEE, 2015.

[55] H. E. Orhon, C. Odabas, I. Uyanik, Ö. Morgül, and U. Saranli, "Extending the lossy spring-loaded inverted pendulum model with a slider-crank mechanism," in *Proceedings of the IEEE International Conference on Advanced Robotics*, pp. 99–104, IEEE, 2015.

[56] L. R. Hunt and R. Su, "Linear equivalents of nonlinear time varying systems," in *Proc. MTNS, Santa Monica, CA*, pp. 119–123, 1981.

[57] M. W. Spong, "Partial feedback linearization of underactuated mechanical systems," in *Intelligent Robots and Systems '94. 'Advanced Robotic Systems and the Real World', IROS '94. Proceedings of the IEEE/RSJ/GI International Conference on*, vol. 1, pp. 314–321, Sept. 1994.

[58] B. d'Andréa Novel, G. Campion, and G. Bastin, "Control of nonholonomic wheeled mobile robots by state feedback linearization," *The International Journal of Robotics Research*, vol. 14, no. 6, pp. 543–559, 1995.

[59] M. Gienger, K. Loffler, and F. Pfeiffer, "Towards the design of a biped jogging robot," in *Proceedings 2001 ICRA. IEEE International Conference on Robotics and Automation (Cat. No.01CH37164)*, vol. 4, pp. 4140–4145, 2001.

[60] K. Mitobe, N. Mori, K. Aida, and Y. Nasu, "Nonlinear feedback control of a biped walking robot," in *Proceedings of 1995 IEEE International Conference on Robotics and Automation*, vol. 3, pp. 2865–2870, May 1995.

[61] K. Pathak, J. Franch, and S. K. Agrawal, "Velocity and position control of a wheeled inverted pendulum by partial feedback linearization," *IEEE Transactions on Robotics*, vol. 21, pp. 505–513, June 2005.

[62] G. Piovan and K. Byl, "Enforced symmetry of the stance phase for the spring-loaded inverted pendulum.," in *2012 IEEE International Conference on Robotics and Automation*, pp. 1908–1914, May 2012.

[63] G. Piovan and K. Byl, "Approximation and control of the SLIP model dynamics via partial feedback linearization and two-element leg actuation strategy," *IEEE Transactions on Robotics*, vol. 32, pp. 399–412, Apr. 2016.

[64] H. Hamzaçebi and Ö. Morgül, "Enlarging the region of stability using the torque-enhanced active SLIP model," in *2015 International Conference on Advanced Robotics (ICAR)*, pp. 345–350, July 2015.

[65] H. Hamzaçebi and Ö. Morgül, "On the periodic gait stability of a multi-actuated spring-mass hopper model via partial feedback linearization," *Nonlinear Dynamics*, vol. 88, pp. 1237–1256, Apr. 2017.

[66] R. Altendorfer, U. Saranli, H. Komsuoglu, D. Koditschek, H. B. Brown, M. Buehler, N. Moore, D. McMordie, and R. Full, *Evidence for Spring Loaded Inverted Pendulum Running in a Hexapod Robot*, pp. 291–302. Berlin, Heidelberg: Springer Berlin Heidelberg, 2001.

[67] I. Poulakakis and J. W. Grizzle, "The spring loaded inverted pendulum as the hybrid zero dynamics of an asymmetric hopper," *IEEE Transactions on Automatic Control*, vol. 54, pp. 1779–1793, Aug. 2009.

[68] Z. H. Shen and J. E. Seipel, "A fundamental mechanism of legged locomotion with hip torque and leg damping," *Bioinspiration & Biomimetics*, vol. 7, p. 046010, Sept. 2012.

[69] G. Secer and U. Saranli, "Control of hopping through active virtual tuning of leg damping for serially actuated legged robots," in *2014 IEEE International Conference on Robotics and Automation (ICRA)*, pp. 4556–4561, May 2014.

[70] J. Schmitt and J. Clark, "Modeling posture-dependent leg actuation in sagittal plane locomotion," *Bioinspiration & Biomimetics*, vol. 4, no. 4, p. 046005, 2009.

[71] F. Peuker, A. Seyfarth, and S. Grimmer, "Inheritance of SLIP running stability to a single-legged and bipedal model with leg mass and damping," in *2012 4th IEEE RAS EMBS International Conference on Biomedical Robotics and Biomechatronics (BioRob)*, pp. 395–400, June 2012.

[72] M. Hutter, C. D. Remy, M. A. Hoepflinger, and R. Siegwart, "Efficient and versatile locomotion with highly compliant legs," *IEEE/ASME Transactions on Mechatronics*, vol. 18, pp. 449–458, Apr. 2013.

[73] J. Seipel and P. Holmes, "A simple model for clock-actuated legged locomotion," *Regular and Chaotic Dynamics*, vol. 12, pp. 502–520, Oct. 2007.

[74] I. Uyanik, "Adaptive control of a one-legged hopping robot through dynamically embedded spring-loaded inverted pendulum template," Master's thesis, Bilkent University, Aug. 2011.

[75] A. Long, R. Gregg, and K. Lynch, "The simplest parkour model: Experimental validation and stability analysis," in *Proceedings of the International Conference on Climbing and Walking Robots and Support Technologies for Mobile Machines*, Citeseer, 2011.

[76] H. Geyer, A. Seyfarth, and R. Blickhan, "Compliant leg behaviour explains basic dynamics of walking and running," *Proceedings of the Royal Society of London B: Biological Sciences*, vol. 273, no. 1603, pp. 2861–2867, 2006.

[77] J. Rummel, Y. Blum, and A. Seyfarth, "From walking to running," *Autonome Mobile Systeme 2009*, pp. 89–96, 2009.

[78] H. R. Martinez and J. P. Carbajal, "From walking to running a natural transition in the SLIP model using the hopping gait," in *2011 IEEE International Conference on Robotics and Biomimetics*, pp. 2163–2168, Dec. 2011.

[79] S. Collins, A. Ruina, R. Tedrake, and M. Wisse, "Efficient bipedal robots based on passive-dynamic walkers," *Science*, vol. 307, no. 5712, pp. 1082–1085, 2005.

[80] D. G. E. Hobbelen and M. Wisse, "Swing-leg retraction for limit cycle walkers improves disturbance rejection," *IEEE Transactions on Robotics*, vol. 24, pp. 377–389, Apr. 2008.

[81] N. Shemer and A. Degani, "Analytical control parameters of the swing leg retraction method using an instantaneous slip model," in *2014 IEEE/RSJ International Conference on Intelligent Robots and Systems*, pp. 4065–4070, Sept. 2014.

[82] J. Rummel, Y. Blum, and A. Seyfarth, "Robust and efficient walking with spring-like legs," *Bioinspiration & Biomimetics*, vol. 5, p. 046004, Nov. 2010.

[83] L. C. Visser, S. Stramigioli, and R. Carloni, "Robust bipedal walking with variable leg stiffness," in *2012 4th IEEE RAS EMBS International Conference on Biomedical Robotics and Biomechatronics (BioRob)*, pp. 1626–1631, June 2012.

[84] J. Rummel, Y. Blum, H. M. Maus, C. Rode, and A. Seyfarth, "Stable and robust walking with compliant legs," in *2010 IEEE International Conference on Robotics and Automation*, pp. 5250–5255, May 2010.

[85] G. Garofalo, C. Ott, and A. Albu-Schäffer, "Walking control of fully actuated robots based on the bipedal SLIP model," in *2012 IEEE International Conference on Robotics and Automation*, pp. 1456–1463, May 2012.

[86] J. G. Ketelaar, L. C. Visser, S. Stramigioli, and R. Carloni, "Controller design for a bipedal walking robot using variable stiffness actuators," in *2013 IEEE International Conference on Robotics and Automation*, pp. 5650–5655, May 2013.

[87] M. Shahbazi, R. Babuška, and G. A. D. Lopes, "Unified modeling and control of walking and running on the spring-loaded inverted pendulum," *IEEE Transactions on Robotics*, vol. 32, pp. 1178–1195, Oct. 2016.

[88] M. Shahbazi, U. Saranlı, R. Babuška, and G. A. D. Lopes, "Approximate analytical solutions to the double-stance dynamics of the lossy spring-loaded inverted pendulum," *Bioinspiration & Biomimetics*, vol. 12, p. 016003, Dec. 2016.

[89] A. Arampatzis, G.-P. Brüggemann, and V. Metzler, "The effect of speed on leg stiffness and joint kinetics in human running," *Journal of Biomechanics*, vol. 32, no. 12, pp. 1349–1353, 1999.

[90] M. Farkas, *Periodic Motions*, vol. 104 of *Applied Mathematical Sciences*. Springer-Verlag, New York, NY, USA, 1994.

[91] W. J. Schwind, *Spring loaded inverted pendulum running: A plant model*. PhD thesis, University of Michigan, 1998.

[92] H. K. Khalil, *Nonlinear Systems*. Prentice Hall, Upper Saddle River, NJ, USA, 3rd ed., 2002.

[93] B. Miller, J. Schmitt, and J. E. Clark, "Quantifying disturbance rejection of SLIP-like running systems," *The International Journal of Robotics Research*, vol. 31, no. 5, pp. 573–587, 2012.

[94] P. Welch, "The use of fast fourier transform for the estimation of power spectra: A method based on time averaging over short, modified periodograms," *IEEE Transactions on Audio and Electroacoustics*, vol. 15, pp. 70–73, June 1967.

[95] W. Romberg, "Vereinfachte numerische integration," *Det Kongelige Norske Videnskabers Selskab Forhandlinger*, vol. 28, no. 7, pp. 30–36, 1955.

[96] H. R. Vejdani, A. Wu, H. Geyer, and J. W. Hurst, "Touch-down angle control for spring-mass walking," in *2015 IEEE International Conference on Robotics and Automation (ICRA)*, pp. 5101–5106, May 2015.

[97] C. de Boor, *A Practical Guide to Splines*, vol. 27 of *Applied Mathematical Sciences*. Springer-Verlag, New York, NY, USA, 1978.